UNIVERSITÀ DEGLI STUDI DI PADOVA
DIPARTIMENTO DI INGEGNERIA INDUSTRIALE DII

TESI DI LAUREA MAGISTRALE IN INGEGNERIA AEROSPAZIALE

MISSUS experiment on BEXUS programme: Temperature data analysis and correlation

Relatore: Prof. Stefano Debei
Correlatori: Dott. Giacomo Colombatti
Ing. Francesca Cucciarrè

Laureanda: CHIARA PALLA

ANNO ACCADEMICO 2012 – 2013

“Quanto più ci innalziamo,
tanto più piccoli sembriamo a quelli che non possono volare.”
F. Nietzsche, Aurora, 1881

Abstract

MISSUS is a multi-sensors scientific package for the measurement of temperature, pressure, humidity, velocity, magnetic field, attitude, that flew on-board BEXUS 15 stratospheric balloon. The flight constituted a unique opportunity to test an innovative temperature sensor (MarsTem, which will be accommodated on DREAMS suite onboard ExoMars 2016 mission), based on-previous CISAS know-how. The goal was to collect meteorological and attitude data and validate the atmospheric models basing on a synergic approach in the data analysis.

In the first part of the thesis the project management of the experiment has been undertaken, from the preliminary definition to the post flight analysis, in particular four main activities are described: work areas identification, resources analysis, schedule and risks definition.

In the second part the data analysis has been carried out, according to the data fusion concept which relies on the cross correlation between measurements. After the preliminary operation of data filtering, the analysis of the meteorological data has been performed, in particular temperature data provided by the innovative RTD, and the influences of environmental factors which affected measurements have been studied (e.g.: clouds, solar radiation, etc). The work focused on two main aspects: atmospheric analysis and correlation between gondola attitude and RTD measurements.

From this starting point thermal vacuum tests with solar simulator are proposed in order to verify data collected by the sensor during flight and compare the thermal behavior of the prototype which flew on MISSUS with that of the Flight Model of the sensor, which will be part of DREAMS suite.

Index

Introduction

This thesis work concerns the development of MISSUS experiment, within BEXUS programme, with focus on two main subjects which are examined in detail:

- Project management of the experiment together with objectives and requirements definition (in the first part).
- Analysis of the collected data during flight (in the second part), in particular meteorological data and the temperature measurements provided by the MarsTem prototype.

Chapter 1 introduces MISSUS and Stratospheric Balloon flight. It starts with an overview on the BEXUS programme, followed by a detailed description of MISSUS. At first the motivations that led to the development of the experiment are presented, followed by the identification of the mission objectives. In the second part the configuration onboard of the experiment with particular focus on the sensors and their main specifications is explained. Finally are presented the specific requirements of MISSUS performed by means of the technical design in order to achieve the objectives listed before.

In Chapter 2 the Project Management work is described. There are two main sections: the first one concerns the project planning, the second one about the management of the risks. The project planning paragraph focuses on how achieve the experiment by defining the work packages, the identification of the resources available and the schedule forced by deadlines and time constraints. In the risk section the identification process and the classification methods adopted are presented, the experiment risks that were identified and mitigated during the whole programme follow.
The last part of the Chapter is devoted to a critical comparison between the planned work and what has been in fact realized.

Chapter 3 is dedicated to the launch campaign. It contains an overview of the activities performed in order to get the experiment ready for launch, followed by the flight performance onboard the stratospheric balloon. A summary of the recovery procedure and post flight investigation is reported in the last paragraphs.

The data analysis and results are presented in Chapter 4. The chapter is divided in three main sections: the preliminary procedure of data filtering; the cross-correlation among temperature measurements, meteorological data and environmental factors; the future tests on the MarsTem prototype.

In addition, the second paragraph is split up in two parts: the atmospheric analyses and the correlation between gondola attitude and temperature data. The atmospheric analyses have been performed in order to characterize the environment up to the floating phase, validate the atmospheric models and study the stability of troposphere and stratosphere regions during flight. In the second section the correlation allows to study how the sun influences temperature measurement during the cruise phase.

Chapter 1

BEXUS Programme and MISSUS experiment

1.1 Balloon flights

Nowadays stratospheric balloon missions play an increasingly important role for the international scientific community since the experiments can be hold in space-like environment with a significant reduction in costs, timelines and mission constraints.
Furthermore balloon flights give the opportunity to test untried technologies and space mission prototypes in operative conditions of thin atmosphere. This allows comparison with other planets similar atmosphere conditions based on real flight data rather than simulations.
Another significant meaning of Ballooning is the possibility to develop and validate techniques and procedures that will be implemented and applied in real space missions.

1.2 BEXUS

BEXUS programme allows students from universities across Europe to carry out scientific and technological experiments on stratospheric research balloons.
Each year, two balloons are launched, carrying up to 20 experiments designed and built by student teams.
The BEXUS programme is realised under a bilateral Agency Agreement between the German Aerospace Center (DLR) and the Swedish National Space Board (SNSB). The Swedish share of the payload is made available to students from other European countries through a collaboration with the European Space Agency (ESA).
EuroLaunch, a cooperation between the Esrange Space Center of SSC and the Mobile Rocket Base (MoRaBa) of DLR, is responsible for the campaign management and operations of the launch vehicles. Experts from ESA, SSC and DLR provide technical support to the student teams throughout the project.
The main aim behind of this educational programme is to motivate and promote study project and design in the field of science and aerospace technology. Moreover the students

gain experience in scientific experimental probe design and realization, team work and management which are important for involvement in projects work and their future careers.

The typical BEXUS balloon has a volume of 12,000 m^3 and a diameter of 14 m when filled with Helium gas. The total mass available for the experiments is between 40 and 100 kg. The maximum altitude is 35 km and the flight duration can varies between 2 and 5 hours.
The experiments are placed in the payloads gondola. There are different available configurations depending on the dimension, mass and numbers of the selected experiments. Available for BEXUS there are a large, medium and small gondola. The gondola payload mass influences the maximum reachable altitude. This can be simply explained by the Archimedes principle. The forces acting on the balloon are gravity, due to the mass of balloon, Helium gas and payload, (directed downwards) and buoyancy, equal to the weight of the air moved by the balloon volume (directed upwards). The balloon will lift until the Archimedes lift will fully compensate gravity.

The collaboration with the Air Traffic Control (ATC) permits to track the balloon position during flight. The balloon trajectory is predicted in real time, based on wind profile, meteorological models and GPS trajectory tracking.
Main flight termination criteria are: no inhabitants under cut down point, authorization from ATC and good recovery conditions.
The payload gondola is picked up by a helicopter and returned to the launch base, after landing with parachute.

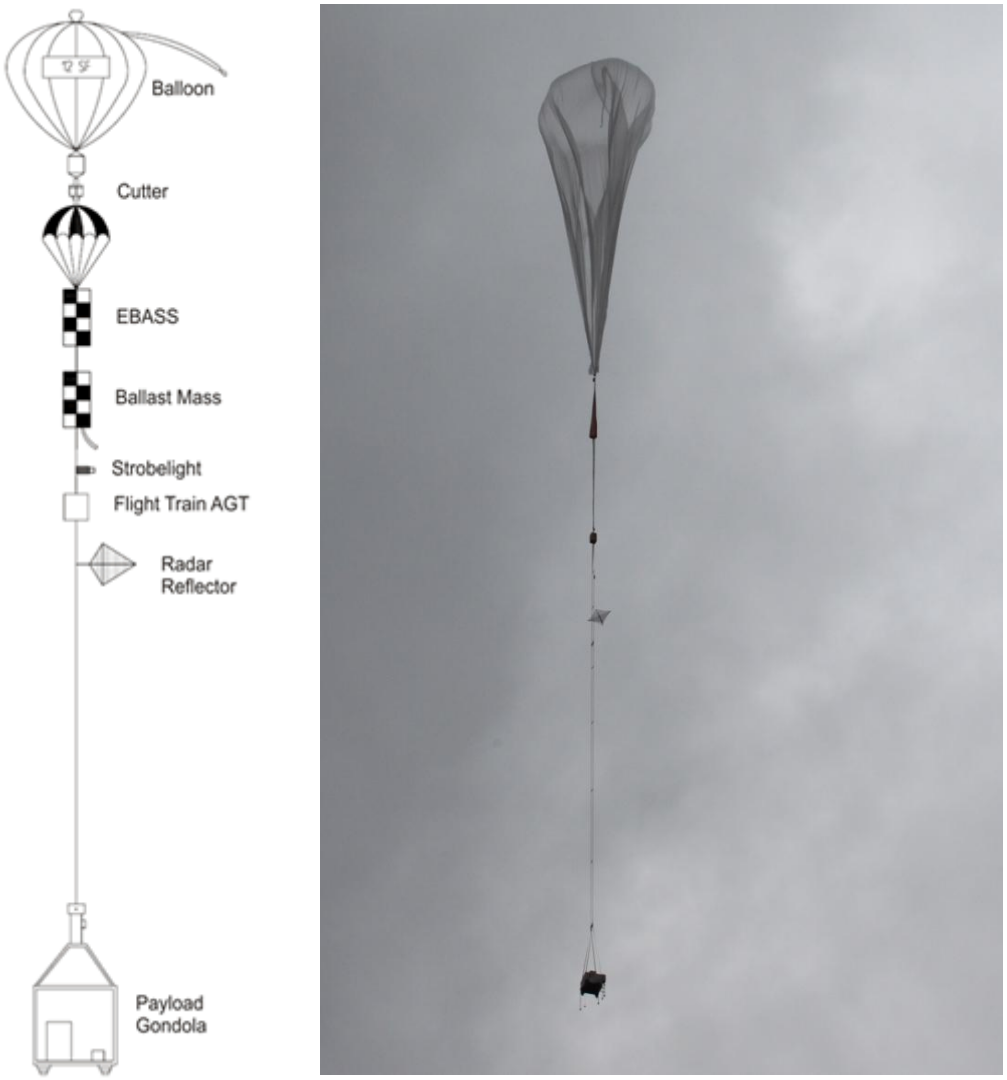

Figure 1 BX balloon flight train and the BX15 balloon a few seconds after launch

The experiment design has to be compatible with the environmental conditions of the flight: temperatures as low as -70 °C, air pressure of 6-10 mbar.
Loads are also fundamental constrains to be considered for the experiments. They should be able to withstand 10 g vertically and 5 g horizontally. The maximum accelerations are during parachute deployment and at impact with ground surface.
The ascent velocity is about 5 m/s and the landing velocity is approximately 8 m/s. The shock at impact depends on the nature of the ground surface.

On the 25th of September 2012 MISSUS experiment on-board BEXUS 15 lifted off at 12:18 CEST (10:18 UTC) from the launch pad at SSC Esrange Space Centre in Northern Sweden. After a 2-hour ascent phase, it reached its floating altitude of around 25 km. The balloon and gondola floated for about six hours until they were cut down.

Figure 2 View of the timing from the launch of BX15

1.3 MISSUS

MISSUS is a Meteorological Integrated Sensor SUite for Stratospheric analysis developed at the University of Padova by a team of students in aerospace, electronics and software engineering.

The role of meteorological instrumentation is central for planning a surface mission on a planet because the study of the atmosphere allows to go deeply into the dynamics of the atmosphere formation and to investigate the evolution processes of the whole Solar System.
In particular the recent ESA programs have focused on Mars for 2016-2018 and beyond with the ExoMars mission, to investigate the environment of the planet, focusing on the research of present and past life traces and demonstrate new technologies for future missions and landings.

At the moment, CISAS is involved in the design and realization of DREAMS package (Dust characterization, Risk assessment and Environment Analyzer on the Martian Surface), which will be part of the payload on ExoMars 2016 Mission, (see next paragraph).

From this starting point the need of realizing a meteorological package conceived for applications in Mars-like environments arises.
In particular MISSUS, composed of several sensors for the measurement of temperature, pressure, humidity, velocity, magnetic field, attitude, gives a useful contribution in the development of integrated multi-sensors packages for harsh atmosphere exploration. The goal was to collect meteorological and attitude data and validate the atmospheric models

during the ascent, cruise and descent phases, basing on a synergic approach in the data analysis.

At an altitude of 20-30 km, Earth atmosphere is similar to Mars ground environment for what concern the pressure and the thermal exchange mechanisms. In particular convective motions in the daytime are primarily driven by radiative contributions, which have stronger effect due to low density (see Ref.[1]).

Differences respect to Earth atmosphere are related to the thermal conductivity and thermal capacity of CO_2 (about 95% of Martian atmosphere), temperature and dust storms.

The balloon flight constituted a unique opportunity to test an innovative temperature sensor (MarsTem) on board MISSUS, developed to measure fast temperature fluctuations, basing on previous Cassini-Huygens experience on Titan and past balloon missions HASI and Sora. MarsTem on board MISSUS is the prototype of the sensor which will be used to measure the temperature profile of Mars atmosphere on the Entry Descent Module (ExoMars 2016).

Moreover the flight offered a very interesting possibility to measure a wide range of parameters in a changeable environment during ascent, cruise and descent phases.

The verification of the metrological behaviour of the instruments thanks to the cross correlation of the data (data fusion) in post processing will be a useful input and reference for the future missions.

1.3.1 Motivations: ExoMars programme and DREAMS package

ExoMars programme has been established by ESA to investigate the Martian environment and to demonstrate new technologies paving the way for a future Mars sample return mission in the 2020's.

The ExoMars programme foresees two missions: the first, consisting of an Orbiter plus an Entry, Descent and Landing Demonstrator Module (to be launched in 2016), the second, featuring a rover, with a launch date of 2018 (see Ref.[2]). Both missions will be carried out in cooperation with Roscosmos, which will provide a Proton launcher.

Figure 3 Elements of the ExoMars programme 2016-2018, *Credit: ESA*

The first mission of the ExoMars programme, scheduled to arrive at Mars in 2016, includes:

- A Trace Gas Orbiter (see Ref. [2] for further information);
- An Entry, Descent and Landing Demonstrator Module (EDM) which will host the DREAMS package.

The main objectives of this mission are to search for evidence of methane and other trace atmospheric gases that could be signatures of active biological or geological processes and to test key technologies in preparation for ESA's contribution to subsequent missions to Mars.

The Orbiter and EDM will be launched together in January 2016 and will fly to Mars in a mated configuration. Thanks to the positioning of Earth and Mars the cruise phase can last about 9 months. Three days before reaching the atmosphere of Mars, the EDM will be ejected from the Orbiter towards the Planet. The EDM capsule will head towards its destination, entering the Martian atmosphere and finally landing. The EDM will arrive at Mars during the global dust storm season, which means that it may encounter a highly dust-loaded atmosphere.
A communication link between the EDM and the Orbiter will facilitate the real-time transmission of the most important data measured by the module. The complete set of data acquired will be transmitted to the Orbiter within 8 sols after the landing (a solar day on Mars, or sol, is 24 hours and 39 minutes). Then the EDM mission will officially end and the Orbiter will sweep through the atmosphere to reach its final science orbit. The ExoMars Entry, Descent and Landing Demonstrator Module will provide Europe with the technology for landing on the surface of Mars with a controlled landing orientation and

touchdown velocity. The design of the EDM maximizes the use of the following technologies: special material for thermal protection, a parachute system, a radar Doppler altimeter system and a final braking system controlled by liquid propulsion.

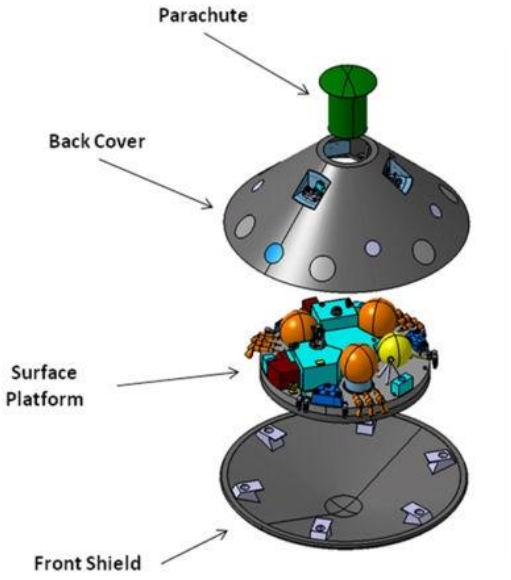

Figure 4 ExoMars EDM exploded view, *Credit: TAS-I*

One of the core scientific goals of any mission to Mars is the search for evidence of life. The best approach is to investigate the surface where the evidence may lie. That's why the EDM will also host a science package that will operate on the surface of Mars for a short duration after landing.

The EDM is expected to survive on the surface of Mars for a short time (planned to last approximately 2-8 days) by using the excess energy capacity of its batteries. The science possibilities of the EDM are limited by the absence of long term power and the fixed amount of space and resources that can be accommodated within the module; however, thanks to the scientific sensors package, will be performed useful surface science.

The EDM surface payload is based on the proposed DREAMS (Dust Characterisation, Risk Assessment, and Environment Analyser on the Martian Surface) package in which CISAS is involved. It consists of a suite of sensors to measure:

- the wind speed and direction, the sensor is MetWind
- the humidity, the sensor is MetHumi,
- the pressure, the sensor is MetBaro,
- the surface temperature, the sensor is MarsTem,
- the transparency of the atmosphere, the sensor is Optical Depth Sensor (ODS),
- the atmospheric electrification, the sensor is MicroARES.

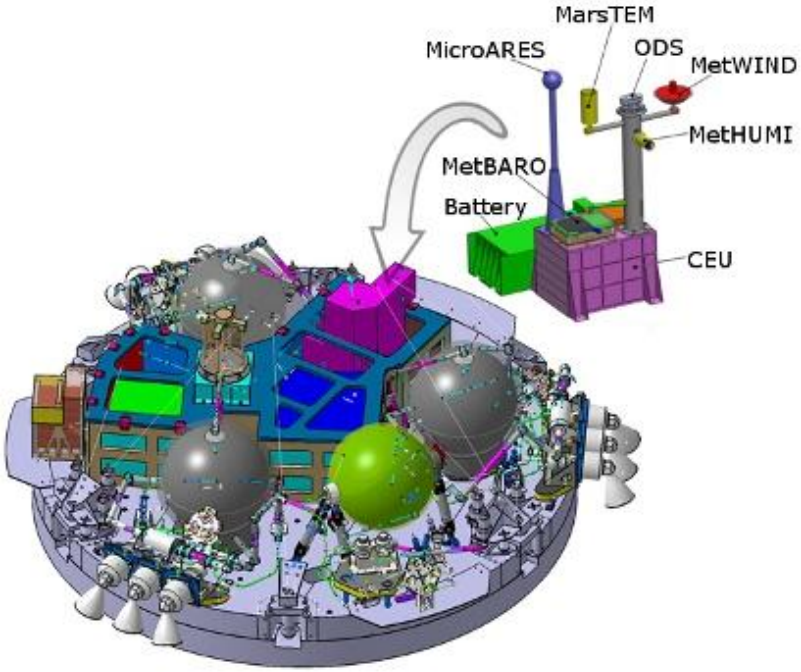

Figure 5 The science package accommodated on the ExoMars Entry, Descent and Landing Demonstrator Module surface platform, *Credit: TAS-I, DREAMS team, ESA - P. Reizi*

DREAMS will provide the first measurements of electric fields on the surface of Mars (with MicroARES). Combined with measurements (from ODS) of the concentration of atmospheric dust, DREAMS will provide new insights into the role of electric forces on dust lifting, the mechanism that initiates dust storms.
In addition, the MetHumi sensor will complement MicroARES measurements with critical data about humidity; this will enable scientists understand better the dust electrification process.

1.3.2 Objectives

In space missions the objectives are precisely formulated, defined and described in detail. It is necessary that the customer, the mission developer and the foreseen mission operator develop common understanding of the mission objectives [7].
In MISSUS project the previous subjects of interaction are reduced and unified into the team members, but anyway the starting point to begin the project was to define what shall be measured, tested and investigated; i.e. all the objectives had to be identified and listed.
It was useful to introduce a flat hierarchy into the mission objectives (e.g.: a division into primary and secondary objectives) of MISSUS experiment.
The main objectives of MISSUS experiment were distinguished into scientific and technological. The former goals are reached thanks to the latter ones.

1. The scientific goals of the experiment are:
   1.1. Environment characterization up to 20-30 km of altitude.
   1.2. Validation of the atmospheric models.
   1.3. Comparison between Earth thin atmosphere and similar planets atmospheres. In particular Mars.
   1.4. Gondola attitude and trajectory reconstruction.

2. The technical objectives of the experiment are:
   2.1. Primary:
      2.1.1. Integrated multi-sensor scientific payload design and realization.
      2.1.2. Innovative temperature sensor development.
   2.2. Secondary: Sensors system for probe impact detection

Considering the whole experiment project its concept was derived from the requirements (see paragraph 1.3.4) and constraints of the mission. The requirements of the experiment were derived from the objectives, described above.

1.3.3 The experiment

MISSUS experiment instrumentation, following DREAMS concept, has allowed to provide:

- Meteorological measurements;
- Attitude and trajectory measurements.

After the flight all sensors measurements have been cross-correlated to understand metrological behaviour and increase the accuracy of the results, based on a synergic approach.

The experiment is split up in two parts: some sensors are placed outside the gondola, on a 1.2 meter length Aluminium mast attached to the gondola rails, for the meteorological measurements; the other sensors are placed inside the gondola, facing the external side. Inside the gondola are placed also the electronics, which controls the sensors by acquisition and conditioning boards, manages the power supply and activates heaters; the batteries and the PC104, for the data-sampling, data-handling and transmission to ground station. Power supply for all the sensors is provided by the batteries through the electronics.

The experiment is provided with the following sensors:

- An innovative resistance temperature sensors - MarsTem prototype (fine RTD), placed on the tip of the external mast, on a Aluminium support, in order to get the temperature of the external environment as a function of the altitude;

- A RTD commercial temperature sensor (coarse RTD), used as reference sensor for the innovative temperature sensor and for redundancy reasons; placed near to the innovative temperature sensors;
- A humidity sensor, placed on the mast, used for the measurement of humidity during the ascending and descending phases;
- Two USB camera in order to monitor the experiment (e.g. to assess the position of the Sun by the observation of the shadows) and for public outreach contribution;
- A fluxgate tri-axial magnetometer for the measurement of Earth magnetic field; placed on the mast, far from the gondola in order to minimize spurious effects due to the magnetic field of the gondola and its subsystems: it gives a contribution to completely reconstruct the gondola attitude;
- An absolute pressure sensor, placed inside the gondola, near to the electronics, to get the absolute pressure as a function of the altitude;
- A differential pressure sensor, placed inside the gondola, and connected to the external Pitot tube, placed on the tip of the mast, in order to obtain the descending velocity measurements by the measure of the differential pressure;
- An IMU, provided with GPS receiver, in order to reconstruct the gondola attitude and trajectory;
- A tri-axial accelerometer, specific for shock measurements.

Combining the signals provided by the tri-axial accelerometer, which detects probe impact, and the absolute pressure sensor, a cut away sensor system has been developed to detect the probe impact with the ground. It's important to demonstrate the feasibility of this system since one of the most critical issues in stratospheric balloon missions is the separation of the payload from the parachute after probe landing, considering that parachute may drag the payload for long distances before being recovered, with consequent damage of the instrumentation. The absolute pressure sensor signal is fundamental to measure absolute pressure on ground, avoiding accidental separation during the flight (e.g. when parachute is deployed).

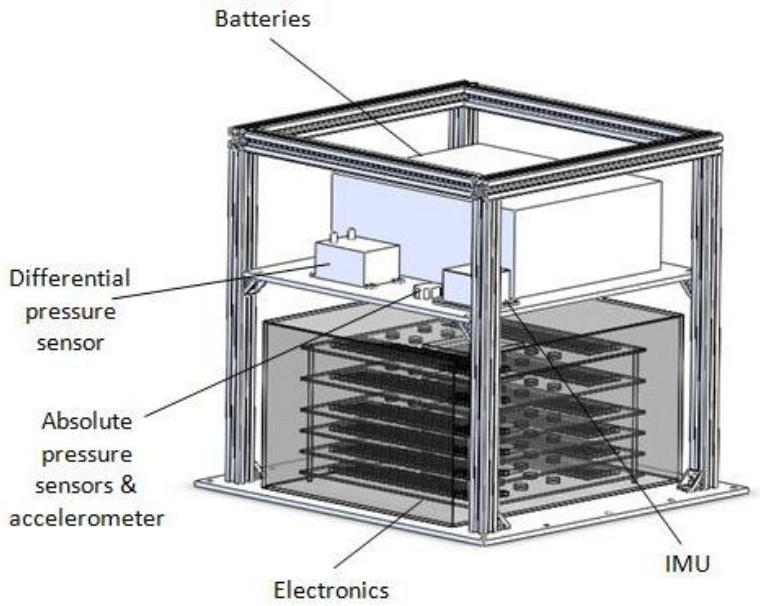

Figure 6 Layout of internal part of MISSUS experiment, placed inside the gondola

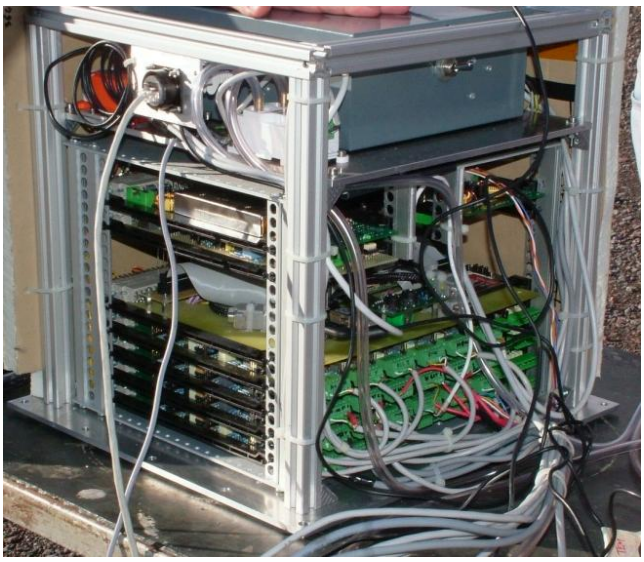

Figure 7 Internal part of MISSUS experiment

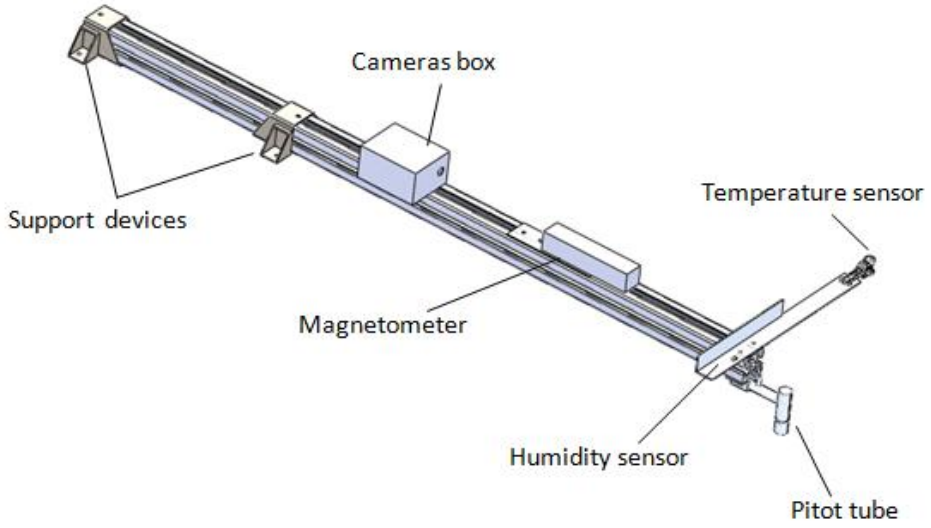

Figure 8 Layout of external part of the experiment, fixed on the gondola and exposed to the atmosphere

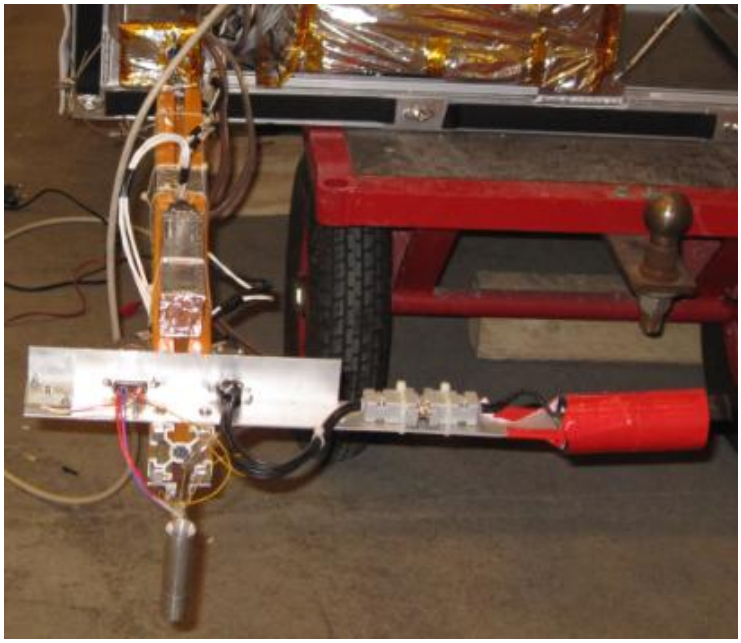

Figure 9 External boom fixed on the gondola; the temperature sensor is protected by the red cylindrical shield

1.3.3.1 Configuration

The structure of MISSUS experiment consists of two main parts: an edged box and a cantilever boom. The box (380x360x364) mm^3 is placed into the gondola, close to its external side, in order to be easily accessible and close to the boom. It has a bottom plate (4

mm thick), on which electronics rack is placed, and another support plate (placed 240 mm above the bottom one), which hosts most of the internal components: the batteries box, the absolute pressure sensor, the relative pressure sensor, the accelerometer, and the IMU. The boom is a 1.2 meter long Bosch profile fixed to the bottom of the box through a support frame; it supports the external sensors: the temperature sensors, the humidity sensor, the magnetometer, the Pitot tube and the cameras. The aim of the boom is to allow to the external sensors to operate as far as possible from the gondola that represents a significant perturbing source for almost all the atmospheric parameters to be measured.

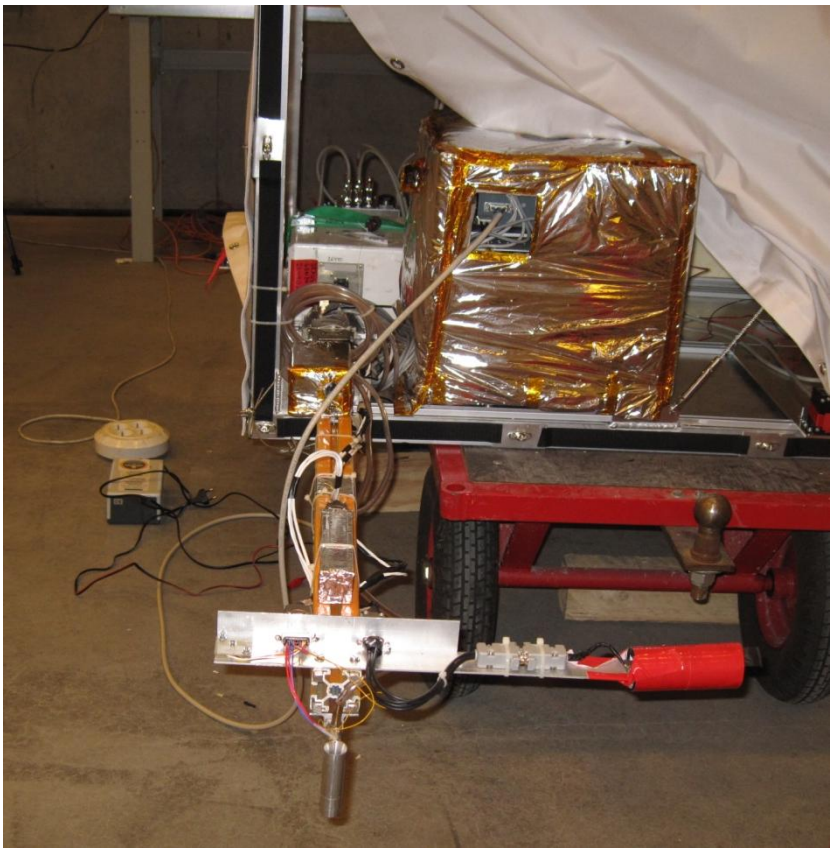

Figure 10 MISSUS experiment placed on BX15 gondola

A housekeeping system (e.g. additional temperature sensor) and active thermal control system are used for monitoring and controlling the experiment respectively.

Data conditioning and telemetry subsystem collects data coming from sensors to send part of them to the ground through the E-link unit, while the whole data volume is stored in a solid state memory.

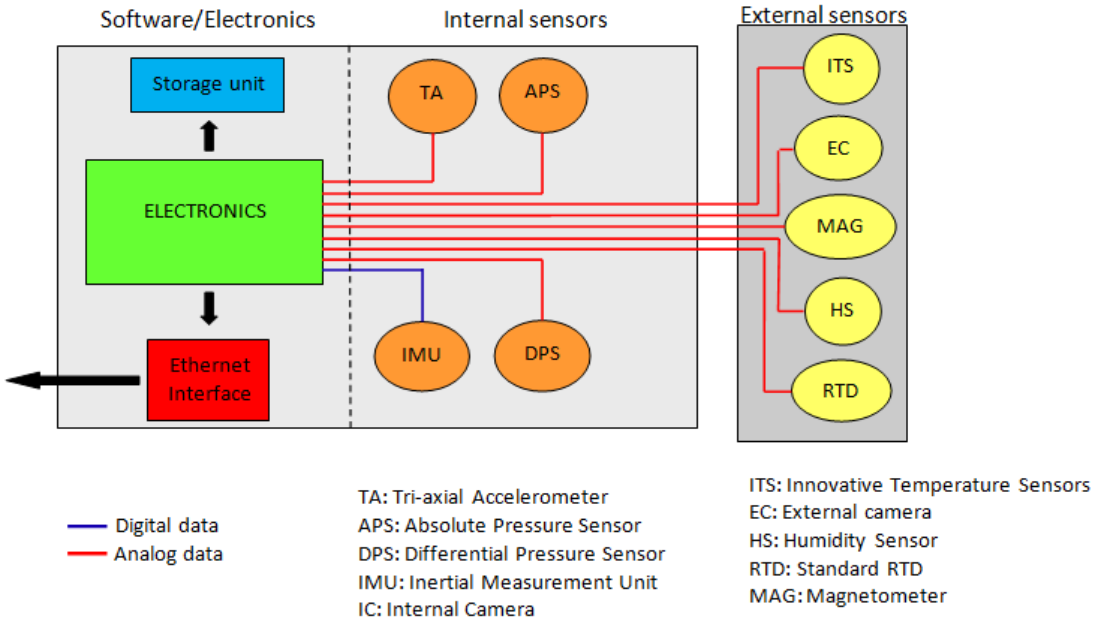

Figure 11 MISSUS setup

1.3.3.2 Sensors on board

1.3.3.2.1 Innovative RTD Sensor

The sensor is a platinum resistance thermometer with a thin platinum wire wrapped around a PEEK support.

To measure the fast temperature fluctuations that characterize a thin atmosphere, a sensor based on the RTD principle has been chosen. The platinum RTD signal is characterized by a high linearity, which allows, together with the high stability, a good reproducibility even though significant variations of the operative conditions occur. The physical behavior of the platinum sensors is well-known because they are widely used in scientific applications; moreover the International Scale of Measure of 1990 is based on measures provided by this type of RTD.

In addition the sensor is characterized by large dimensions w.r.t. thermocouples: resistive elements are wider, directly exposed to the flux and less sensitive to local perturbing effects (e.g. a dust grain on a thermocouple could affect the measurement process due to the very low exchange area of the sensor).

The chosen geometric configuration is represented in the following figures and derives from CISAS previous experience.

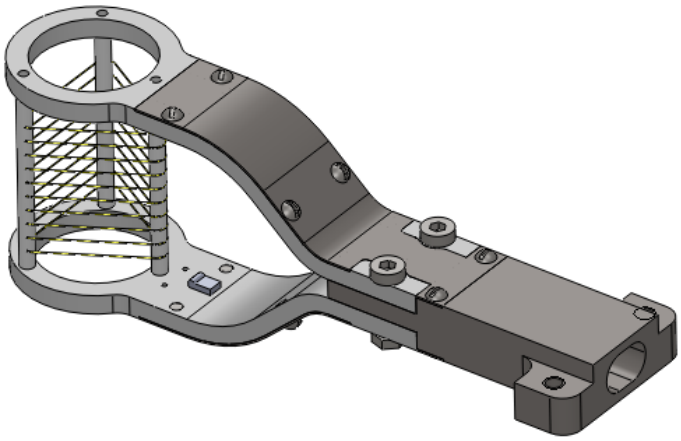

Figure 12 RTD Sensor layout

The main structure consists of two titanium arms internally hollowed in order to accommodate and shield the electric cables.
At the tips of the arms two rings support 3 PEEK bars (450GL30) and the platinum sensitive wires are wrapped around them and fixed thanks to glue. The edges of the structure are smoothed, in order to reduce fluid perturbations due to the stem. Two holes per ring allow the connection between the sensitive platinum wire with the internal electric cables.
Thanks to the platinum net, the exchange surface between the wire itself and the air flux is maximized.
Conductive thermal exchange between sensitive element and Titanium structure is considered negligible thanks to the PEEK insulating properties.
The PEEK polymer is characterized by excellent resistance, rigidity and dimensional stability at temperature extremes; gamma rays resistance and high wear resistance without the need for lubrication; it is chemically resistant and insoluble in all common solvents including acids, salts and oils. Moreover PEEK is a good electrical insulator.

The following figures show the cables and the electrical interconnections.

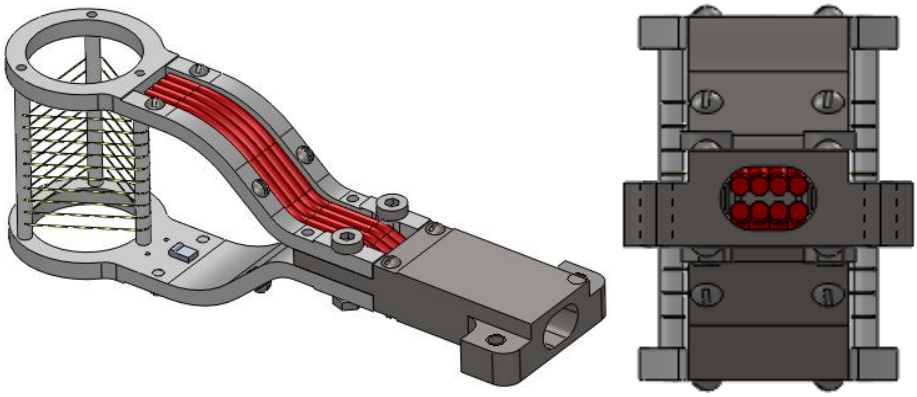

Figure 13 RTD cable position

Figure 14 Sensor's components compared with a euro coin (left), assembling of the RTD Sensor (right)

1.3.3.2.2 Commercial RTD sensor

The coarse RTD temperature sensor is a commercial Pt100. This sensor (Discoil™ thermal-ribbon, response time: 0.15 s, accuracy: ±0.01°C) has been used for redundancy reasons and as a reference for the measurements provided by the fine sensor. The following figure shows the commercial sensor position.

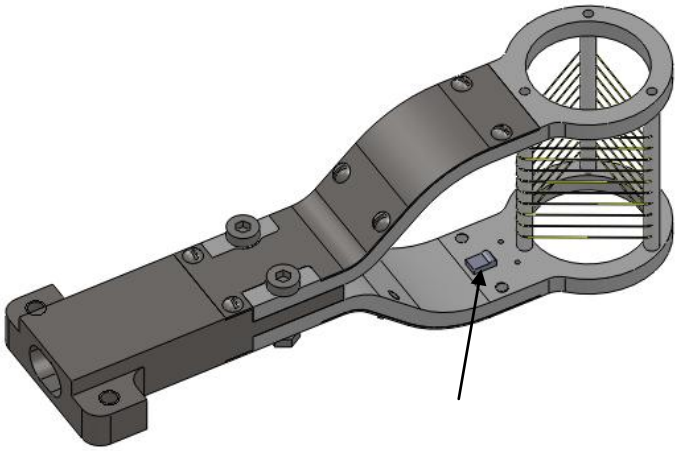

Figure 15 Commercial RTD Sensor position

1.3.3.2.3 Humidity sensor

The relative humidity sensor is a HIH-4000 Series. It is a laser trimmed, thermo-set polymer capacitive sensing element with on-chip integrated signal conditioning.

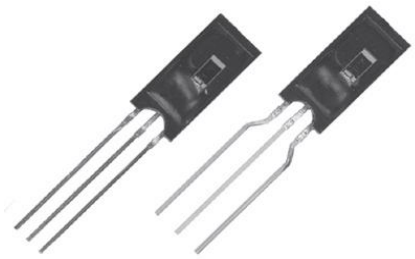

Figure 16 Humidity sensor

Among its main features the instrument has a low power consumption and a high accuracy. This kind of sensor is usually adopted for metrological measurements.
In the tables below are reported the principal characteristics of the instrument:

Supply voltage	5 Vdc
Operative temperature	-40°C to +85°C
Measurement Range	0-100 % RH
Accuracy	±3.5 % RH
Response time	5.0 s

Table 1 Humidity sensor specifications

1.3.3.2.4 Magnetometer

A tri-axial magnetometer (Bartington Mag-03MS1000) is used for the measurements for the Earth magnetic field outside the gondola.
This sensor with integral electronics provides measurements of static and alternating magnetic fields in three axes; it converts magnetic flux density measured in three axes, into a bipolar analog voltage.
Analog output voltages Vx, Vy and Vz are linearly proportional to the flux density. Three fluxgate sensing elements are mounted orthogonally at one end of an enclosure, which also contains the electronic circuitry.

Figure 17 Fluxgate magnetometer

Each axis produces an analog output V_a in response to flux density B in the relationship:

$$V_a = B \cdot \cos\theta$$

where θ is the angle between the flux direction and the direction of the individual sensing element. The scalar value of the magnetic field may be computed from the individual X, Y and Z vector components using the following relation:

$$B = \left(V_x^2 + V_y^2 + V_z^2\right)^{\frac{1}{2}}$$

The following table shows the main properties of the instrument:

Supply voltage	±12 V
Measuring range	±100 μT
Operative temperature	-40°C to +70°C
Linearity error	<0.0015%

Table 2 Magnetometer specification

1.3.3.2.5 Absolute pressure sensor

The absolute pressure sensor is a Freescale MPX-2200 series. This is a silicon piezoresistive sensor providing a highly accurate and linear voltage output, directly proportional to the applied pressure.

Figure 18 Absolute pressure sensor

The sensor is a single, monolithic silicon diaphragm with the strain gauge and a thin–film resistor network integrated on–chip. The chip is laser trimmed for precise span and offset calibration and temperature compensation.
These are the principal characteristics of the instrument:

Supply voltage	12 Vdc
Supply current	9 mA

Temperature range	-40°C to 125°C
Measurement Range	0-200 kPa
Sensitivity	0.2 mV/kPa
Linearity error	±1% V_{fss}

Table 3 Absolute pressure sensor specifications

1.3.3.2.6 Differential pressure sensor

The Differential Pressure Transmitter is a Vaisala PDT10. It is the sensing element of the Pitot tube. It offers high accuracy and sensitivity. The sensor also uses a micro-machined, ultra-thin silicon diaphragm which provides inherent sensor repeatability and stability.

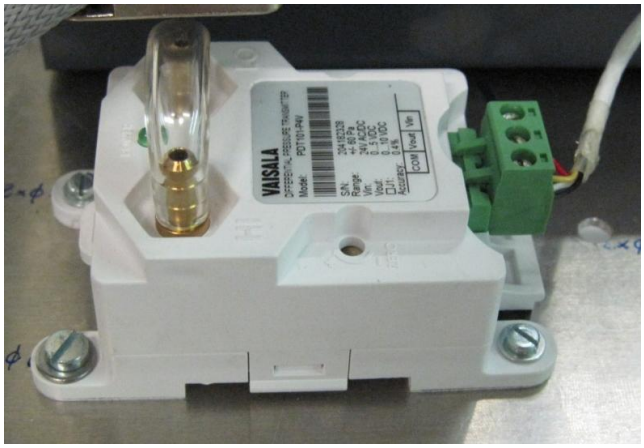

Figure 19 Differential pressure sensor

These are the principal characteristics of the sensor:

Supply voltage	12 V
Supply current	22 mA
Temperature range	-18°C to +70°C
Measurement Range	±60 Pa
Accuracy	0.4% span

Table 4 Differential pressure sensor specifications

Combining relative pressure obtained by this sensor and air density (achievable by atmospheric models) through the Bernoulli law, a new Pitot tube configuration has been developed in order to estimate the flow velocity, compensating possible issues arising from misalignment between total pressure axes and flow direction.
Flow speed can be measured connecting the total and the static hold to the differential pressure transducer.

$$U_M = k\sqrt{\frac{2(p_{tot} - p_{st})}{\rho}}$$

The ideal correlation considers an ideal fluid and a potential motion; this has been modified for the real case introducing an experimental coefficient *k*. The coefficient *k* has been experimentally estimated through the calibration procedure.

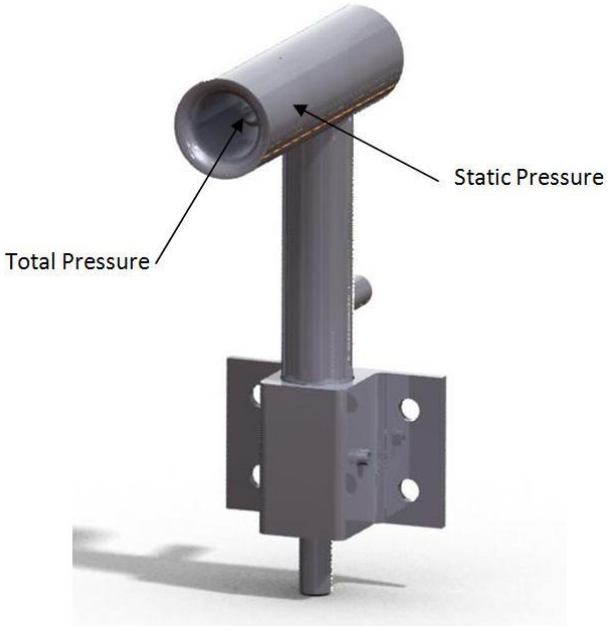

Figure 20 Pitot tube assembly

1.3.3.2.7 IMU

The IMU is a XSENS MTi-G miniature size and low weight 6DOF Attitude and Heading Reference System (AHRS). It is necessary for the reconstruction of the trajectory and the attitude of the gondola.

The selected IMU contains accelerometers, gyroscopes, magnetometers in 3D, an integrated GPS receiver, a static pressure sensor and temperature sensor.

Figure 21 IMU

Its internal low-power signal processor provides real time and drift-free 3D orientation as well as calibrated 3D acceleration, 3D rate of turn, 3D earth-magnetic field, 3D position and 3D velocity data.
In table below are reported the principal characteristics of the instrument:

Supply voltage	5 V
Power consumption	+610 mW to +910 mW
Temperature range	-40°C to +85°C
Full Scale	Rate of turn ±300 deg/s Acceleration ±50 m/s^2 Magnetic field ±750 mGauss Static Pressure 30 to 120 kPa
Linearity error	Rate of turn 0.1% FS Acceleration 0.2% FS Magnetic field 0.2% FS Static Pressure 0.5% FS

Table 5 IMU specifications

1.3.3.2.8 Tri-axial accelerometer

The tri-axial accelerometer is a Dytran7523A5 piezoelectric accelerometer. It has a wider bandwidth than those inside the IMU and it was selected mainly for an accurate detection of the shock due to the impact with the ground and also for redundancy.

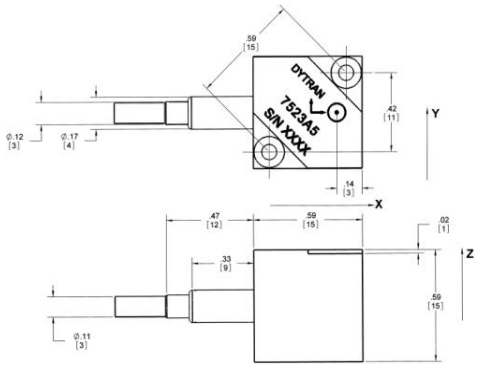

Figure 22 Tri-axial accelerometer

The sensor contains elements that are subjected to strain under acceleration-induced loads. This strain displaces electrical charges within the elements and charges accumulate on opposing electrodes surfaces.

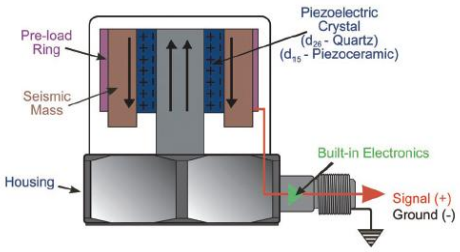

Figure 23 Tri-axial accelerometer working principle

In the table the main characteristics of this sensor are reported:

Range	±50 g
Supply voltage	5 VDC
Supply current	0.5 mA
Operative temperature	-55°C to 125°C
Maximum Mechanical Shock	5000 g
Sensitivity	22 mV/g
Linearity error	0.3%

Table 6 Tri-axial accelerometer specifications

This sensor is related to the cut away sensor system (see beginning of paragraph 1.3.3): it consists in the combination of the data achievable by this accelerometer and the absolute pressure sensor through an *AND* logical operator. In this way it is possible to recognize the desired shock avoiding the provision of the expected signal due to any possible high shock occurring during the cruise phase (for example when the parachute is deployed). It is a system of sensors that provides only a signal in order to validate the technology: no actuator will be present (e.g. pyro).

1.3.4 Requirements

In order to achieve the objectives (see paragraph 1.3.2) the experiment has to have specific functionalities, which will be performed to the desired standard by means of the technical design, which is operated during the flight.
Before starting the detailed experiment design the requirements need to be determined.
After having analyze the experiment objectives the requirements were listed, in a iterative process during the different milestones of the project.
Requirements are “something that will be done” and they can be defined as the practical translation of the objectives and how to achieve them. They identify the right path and the wrong path of the experiment.

Depending on the constraints each requirement shall, should or may be done; the verbs clearly indicate a decreasing scale of binding conditions.
After finishing the design of the experiment, all requirements were checked to verify whether they were fulfilled. This process is called verification and it has been done in the Test phase.

Following the ECSS-E-ST-10C [6] the differing types of technical requirements for a space mission to be fulfilled are as follows:

- functional requirements,
- mission requirements,
- interface requirements,
- environmental requirements,
- operational requirements,
- human factor requirements,
- (integrated) logistics support requirements,
- physical requirements,
- product assurance (PA) induced requirements,
- configuration requirements,
- design requirements,
- verification requirements.

BEXUS can be considered a small students space mission, for this reason the requirements above are reduced to four main categories:

- Functional Requirements
- Performance Requirements
- Design Requirements
- Operational Requirements

1.3.4.1 Functional Requirements

Functional requirements define what the product shall perform, in order to conform to the needs/mission statement or requirements of the user. In particular for BEXUS they define the functionality that the experiment needs to have or the tasks it needs to fulfil in order to achieve the experiment objectives.

MISSUS had to fulfil the following requirements:

The experiment shall:

F.1.	Characterize the external environment up to 20-30 km

F.1.1.	Measure external temperature by means of an innovative RTD sensor during the whole flight
F.1.2.	Measure external temperature by means of a commercial RTD sensor during the whole flight
F.1.3.	Measure environment absolute pressure during the whole flight
F.1.4.	Measure humidity during ascending and descending phases
F.1.5.	Provide descending velocity by means of a Pitot tube
F.2.	Reconstruct gondola attitude and trajectory by means of a tri-axial magnetometer and an IMU during the whole flight
F.3.	Detect probe impact with ground
F.3.1.	Detect shocks by means of a tri-axial accelerometer
F.3.2.	Measure atmospheric pressure
F.4.	Store data
F.4.1	Collect sensors data during the whole flight
F.4.2	Record videos during the whole flight
F.5.	Provide telemetry packages during the whole flight
F.6.	Calibrate the innovative temperature sensors by means of ITS90 normative
F.7.	Calibrate the Pitot tube

Table 7 MISSUS Functional requirements

1.3.4.2 Performance Requirements

Performance requirements quantify to what level the functional requirements will be fulfilled. In the case of measurements, they typically define the range, the precision and the frequency.

They define how good the function will be fulfilled, i.e. the quality of the experiment. For MISSUS experiment each performance requirement is in response to a precise functional requirement, described in the previous paragraph.

Response to F.1

P.1.1.	Measure the temperature outside the gondola in the range -90°C up to +20°C
P.1.2.	Measure the temperature outside the gondola by means of the innovative RTD sensors with accuracy better than ±0.1°C
P.1.3.	Sample the temperature by means of the innovative temperature sensors with a frequency of 256 Hz
P.1.4.	Measure the temperature outside the gondola by means of the innovative RTD sensors with a response time lower than 0.04 s
P.1.5.	Measure the temperature outside the gondola by means of a commercial RTD

	sensor with accuracy better than ±0.1°C
P.1.6.	Sample the temperature by means of a commercial RTD sensor with a frequency of 256 Hz
P.1.7.	Measure the absolute pressure outside the gondola from 6 mbar up to 1.5 bar
P.1.8.	Measure the absolute pressure outside the gondola (from 30000 Pa up to 100000 Pa) with accuracy better than ± 500 Pa
P.1.9.	Sample the absolute pressure outside the gondola with a frequency of 256 Hz
P.1.10.	Measure differential pressure in the range -60 to +60 Pa
P.1.11.	Measure differential pressure with accuracy better than 0.24 Pa
P.1.12.	Sample differential pressure with a frequency of 256 Hz
P.1.13.	Measure relative humidity outside the gondola in the range 0 to 100%
P.1.14.	Measure relative humidity with accuracy better than 3.5%
P.1.15.	Sample relative humidity with a frequency of 256 Hz
P.1.16.	Measure relative humidity with a response time of 5 s

Table 8 MISSUS Performance requirements in response to F.1

Response to F.2

P.2.1.	Measure Earth magnetic field by means of the external magnetometer with accuracy better than ±0.0015 μT
P.2.2.	Sample Earth magnetic field by means of the external magnetometer with a frequency of 256 Hz
P.2.3.	Measure gondola internal magnetic field with accuracy of ±0.15 μT
P.2.4.	Collect data of internal magnetic field with a response time of 0.1 s
P.2.5.	Measure acceleration in the range ±50 g
P.2.6.	Measure acceleration with accuracy of ±0.1 g
P.2.7.	Collected data of acceleration with a response time of 35 ms
P.2.8.	Measure rate of turn in the range ±300 deg/s
P.2.9.	Measure rate of turn with accuracy of 0.3 deg/s
P.2.10.	Collected data of turn with a response time of 25 ms
P.2.11.	Collected GPS data every 250 ms

Table 9 MISSUS Performance requirements in response to F.2

Response to F.3

P.3.1.	Measure acceleration in the range -50 up to 50 g
P.3.2.	Sample acceleration with a frequency of 1024 Hz
P.3.3.	Measure the absolute pressure outside the gondola in the range 0 kPa up to 200 kPa
P.3.4.	Measure the absolute pressure outside the gondola with accuracy better than ± 500 Pa

P.3.5.	Sample the absolute pressure outside the gondola with a frequency of 256 Hz

Table 10 MISSUS Performance requirements in response to F.3

Response to F.4

P.4.	Store a total data volume lower than 32 GiB

Table 11 MISSUS Performance requirements in response to F.4

Response to F.5

P.5.	Transmit data with a data rate from 60 to 100 kbit/s

Table 12 MISSUS Performance requirements in response to F.5

1.3.4.3 Design Requirements

Design requirements define all design (system engineering) aspects that the experiment needs to fulfil in order to achieve the experiment objectives, they document the limits to take into account. While functional requirements and performance requirements originate from the experiment team, design requirements can come from other sources, such as:

- the flight environment (e.g. the need to withstand mechanical and thermal stress)
- the launch vehicle (e.g. certain components may be forbidden)
- legal limitations (e.g. frequency allocation)
- safety restrictions (e.g. high voltage or ionisation)

An important subset of design requirements are the interface requirements, which determine that the mechanical and electrical interfaces to the launch vehicle are correct.
The following table provides the list of MISSUS design requirements. The main design constraints considered are on the whole experiment, on the electronics and on the software (onboard and GSE).

The experiment shall:

D.1.	Have a structure able to outstand a maximum vertical static load of -10 g
D.2.	Have a structure able to outstand a maximum horizontal load of +/-5 g
D.3.	Have a structure able to outstand low frequency vibration loads expected during flight (BEXUS13 flight data have been taken as reference)
D.4.	Operate in the temperature profile from -90°C up to +50°C
D.5.	Operate in environment from 1 bar down to 5 mbar
D.6.	Have rechargeable batteries able to provide power supply for a duration of 8 hours
D.7.	Have batteries placed close to the accessible side of the experiment and easy to be removed and substituted
D.8.	Be easily and quickly accessible from the outside

D.9.	Have batteries separated from the electronics and enclosed in a security box
D.10.	Be equipped with passive thermal control systems (such as MLI, insulating materials, coatings with appropriate thermal-optical properties)
D.11.	Be equipped with active thermal control systems (heaters) able to guarantee the operative range of the components
D.12.	Be equipped with heaters in order to avoid ice formation on the Pitot tube
D.13.	Have active thermal control system electrically insulated from the rest of the electronics
D.14.	Have shielded electrical components
D.15.	Keep an always powered-on RTC

Table 13 MISSUS Experiment design requirements

The electronics shall:

D.16.	Operate from -30°C up to +50°C
D.17.	Operate for 8 hours continuously
D.18.	Not generate EM interferences
D.19.	Be subjected to voltages lower than 50 V
D.20.	Not overheat
D.21.	Not have digital – analog interferences between the 2 different circuits
D.22.	Have a noise lower than 100 µV in the conversion stage
D.23.	Have a power supply able to provide 5 V, ±15 V
D.24.	Be connected to the E-link system by means of the umbilical connector
D.25.	Have a shielding system to be connected to gondola power system ground
D.26.	Be equipped with leds to monitor status (e.g. power supply)
D.27.	Guarantee the protection of data on SSD after landing

Table 14 MISSUS Electronics design requirements

The onboard software shall:

D.28.	Be compliant with IEEE 802.3 and with TCP/IP specifications
D.29.	Not fail in case of connection error
D.30.	Record all the samples
D.31.	Preserve recorded data integrity
D.32.	Restart in case of failure
D.33.	Be compatible with hardware
D.34.	Be compatible with ext file-system
D.35.	Continue to work in case of failure of some devices
D.36.	Allow GSE to monitor power supply from remote

D.37.	Send a subset of sampled data to the GSE
D.38.	Not be crashed by GSE errors
D.39.	Not be damaged or lose previously recorded data (on SSD) after an unexpected power loss
D.40.	Allow remote storage management

Table 15 MISSUS onboard software design requirements

The GSE shall:

D.41.	Log and display received data
D.42.	Allow users to send commands to the onboard software

Table 16 MISSUS GSE design requirements

The experiment should:

D.43.	Have a structure inside the gondola with a maximum volume of 51 dm^3.
D.44.	Have an external mast of 1.2 m length.
D.45.	Have a maximum internal total mass of 15.0 kg.
D.46.	Have a maximum external total mass of 3 kg.

Table 17 MISSUS Experiments design requirements less binding

1.3.4.4 Operational Requirements

Operational requirements are related to the system operability, they define what the experiment has to fulfil to be handled and operated safely and reliably. Operation not only refers to operation during flight but also to the handling of the experiment prior and after flight. Some of the operational requirements are related to experiment safety.
The following table reports the operational requirements the experiment shall and should fulfil.

The experiment shall:

O.1.	Fly with sun light
O.2.	Be rotated 360° around the vertical axis and shifted by 30° from the vertical axis before launch
O.3.	Collect measurements automatically during flight
O.4.	Accept a request for radio silence before launch
O.5.	Be able to be switched on and off from ground segment
O.6.	Be able to modify the operational sequence from the ground segment
O.7.	Have a test operational sequence to be activated before the launch as last check

Table 18 MISSUS Experiments operational requirements

The experiment should:

O.8.	Switch ON and switch OFF sensors with a switch ON time of 30 s and a switch OFF time of 1ms

Table 19 MISSUS Experiments operational requirements less binding

Chapter 2

Project Management

2.1 Project Planning

Project planning and its implementation includes all the processes and activities required in order to plan and execute a project. Programming shall consider all levels and stages of development, from beginning to completion, in a coordinated, efficient and structured manner.

The inputs of this activity come from all the project disciplines, moreover it is necessary a close co-operation across the different fields involved.

The design and development of the MISSUS experiment required a preliminary starting Project planning to organize all the expected activities.

We can summarize the main objectives of this task with four big questions that have to be answered:

- What must we achieve?
- What are the resources?
- How long have we got?
- What are the risks?

In the following paragraphs each question will be clarified with the explanation of the work performed and the procedure adopted to plan the project of the experiment. For what concern the risk management a specific paragraph has been considered to analyze the matter in detail.

2.1.1 Identification of the different work areas

The answer to the first question is the identification of all the tasks and subtasks necessary to achieve MISSUS experiment.

To do this the different work packages of the project were identified defining a work breakdown structure.

The WBS decomposes the project into smaller components, the work packages (WP). It defines and groups the discrete work elements in a way that helps to:

- Identify the tasks and responsibilities of each actor;
- Facilitate the coherence between all activities of the whole project;
- Perform scheduling and costing activities [9].

The WP breakdown of MISSUS was made by the required activities during the BEXUS program (100% of the whole project), from the proposal to the post flight analysis at University.
No scheduling information is present in the WBS, in fact the WP can be carry out at the same time by different team members or in subsequent periods during the year.
A preliminary split up of the work, shown by Figure 24, considered six packages:

1. Project management
2. System engineering
3. Experiment design
4. Test activity
5. Operation
6. Data analysis

The lowest level boxes show the tasks that have been allocated to either individual team members or working groups [4].
The WPs of management, system engineering, experiment subsystems and data analysis provide a division into sub-teams to assure each team member work in their field of studies, according to their personal attitude and skills. All the team is involved for the test activity and the operational phase.
During the development of the project was better to divide the work further and add other WPs with their responsible, the division provided nine packages:

1. Project management
2. System engineering
3. Experiment design:
    a. Mechanical design
    b. Thermal design
    c. New sensors design
    d. Electric & electronics design
    e. Software design
4. Procurement
5. Assembling
6. Calibration
7. Testing
8. Operational phase
9. Data analysis

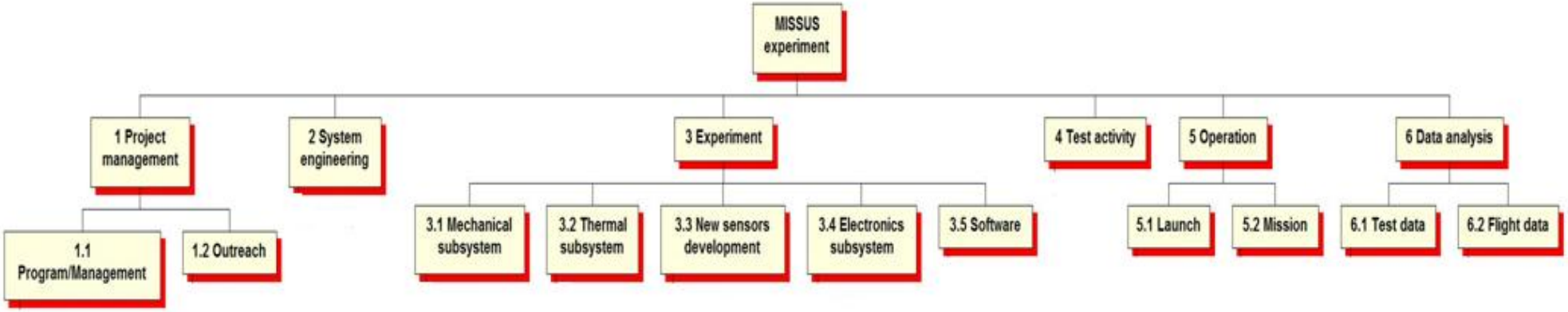

Figure 24 Work Breakdown Structure

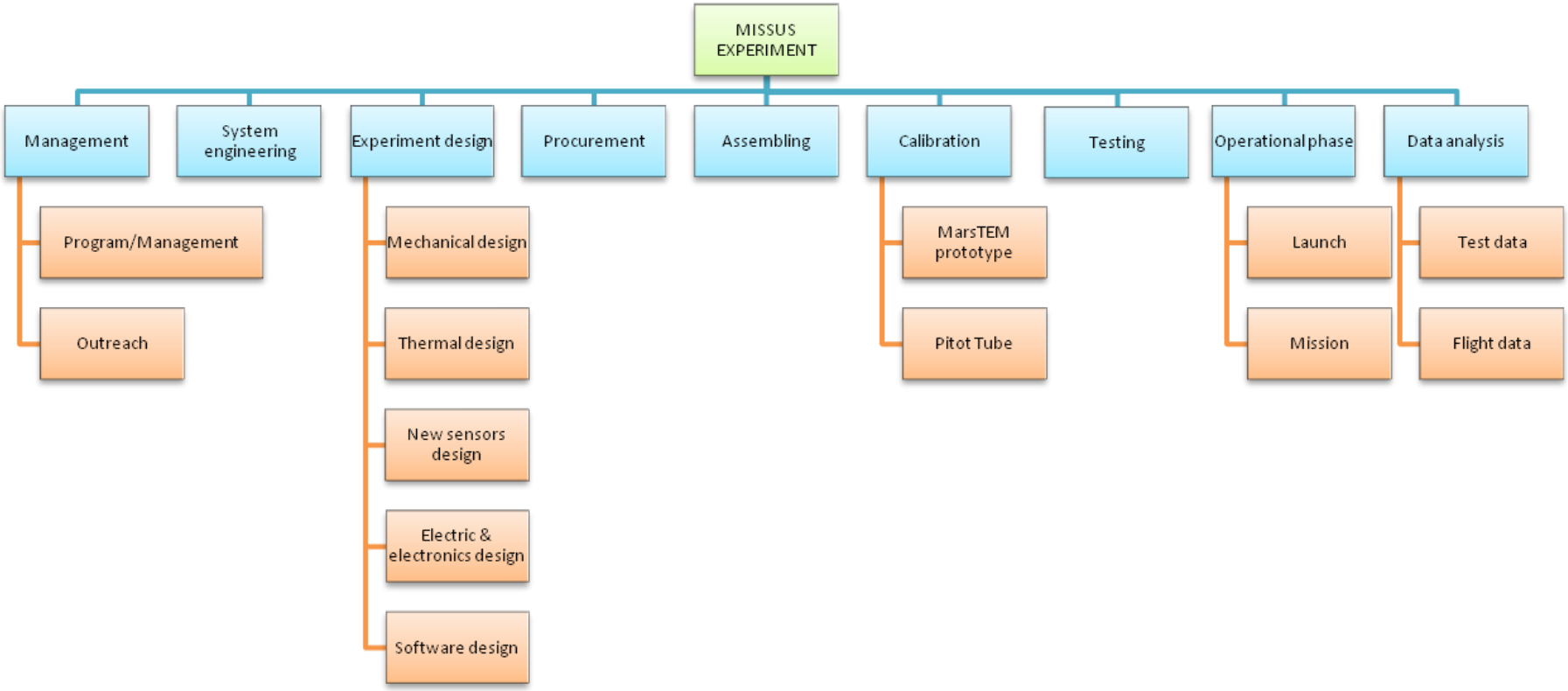

Figure 25 Work Breakdown Structure updated

The additional packages were procurement, assembling and calibration. The procurement involved almost all purchasing decisions include factors such as delivery and handling, comparison between offers and best possible cost of the components; so it needed a specific responsible. Also the assembling was committed to a responsible to better organize the practical building of the experiment.
It was necessary to point out also the calibration, since it is a fundamental activity to have correct reference measurements for the custom sensors (MarsTem, Pitot Tube) on board the experiment.

2.1.2 Analysis of the resources available

Once the tasks have been identified the resources available must be analyzed, this is the answer to the second question of the project planning. The resources for the project comprehend:

- the team
- the funding
- the support
- the facilities

Facilities were provided by University and the team had access to laboratory and workshop for the realization and the integration of mechanical and electric/electronic parts of the experiment; concerning the test activity, the team had access to CISAS facilities, for testing components, sensors and units in thermal-vacuum chamber.
The human and economic resources required to be studied in detail.

2.1.2.1 Human resources

The human resources available include the members of the team and their related expertise and skills, University support staff, coordinators and external partners.
After having identified the different work packages is possible to distribute them inside the team and looking for other team members or external help if there are no resources available. In particular this happened at the very beginning of the project where in the team were not present software and electronic members.
Except for the operational phase, each work package must be assigned to a primary responsible helped by a second/vice responsible of the team and if necessary supported by external members such as University professors, researchers, technicians, etc.
MISSUS Team is composed of ten students: one of them is PhD Student in Sciences, Technologies and Measurements for Space at CISAS, four of them are Master students of

"Aerospace Engineering", three of them are Bachelor students of "Aerospace Engineering", two of them are Bachelor students of "Information Engineering".
Since the human resources were those described above and the team was already quite big, has been decided to split up the work areas among the members available without adding other members.
External support was required where there was a lack in the expertise and skills. In particular the Electronics and Software area needed external support since the responsibles were both Bachelor students.
The following table provides the work division of the project. The members of the team have been indicated with their ongoing level of study:

- PhD: PhD Student in Sciences, Technologies and Measurements for Space at CISAS;
- Master AS: Master student of "Aerospace Engineering";
- Bachelor AS: Bachelor student of "Aerospace Engineering";
- Bachelor I: Bachelor student of "Information Engineering".

The capital letters in parenthesis (from A to J) represent the members of the team.

Task	Responsible	Second responsible	External support
Management	Master AS (A)	PhD (F)	
Outreach	Bachelor AS (G)	Master AS (A)	
System engineering	PhD (F)	Master AS (J)	
Mechanical design	Master AS (I)	Bachelor AS (H)	
Innovative RTD design & calibration	Master AS (J)	Bachelor AS (C)	CISAS researcher
Custom Pitot tube probe design & calibration	Master AS (E)	Bachelor AS (G)	Professor (wind gallery resp.)
Thermal design	2 Bachelors AS (C) (H)	Bachelor AS (G)	
Electronics	Bachelor I (D)	Bachelor I (B)	Electronic engineer
Software	Bachelor I (B)	Bachelor I (D)	CISAS researcher PhD
Procurement	Master AS (A)	PhD (F)	

Assembling	Master AS (I)	2 Masters AS (E)	
Test activity	PhD (F)	2 Masters AS (A) (J)	Lab. technicians
Data analysis	Master AS (E)	Master AS (A)	CISAS researchers

Table 20 Work division

Moreover at the beginning of the project, indeed more in detail after the preliminary phase, every team member gave his/her availability to the design and development of MISSUS. The following table provides the availability hours initially planned for each member (A to J).

Periods	Availability (hours per week)									
	A	B	C	D	E	F	G	H	I	J
II Semester (2011-2012) 5th March – 17th June	10-15	10-20	10+	10-20	10-15	10-15	10+	5-10	10-15	10-15
Exams Period 18th June – 15th July	10-15	10-15	5-10	10-15	10-15	10-20	5-10	5-10	10-15	10-15
Summer holiday 16th July – 19th August	20+	20+	20+	20+	20+	20+	20+	20+	20+	20+
Recovery Exams Period 20th August – 22nd Septem.	15-20	15-20	5-10	15-20	15-20	15+	5-10	5-10	15-20	10-15
I Semester (2012-2013) 1st October – 30th January	10-15	5-10	5-10	1-5	10-15	10-15	5-10	1-5	1-5	5-10

Table 21 Team members availability

2.1.2.2 Economic resources

The economic resources available include the funding provided by institutional bodies and sponsors. In particular for the project there were involved:

- University, in particular for workshop and facilities utilization;
- CISAS;
- ESA which sponsored four team members (travel costs);
- Private local companies interested in supporting the project;
- Cultural association/Charity interested in promote the scientific knowledge.

The analysis of economic resources is essential for the development of the project and even more the distribution of the cost during the different phases of progressing.

A preliminary estimation of the costs has been provided to establish the economic resources required to achieve MISSUS, even if the resources at first were not totally available.

The price breakdown form 1 (see Appendix) is a preliminary estimation of the expected costs of the experiment at the beginning of the project. In this budget the travel costs of the team are not included, while are considered:

- Direct cost,
- Machining,
- Funding.

The cost of the sensors are the real prices of the items available on the market.
The costs of materials and machining were estimated taking into account previous missions and balloon flights. In particular the cost estimation of the components for the custom sensors was assumed as hypothesis since the design was still not frozen at that stage.

The following table shows the components already available at CISAS, so for these sensors no economic resources are considered.

Available at CISAS	**Quantity**
Magnetometer	1
IMU	1
Camera	2
Absolute pressure sensor	1

Table 22 Components availability

As can be seen from the breakdown form the very preliminary design of the experiment provided a sonic anemometer. The wind sensor has been eliminated from the experiment after a detailed evaluation for different reasons; from an economic point of view its cost was prohibitive. The other motivations must be underlined: scientific outcome was not relevant since heating effect could heavily interference with the measurements; in addition the requested power to heat up the sensor was too high.

A more detailed cost breakdown form (see Appendix) was listed with the progress of the project and after the experiment design was frozen.
The costs derive directly from the quotations received for the following components of the experiment: differential pressure sensor, sensors and devices for diagnostic and thermal control (thermometers and heaters), commercial Pt100, components for the innovative

RTD, Pitot tube, structural components, batteries. The other costs are realistically estimated from previous balloon missions.
In the table are also listed the travels expenses since affected in a considerable way the cost of the project.

2.1.3 The Schedule

The schedule can be planned after the identification of the tasks, their interdependences and their distribution to the human resources, taking in account the economical resources available. Anyway the most important aspect to consider were the project milestones.
The deadlines were set, therefore you had to adapt the scopes and optimize costs in order to remain on schedule.
The main key milestones of the project that the team had to face with were:

- DP (23/10/2011): delivery of proposal, at the beginning of the project before pre-selection.
- WS (08/12/2011): Workshop, presentation of the planned experiment project to the panel of expert.
- PDR (27/02/2012): Preliminary Design Review. Before it the experiment objectives are already fixed. It is required to carefully define the requirements and producing a complete preliminary design of the experiment.
- CDR (24/05/2012): Critical Design Review. Before it the experiment requirements are already fixed. The importance of maturing the experiment design at this stage is fundamental. After the CDR, the design is frozen so that the experiment can be built and verified.
- IPR (03/08/2012): Integration Progress Review. Necessary to monitor the integration is progressing well. The final experiment design should be adjusted according to the inputs received after the CDR.
- EAR (04/09/2012): Experiment Acceptance Review. This takes place upon delivery of the completed experiment to EuroLaunch.
- Launch (25/09/2012)
- Final report (31/12/2012). The launch campaign and the experiment results are documented in the SED.

The planning of the project schedule in a logical time sequence has been illustrated with the use of the Gantt chart.

The Gantt chart illustrates the start and finish dates of all the tasks foreseen, furthermore indicates the key project milestones described above. The chart also shows the dependency

relationships between activities. Gantt chart has been used to show current schedule status using percent-complete shadings; every task is colored as its state of elaboration.
The preliminary version presented at PDR considered the following tasks for monitoring the progress of the project:

- Project management
- System engineering
- Design
- Software development
- MAIT
- Operational phase
- Outreach program

This approach enabled to monitor the activities with respect to the deadlines and to follow subsequent updates with respect to the original planning in case of unexpected problems, delays or test failures.

The progress of the project needed a more accurate planning of all the tasks foreseen, for this reason a detailed Gantt has been developed.
The main tasks considered for monitoring the progress of the project are the same of the WBS, see Figure 25, with detailed listed subtasks. The following table shows the activities in progress during the project. In yellow are the main tasks of the WBS, in light blue the subtasks of the experiment design.

0	MISSUS experiment	20/09/2011	31/01/2013
1	Management	20/09/2011	31/01/2013
1.1	Work packages definition	20/09/2011	24/05/2012
1.2	Schedule & deadlines	20/09/2011	31/01/2013
1.3	Plan team meetings	20/09/2011	31/01/2013
1.4	Relationship with sponsors	10/01/2012	31/01/2013
1.5	Outreach Program	01/11/2011	31/01/2013
1.5.1	Website	01/11/2011	31/01/2013
1.5.2	Relationship with media	01/01/2012	31/01/2013
1.5.3	School & University presentation	01/03/2012	31/01/2013
2	System Engineering	20/09/2011	30/05/2012
2.1	Literary background	20/09/2011	30/01/2012
2.2	Systems coordination	20/09/2011	30/05/2012
2.2.1	Interfaces definition	20/09/2011	30/05/2012

2.2.2	Design plan	01/11/2011	30/05/2012
2.3	Technical supervision	20/09/2011	30/05/2012
3	Experiment design	20/09/2011	01/06/2012
3.1	Mechanical design of the experiment	20/09/2011	05/04/2012
3.1.1	FEM analysis	10/10/2011	15/02/2012
3.1.2	Missus MICD	05/03/2012	05/04/2012
3.2	Thermal design	15/11/2011	15/04/2012
3.2.1	Preliminary Thermal design	15/11/2011	10/02/2012
3.2.2	Detailed design thermal	10/02/2012	05/04/2012
3.2.3	Thermal Control strategy	01/03/2012	15/04/2012
3.3	New Sensors design	10/10/2011	05/04/2012
3.3.1	Temperature sensor	10/10/2011	05/04/2012
3.3.1.1	FEM analysis	10/10/2011	30/01/2012
3.3.1.2	TEM drawings	20/11/2011	05/04/2012
3.3.2	Pitot tube	10/10/2011	05/04/2012
3.3.2.1	FEM analysis	10/10/2011	30/01/2012
3.3.2.2	Fluid dynamic analysis	10/11/2011	10/02/2012
3.3.2.3	Pitot Tube drawings	15/02/2012	05/04/2012
3.4	Electric & electronics design	15/12/2011	15/04/2012
3.4.1	Power supply circuit definition	15/12/2011	10/02/2012
3.4.2	Acquisition & conditioning board definition	15/01/2012	28/02/2012
3.4.3	Digital Interface definition	20/01/2012	05/03/2012
3.4.4	Connectors & harness	25/01/2012	20/03/2012
3.4.5	Select batteries	01/02/2012	15/04/2012
3.5	Software design	15/12/2011	01/06/2012
3.5.1	Flight Software design	15/12/2011	01/04/2012
3.5.2	GSE design	30/01/2012	10/04/2012
3.5.3	Software Development	20/03/2012	01/06/2012
4	Procurement	20/01/2012	15/06/2012
4.1	Quotations Request	20/01/2012	05/04/2012
4.2	Orders	05/02/2012	15/06/2012
5	Assembling	30/06/2012	25/07/2012
6	Calibration	30/07/2012	10/08/2012
7	Testing	01/03/2012	05/09/2012
7.1	Test Plan	01/03/2012	15/04/2012
7.2	Test activity	18/04/2012	05/09/2012

7.2.1	Development test	18/04/2012	25/08/2012
7.2.2	Thermal-vacuum test	25/07/2012	10/08/2012
7.2.3	Vibration test	20/08/2012	30/08/2012
7.2.4	Shock test	25/08/2012	30/08/2012
7.2.5	Software test	15/05/2012	05/09/2012
7.3	Test results analysis	05/08/2012	31/08/2012
7.4	Models validation	15/08/2012	01/09/2012
8	Operational phase	31/08/2012	30/09/2012
8.1	Experiment delivery	06/09/2012	11/09/2012
8.2	Launch campaign preparation	10/09/2012	20/09/2012
8.3	Launch & Mission	20/09/2012	30/09/2012
9	Data analysis	10/03/2012	31/01/2013
9.1	Data Analysis plan	10/03/2012	10/05/2012
9.2	Flight data processing	05/10/2012	15/11/2012
9.3	Flight data report	05/11/2012	31/01/2013

Table 23 Gantt detailed activities during the project

On Figure 26 is reported a snapshot of the Gantt chart of MISSUS project.
The different colors of the tasks on the first column are:

- Pink highlighting: task not started
- Violet writing: task started, still in progress
- Green writing: task completed
- Yellow highlighting: key packages

On the top there are the required milestones marked with the date and reference black dots. On the two following lines there are MISSUS unavailable periods: the first exams period of two weeks between January and February and the second period between the second half of June and the second half of July. The progress is marked by the vertical blue line, representing the status date.

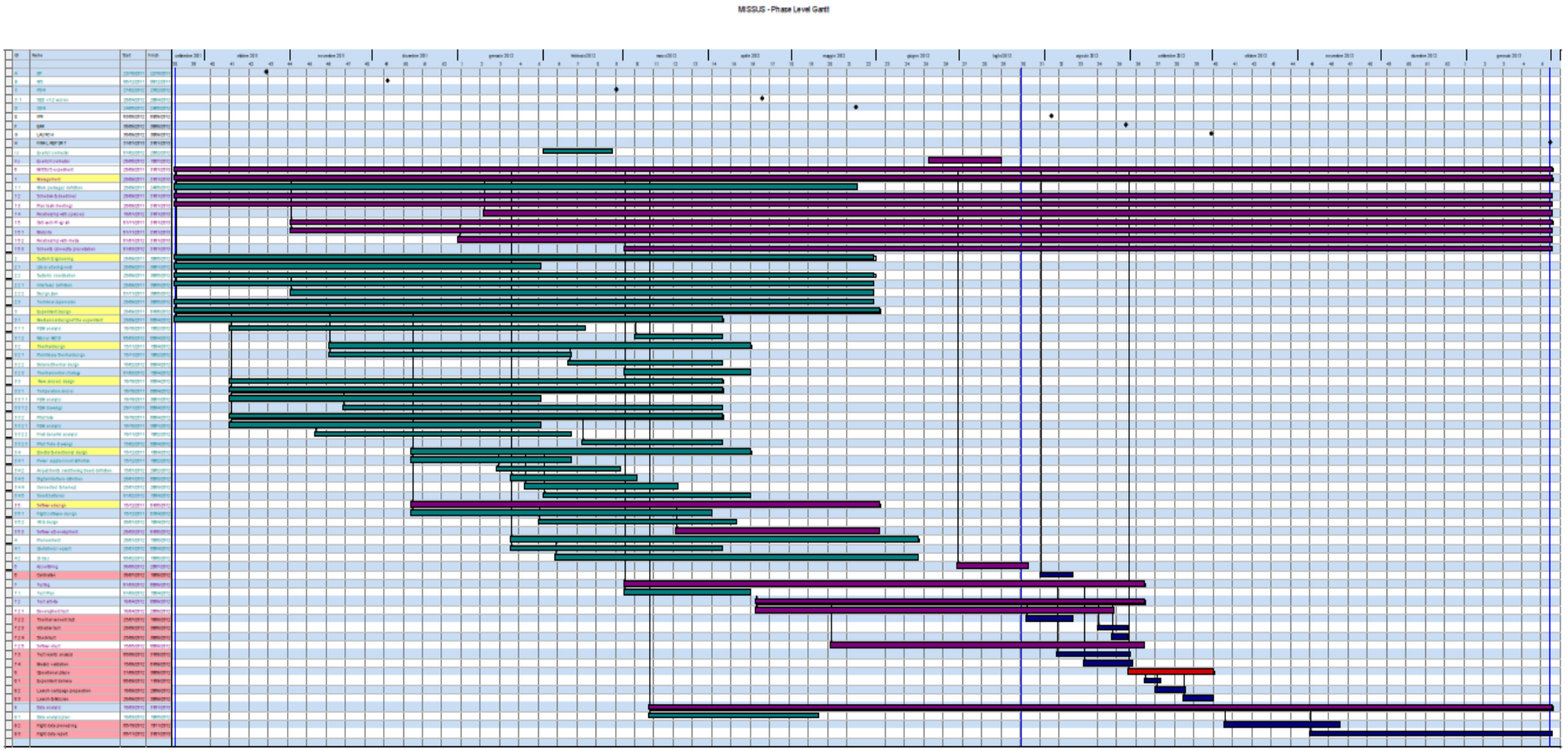

Figure 26 Gantt chart during the project

2.2 Risk management

Evaluation of the risk is a fundamental task of the PM because helps to clarify what are the chances that the project goes exactly as planned.
Obviously it's impossible to predict all the risk but the most must be identified and listed. Thanks to this activity it was possible to dealt with the risks of MISSUS experiment and manage them.
The sooner the risk has been identified and mitigated, the less it has cost.

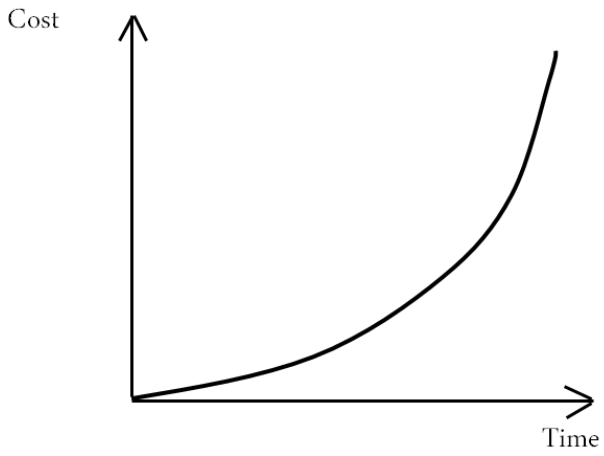

Figure 27 Cost versus time during mission project

The identification of the different risks of the project started using the project management tools. The PM tools include:

- goals and deliverables,
- WBS (see paragraph 2.1.1 for details),
- estimates,
- resources (see paragraph 2.1.2 for details),
- Gantt charts (see paragraph 2.1.3 for details)

At the same time it was also necessary a preliminary brainstorm of the common risk sources for the development and implementation of the project.
The main risk sources considered during this starting phase are:

- Technical: include scalability, integration of the experiment, mechanical and electronic interfaces, standards, compatibility, performance of the sensors (in particular for MISSUS).

- Legal/governmental: include permits for example the frequency allowed or not for the BX experiments, customs, H&S for people during laboratory activities, operational phase and mission.

- Personnel: include illness of a member, conflicts within the team, skill shortage in a work area, motivation level of the team members.

- Project: include budget of the project, schedule (follow up, delay, etc.), scope of the mission, politics, poor estimates.

From the risk sources identified above and their comparison together with the PM tools available derive the risks of the project. The main risks considered are in the:

- Experiment:
    - Technical implementation: malfunction or damage to specific part or components of the experiment.
    - Mission: deadlines, delivery, delay that could jeopardize the whole project and also problems in the operational phase that could bring to failure of the objectives.
- Safety: in the launch area.
- Launch vehicle: possible damage to the BX15 gondola and for other experiments due to MISSUS.
- Personnel: all the problematic related to the human resources.
- Resources: for what concern the economical resources, the funds

The method adopted to manage the risks within the project is the following:

- Identify the risks in certain relevant categories.
- Estimate the probability (P) and severity (S) of each risk.
- Calculate the risk index (P x S).
- Propose actions to mitigate or remove the risks, or reduce them to an acceptable level.
- Record all the risks, their index, magnitude and proposed actions in a risk register (see Table 27).

The level of Probability (P) and Severity (S) described in the risk management method and adopted to classify MISSUS risks are visible in the tables below.

Score	Likelihood	Likelihood of occurence
A	Minimum	Almost impossible to occur, 1of 10000 or more
B	Low	Small chance to occur, 1 of 1000

C	Medium	Reasonable chance to occur, 1 of 100
D	High	Quite likely to occur, 1 of 10
E	Maximum	Certain to occur, maybe more than once

Table 24 Evaluation scale of the risk probability

Score	Severity	Severity of consequences
1	Negligible	Minimal or no impact
2	Significant	Leads to reduced experiment performance
3	Major	Leads to failure of subsystem or loss of flight data
4	Critical	Leads to experiment failure or creates minor health hazards
5	Catastrophic	Leads to termination of the project, damage to the vehicle or injury to personnel

Table 25 Evaluation scale of the risk severity

The rankings for probability (P) and severity (S) are combined to assess the overall risk classification, ranging from very low to very high and being colored green, yellow, orange or red as described below.

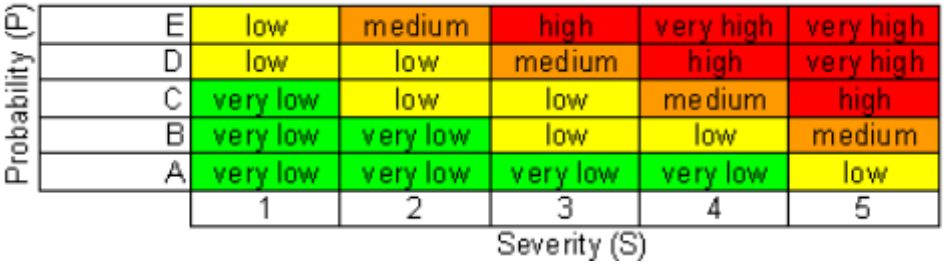

Figure 28 Risk index and magnitude scheme adopted

Risk index (P x S)	Risk Magnitude	Proposed actions
E4, E5, D5	Very High risk	Unacceptable risk: implement new process or change baseline – seek attention at appropriate high level.
E3, D4, C5	High risk	Unacceptable risk: see above.
E2, D3, C4, B5	Medium risk	Unacceptable risk: must be managed. Consider alternative process or baseline – seek attention at

		appropriate level
E1, D1, D2, C2, C3, B3, B4, A5	Low risk	Acceptable risk: control, monitor, consider options
C1, B1, A1, B2, A2, A3, A4	Very Low risk	Acceptable risk: control, monitor

Table 26 Risk magnitude designations and proposed actions for individual risks adopted

The actions considered to reduce risk can either limit the probability of occurrence through prevention or reduce the severity of consequences through mitigation.
The prevention is achieved by means of:

- increase of security: performing analyses and functional tests,
- reviews,
- bread-boarding,
- improve procedures (e.g. data back-ups).

The mitigation is achieved by means of:

- redundancy: using multiple suppliers and spare components/parts,
- recovery plan in place.

MISSUS risk register with the index, magnitude and provided actions can be seen in Table 27. The risks ID adopted for the classification is listed below:

TC – technical/implementation
MS – mission
SF – safety
VE – vehicle
PE – personnel
RE – resources

ID	Risk (& consequence if not obvious)	P	S	P x S	Action
TC12	Alteration of metrological characteristics of sensors	B	4	Low	TVC tests
TC13	Damage of a sensor before the launch	B	3	Low	Pay attention during pre-launch operations, spare components
TC14	Failure of the switching ON/OFF of the sensors	B	3	Low	Development & pre-launch tests
TC20	Impact with flying objects	B	4	Low	Acceptable risk
TC30	Resonances of the boom due to gusts	B	2	Very low	Acceptable risk,

					simulations and vibration tests (TBC)
TC40	Cable failure	A	4	Very low	Development tests
TC50	Electronics doesn't work at low/high temperatures	B	4	Low	Thermal analyses, development (TVC) tests
TC60	Electromagnetic interferences from other experiments	B	2	Very low	Acceptable risk
MS10	Sensor failure during operations phase	C	2	Low	Development and pre-launch Tests
MS20	Breaking of storage units of camera at probe impact	D	2	Low	Acceptable risk
MS30	Electronics components failure	C	3	Low	Functional tests
MS40	Software failure	B	4	Low	Functional and pre-launch tests
MS50	Failure of E-link cable or connector	B	2	Very low	Acceptable risk
MS70	Night-time flight (camera)	E	1	Low	Acceptable risk
MS80	Experiment shipping delay	C	4	Medium	Early delivery of the experiment
MS81	Experiment damage during shipment	C	4	Medium	Spare components
MS90	Late arrival of parts, materials	C	4	Medium	Early orders
SF10	Parts of the experiment falls from the gondola over populated area during flight	B	4	Low	Numerical analyses, functional tests Seek advice from EuroLaunch how to reduce probability
VE10	Damage of the boom and/or its support frame	A	5	Low	Numerical analyses, vibration tests, security cable
VE20	Battery explosion	A	5	Low	Acceptable risk
RE10	Short of funds for the experiment	B	4	Low	Outreach and promotion of the experiment
RE11	Short of funds for team members travels and accommodations	C	2	Low	Acceptable risk

PE10	Unavailability of a team member	D	2	Low	Every work package has a responsible and a co-responsible
PE11	Team member unable to continue with project	C	3	Low	Enough team members to compensate any drop out
PE20	Conflicts within the group	D	2	Low	Try mediation, help by professors
PE30	Overload work for a team member	C	2	Low	Plan the distribution of the work/ Each member must have a margin of spare time to help the mate

Table 27 MISSUS Risk register last version

Following the block scheme provide by the ECSS-M-ST-80C [7] it can be seen that the whole process is iterative.

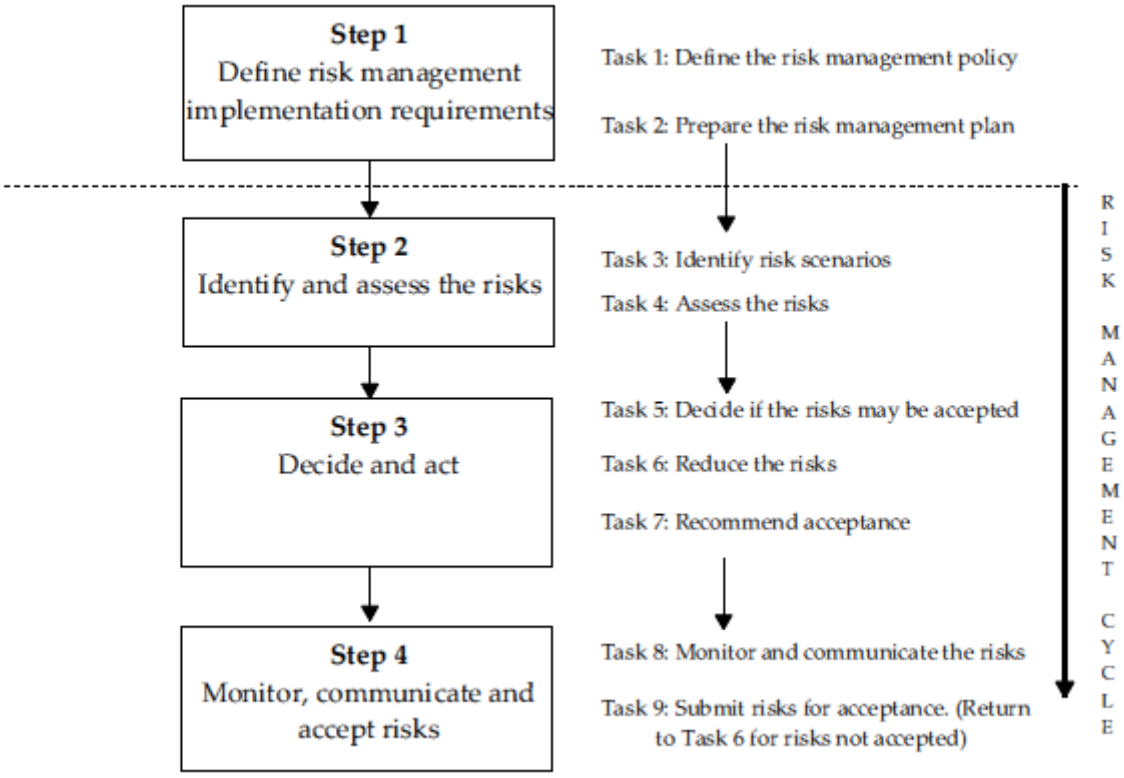

Figure 29 The tasks associated with the steps of the risk management process within the risk management cycle [7]

The process is iterative both in the identification of the risk and both during the different milestones of the project (PDR, CDR, IPR, EAR).
The risk register indeed has been updated in each new SED version provided for the milestones of BX program.
Furthermore the risk magnitude must be possibly reduced during the progress of the project, to bring down at the minimum the level of failure of the project.

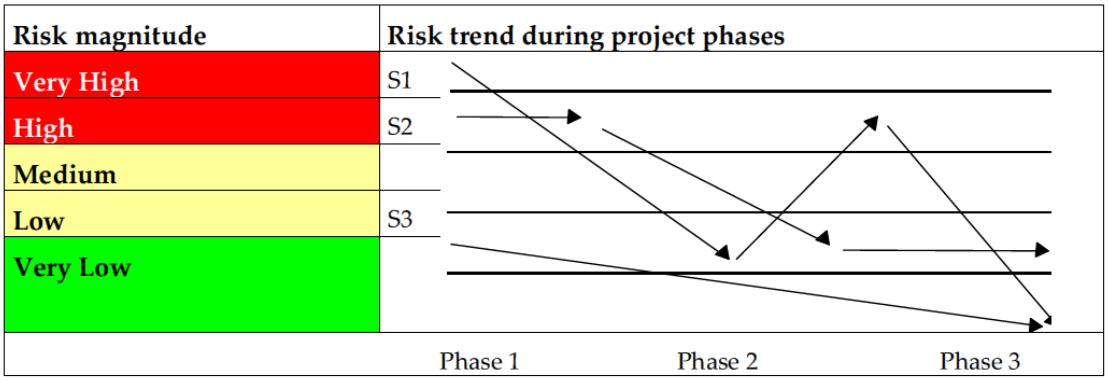

Figure 30 Risk trend and magnitude during the project [7]

2.3 Conclusion

In this section is reported a critical analysis of what was the planned work and what has been indeed realized.

First there's a comparison of the PDR design of the experiment and what has been practically realized for different causes. The reasons considered are related to project management factors: time scheduling, human and economic resources, risks.

What expected	What realized	Notes	Reason
Mass budget: preliminary estimation 40 kg	Mass budget: reduced to 17,4 kg	The mass of the experiment design was excessive, especially as the battery represents ~30kg of the overall mass.	Risk
Sensors on-board: - Accelerometer - IMU - 2 different Absolute Pressure sensors - 1 Differential Pressure sensor - 2 Innovative Temperature sensors - Humidity sensor - Magnetometer - Pitot tube - Wind sensor, i.e. sonic anemometer - 2 fish-eye cameras	Sensors on-board: - Accelerometer - IMU - 1 Absolute Pressure sensors - 1 Differential Pressure sensor - 1Innovative Temperature sensors - Humidity sensor - Magnetometer - Pitot tube - 2 logitec cameras	Number of pressure sensors reduced to unavailability of the item selected. Other sensors not have the specifications required. Number of RTD reduced due to funds reason. Wind sensor removed due to power and economic budget. Type of cameras changed, already available at CISAS	Schedule Economic resources Economic resources & Risk Economic resources
Electronics boards	Electronics boards	Realized as expected, but short amount of time to test them extensively with the whole experiment	Schedule
Battery: LeadAcid	Battery: Rechargeable Lithium-Ion	The battery size and type was considered dangerous to work with, strongly recommended by EuroLaunch	Risk
Hardware/Software: Arm Microcontroller and Custom PCB	Hardware/Software: PC104 System	Too much time required for the development of the custom PCB. Not enough skills and expertise, only one	Schedule Human resources

		member available for the task. The PC104 system was already available at CISAS and previous background available	Economic & human resources

Table 28 Comparison between what planned and what realized

Then are reported the main considerations about the project management tools used; we mean the WBS, the budget form and the schedule.

The update of the WBS and related project schedule (Figure 26) gave a better view of the activities. However, even if the main packages were broken down further, it would have been better to incorporate individual roles and responsibilities for each smaller specific subtask, then allocate them to the human resources. This would have permit a clear division of the work and the identification of the member in charge.

It is important that the planned expenses are as close and accurate as possible to the real costs of components, sensors and materials that will be selected and ordered for manufacturing. Alternatively a safety margin into the project budget from the early estimation should be considered.
In this way a clear amount of the sufficient funds needed respect to those available would have been identified. The budget in fact ran over, in particular for the custom components. One RTD sensor for example had to be removed from the experiment for this reason.
It is fundamental the availability of the funds and identify the contingencies as soon as possible, in the event that you are unable to secure all of the funding. As a matter of fact the delayed availability of the economic resources during the project caused a great shift in the schedule in a crucial period.

The schedule was affected during the project by external factors, not directly dependent from the team. For this reason it is necessary to plan buffer time for critical tasks and monitor well their progress from the beginning. Furthermore the margins must be very wide.
The main external events encountered in the project development and that the team had to deal with were:

- Early launch campaign: at first it was foreseen for the mid of October then it was shifted in the second half of September.
- Delay of the material arrival: sensors, components, electronics. It was due to both delayed confirmation of the funds and late manufacturing of the suppliers.

- Closing of the laboratories in the summer period, during the integration and tests was really critical. Obviously for the reason of delay of material the integration started later and the holiday period had to take in account. The planned schedule shifted in the last month before launch.
- Long time for the shipment of the experiment: risk of delayed experiment arrival.

Regarding the risks, their classification with severity and likelihood must be done carefully, but this can only get better with experience. The risks should not be under or overestimated, and the risks to include are only those you cannot reasonably control.
As an example the risk of ice formation on the Pitot tube that causes the malfunctioning of the sensor isn't a risk. This technical risk was considered at the beginning (PDR phase) but it was then easily avoided by design (with heaters), then was removed from the register.
A real risk instead was the RE10 (see Table 27), the short of funds for the experiment had to be mitigated but maybe it was underestimated. It was one of the critical reason for downsize the experiment components, delay and rescheduling.

Chapter 3

Launch Campaign

The BEXUS-14/15 balloon launch campaign took place between 20th September and 30th September 2012 at Esrange Space Center, SSC. The Launch base Esrange Space Center, SSC is located in northern Sweden, 45 km from the town of Kiruna at 67º N, 21º E.
The campaign programme was approximately organized with the following milestones:

- Delivery of experiment Flight H/W: 10/16.09.12
- Experiment integration: 18/19.09.12
- Nominal day of student arrival: 20.09.12
- Safety briefing: 21.09.12
- Begin of launch campaign: 21.09.12
- Experiment preparation by teams: 21/22.09.12
- Electrical Check-Out: 22.09.12
- Interference test: 22.09.12
- RF interference test: 23.09.12
- First launch date (BX14): 24.09.12
- Second launch date (BX15): 25.09.12
- Recovery of the gondola: 26/27.09.12
- Campaign report: 28.09.12

3.1 Flight preparation activity

In this section a detailed list of the preparation and test activities together with their outcome is reported. These activities were performed by MISSUS team before the launch of the experiment onboard BX15.

#	Activity	Description	Timeline	Results	Notes
1	Visual inspection	Inventory	20.09.2012	OK	
2	Visual inspection	Mechanical integrity check	20.09.2012	OK	
3	Electrical inspection	Check cables and interconnections integrity	21.09.2012	OK	
4	Electrical inspection	Check electronics functionality thanks	21.09.2012	OK	

		to leds, after plug in boards			
5	Functional test (Inside cathedral, without other experiments)	Connection conditioning board to PC104 and acquisition system	21.09.2012	OK	- A short circuit has been detected and repaired on an external connector (pins devoted to the RTD sensor); - humidity sensor doesn't work properly
6	Mechanical assembly	Fixation of MISSUS box to the gondola	22.09.2012	OK	
7	Mechanical assembly	Fixation of the boom to the gondola	22.09.2012	OK	
8	Mechanical assembly	Fixation of the security rope to the boom	22.09.2012	OK	
9	Electrical interconnections	Provide connections between battery & electronics, electronics & sensors	22.09.2012	OK	
10	Check sensors	Plug in sensors & start test sequence	22.09.2012	OK	
11	Mechanical assembly	Ethernet connection, box final assembling (insulating walls, MLI)	22.09.2012	OK	
12	IMU soft & hard iron calibration	Gondola has to be rotated, with all experiments switched on	22.09.2012	See notes	The soft & hard iron calibration software of IMU is inefficient, the magnetic disturbances inside the cathedral are too high
13	Electrical Check-out (Inside Cathedral)	Ethernet simulation	22.09.2012	OK	
14	1st RF interference test	Disturbs quantification with all experiments switched on	22.09.2012	OK	
15	Flight Compatibility Test (i.e.: 2nd RF interference test)	Disturbs quantification with EBASS and all experiments in flight mode	23.09.2012	OK	The PC104 works after 2 power cycles
16	Magnetometer calibration	Gondola has to be rotate, with all experiments switched on	23.09.2012	See notes	The magnetic disturbances caused by Hercules crane are too high
17	Flight Preparation	Recharge batteries Check protections Final definition of countdown timeline	24.09.2012	OK	

18	Functional tests on the launch pad before launch	Final check	25.09.2012	OK	

Table 29 List and outcome of the flight preparation activities during the launch campaign

Hereafter the mandatory tests required by EuroLaunch during the campaign are described in detail, there were three main tests performed in the following order:

- Electrical Check-out,
- Interference Test,
- Flight Compatibility Test (FCT).

The following pictures show the team at work during the flight preparation activity in Esrange.

Figure 31 MISSUS team during launch campaign. Clockwise: Electrical inspection and assembly, functional test of GSE, with the payload manager (on the right), on the launch pad for the calibration activity

After all experiments were mounted and connected on the BEXUS gondola the Electrical Check-Out was performed. The test provided the following operations:

- External power connection,
- Power on/off,
- E-Link communication test.

The check-out was carried out for all experiments, one-by-one. MISSUS had its own power battery supply, no need of external power to be connected.
After the preliminary checks described above, the first interference test was performed:

- All experiment were switched on one by one and then at the same time,
- All the experiments were checked and verified for interference amongst themselves.

If there had been interference between two experiments, the problem would have been discussed and a solution or compromise would have been found.
Anyway the test was performed successfully: no interferences were detected amongst the experiments, the next step was the FCT.

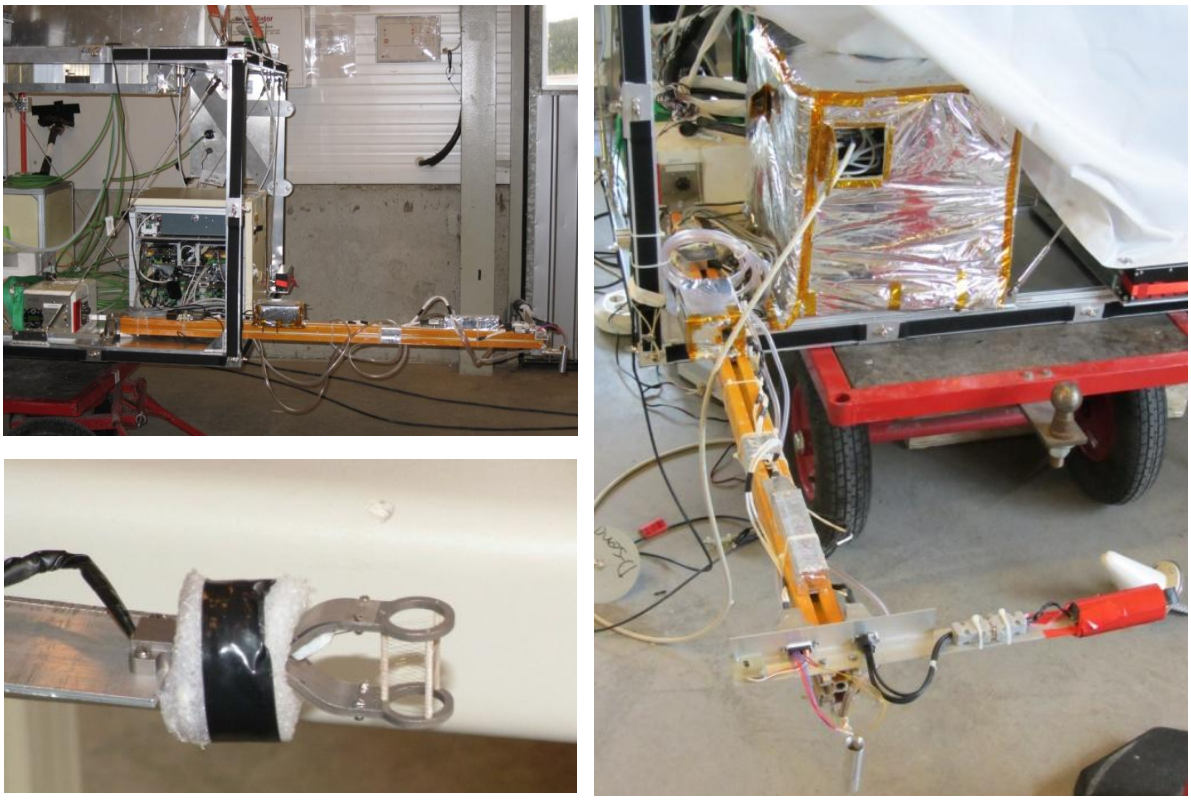

Figure 32 Assembly of the experiment. Clockwise: experiment integration on the gondola, the experiment ready for flight, the innovative RTD on the support placed on the boom

The Flight Compatibility Test (FCT) is a RF interference test. The gondola was picked up by the launch vehicle (Hercules) and placed together with all other transmitting/electrical hardware at the same distances as in a real flight.
The following operations and checks were performed:

- Mass measurement,
- Experiments switched on, one after the other,
- All experiment systems running,
- Test with all electronic equipment as well as experiments operating in flight mode,
- Check for interference with EBASS.

Figure 33 Pick-up of the BX15 gondola by Hercules before the FCT, from this picture MISSUS onboard was placed on the left side

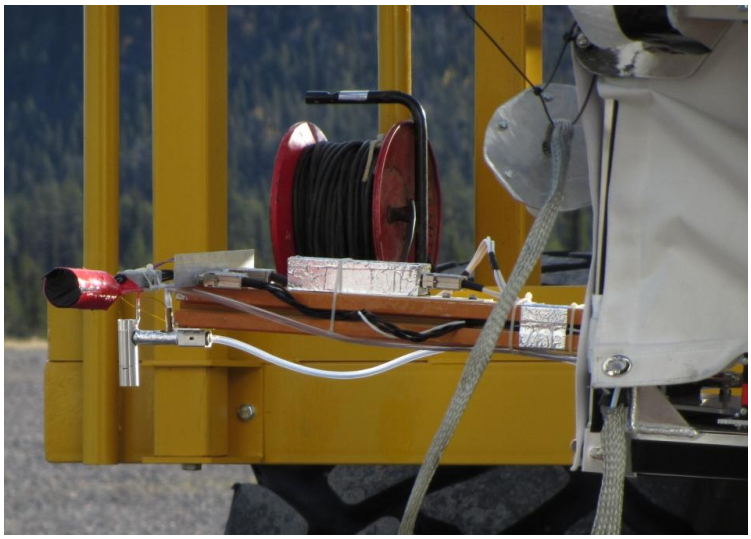

Figure 34 Particular of MISSUS experiment (external boom) during the pick-up

The test lasted more than 3 hours, long waiting times were necessary for all the operations to be carried on. None experiment caused interference with EBASS, on the contrary it wouldn't have been granted permission to fly.

After the RF test, the gondola was sealed and no further changes possible to any experiment. In the case of MISSUS only the batteries were charged.

After the completion of the RF test and ground support stations checkout, the Flight Readiness Review (FRR) was conducted by the EuroLaunch coordinator of the launch campaign. The purpose of the FRR was to authorize start of the count-down phase. In order to do this it was necessary to ensure that all experiments were ready for the flight.
After the successful FRR meeting there was a pre-flight meeting. The objective of this meeting was to verify that all flight hardware was ready, Esrange stations were prepared and other flight conditions were in favour of a possible start of countdown.

MISSUS countdown started at 6.20 a.m. on the 25th of September 2012, however unfavourable weather condition (rain) stopped the countdown sequence few times.
In the following table the time line for countdown and flight of MISSUS is reported: T0 represents lift-off time.

Time	**Action**
Flight preparation	• Charge of Batteries • Functional test • Install of sensor protection cap
T0 – 4h00’	Start of countdown
T0 – 2h30’	Ready for gondola pick-up
T0 – 1h30’	Ready for line-up
T0 – 1h20’	• Manually switch on the experiment • Functional test • Take a picture of the gondola on the launch pad
T0 – 1h10’	Remove protection cap from the temperature sensor
T0 – 1h00’	Balloon unfolding
T0 – 0h40’	Start of inflation
T0	Balloon release and lift off
T0 + time of virtual separation system activation	End of the operations

Table 30 Timeline for countdown and flight

Figure 35 The Hercules vehicle transports BX15 on the launch pad, balloon inflation and release sequence before launch on 25th September 2012

3.2 Flight performance

Once switched on, the experiment worked properly and collected data continuously until 4 hours and 6 minutes after launch: at T0+04:06:00, during the floating phase, the ground station lost contact with the experiment.

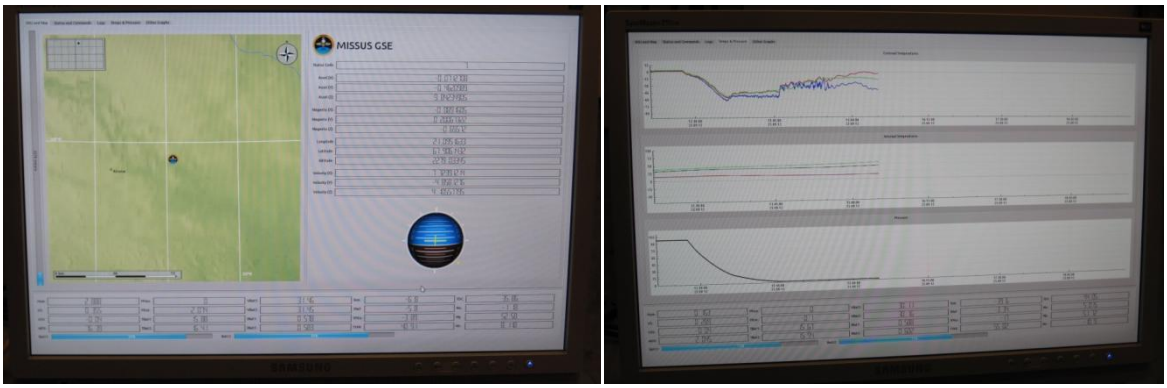

Figure 36 Images of MISSUS GSE graphic interface during flight. Display of sensors data and trajectory at 2500m of altitude (left), monitoring of the temperature and pressure trend during flight - cruise phase (right)

Further investigation clarified that all information on the descent phase were missed: MISSUS definitely stopped working at +04:06:00, both Pitot tube data and sensors system for impact detection data have not been acquired.

However a considerable amount of data have been acquired during the ascent and floating phase.

The following table reports a list of MISSUS sensors and provides some details on the acquired and stored data during flight.

Sensor	Stored data [byte/s]	Transmitted data [Hz]	Operative phase	Status	Notes
Fine Temperature	512	8	Whole flight	OK	
Coarse temperature	512	8	Whole flight	OK	
Absolute pressure sensor	512	8	Whole flight	OK	
Differential pressure sensor	512	8	Descent phase	See notes	MISSUS stopped acquisition during the descending phase
Humidity sensor	512	8	Whole flight	See notes	Malfunctioning is detected during functional tests
IMU Magnetometer (3 signals)	512	8	Whole flight	OK	

Accelerometer	2048	N.A. (Boolean)	Descent phase	See notes	MISSUS stopped acquisition during the descending phase
IMU Accelerometer	512	8	Whole flight	OK	
Rate of turn	512	8	Whole flight	OK	
GPS	512	8	Whole flight	OK	
Flux Gate Magnetometer	512	8	Whole flight	OK	
Battery Voltage	512	8	Whole flight	OK	
Battery Current	512	8	Whole flight	OK	
Cameras	10 frame/s	N.A.	Whole flight	See notes	Images have been recorded on the SD card: however they are useless due to saturation

Table 31 Acquired, stored and transmitted data during flight

Figure 37 Snapshot of the GSE at +04:06:00 (1)

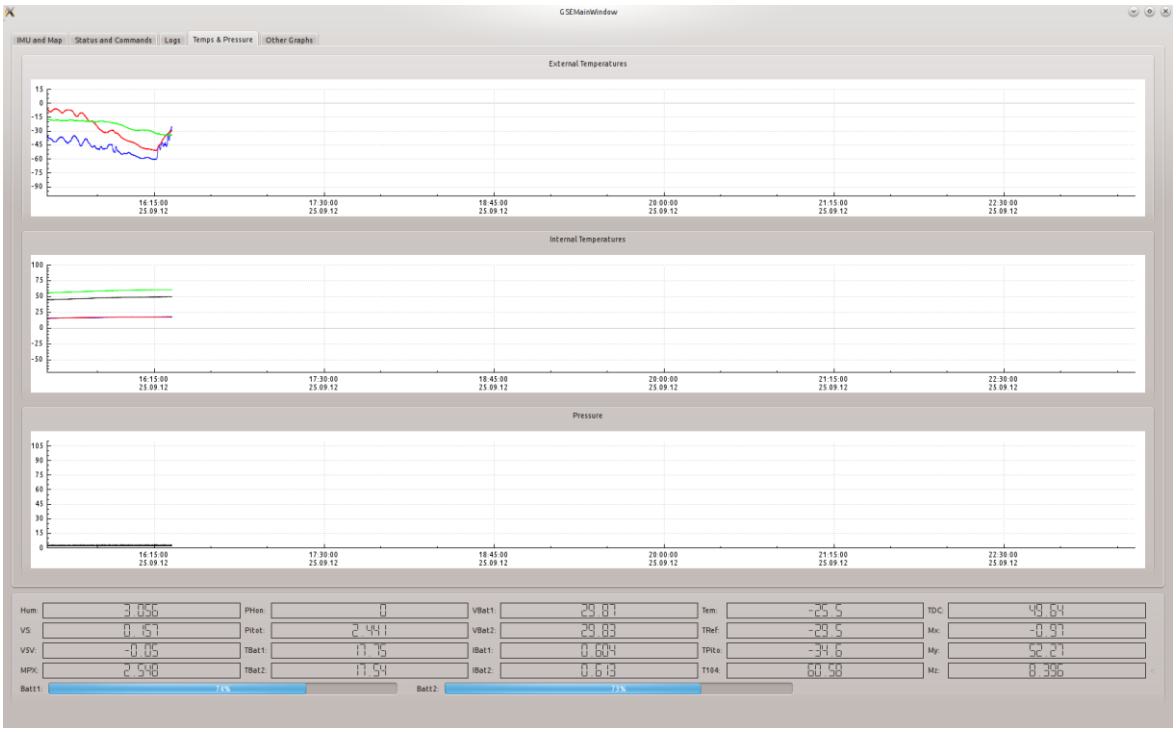

Figure 38 Snapshot of the GSE at +04:06:00 (2)

Once contact has been lost, a preliminary fault investigation started in order to assess any possible failure cause. The investigation started considering some critical parameters and transmitted house-keeping data, such as batteries residual charge, MISSUS internal temperature, eventual voltage peaks or drops.

The following figure shows the voltage (blue line) and the current (green line) of MISSUS batteries: from these graphs any possible problem strictly related to batteries charge were excluded, since at +04:06:00 overall voltage was 29.9V, that means 3.73V/cell and residual capacity of 2Ah.

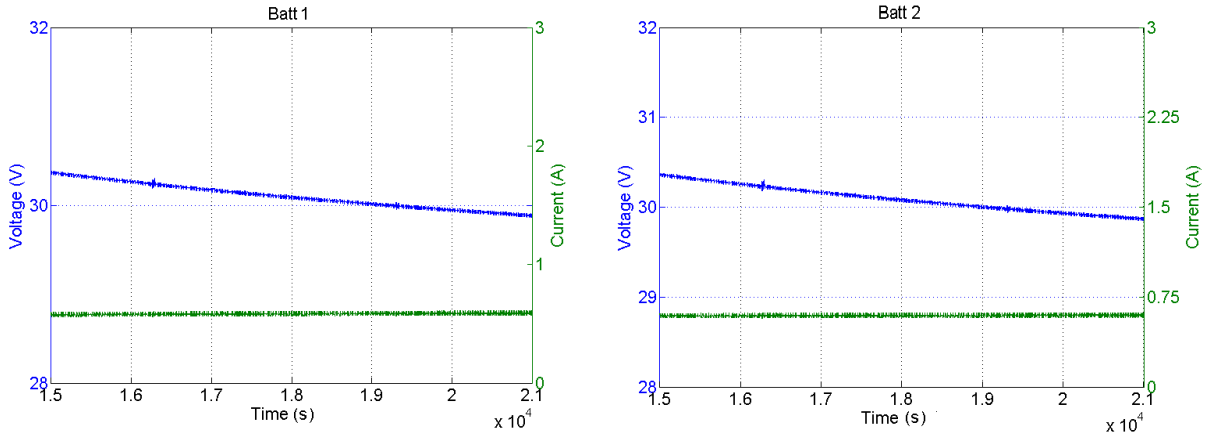

Figure 39 Voltage and Current profiles of MISSUS batteries as a function of time

The following figure shows the temperature of internal MISSUS components (batteries, PC104, DC/DC modules): since all values are within margins (batteries temperature is in the range +10°C/+20°C, PC104 maximum temperature is 62°C, about 20°C lower than its maximum operative temperature), also any thermal issues were excluded.

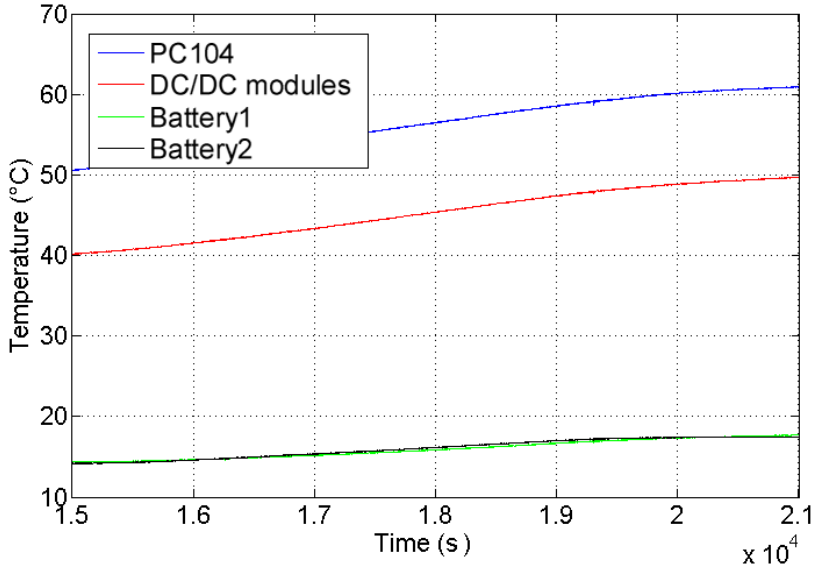

Figure 40 Temperature profile of MISSUS internal components during flight

Since all voltage profiles were in line with nominal and normal behaviour of the experiment, two possible scenarios have been outlined:

- Best scenario:
  - ✓ Loss of the E-link connection;
  - ✓ Data saved properly on the on SD card until landing.
- Worst scenario:
  - ✓ PC104 stopped working;
  - ✓ Unavailability of the data during the descending phase.

The team decided to wait for the recovery of the gondola in order to examine in depth the problem.

3.3 Recovery

MISSUS onboard BX15 gondola was back in ESRANGE in the morning of 27th of September 2012, after a hard landing on a rocky ground in Finland which severely damaged the gondola and some parts of the experiments onboard.

Figure 41 BX15 back in Esrange, MISSUS boom was already been removed

Visual inspection started analysing MISSUS status without removing it from the gondola. Externally the experiment seemed undamaged, as shown in the following figure.

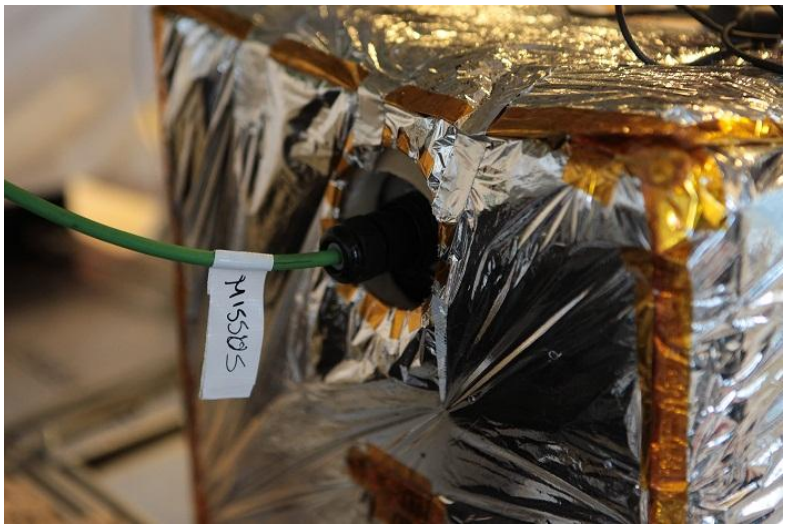

Figure 42 MISSUS on the gondola after the recovery

As prescribed from the recovery procedure, the external boom and the most sensitive part – the temperature sensor – were disassembled from the experiment before the transport by truck.

After the recovery both the boom and the temperature sensor seemed undamaged, as shown in the figure below. Further investigation has demonstrated that the temperature sensor was perfectly undivided and reusable.

Figure 43 Status of the innovative RTD sensor after the recovery

Unfortunately the Pitot tube proved to be damaged: the total probe inside the cylindrical shield was cracked and the main external parts unglued.

3.4 Post flight activity

After the preliminary visual inspection with the experiment still fixed on the BX15 gondola, the fault investigation analysis started in order to identify any possible cause of the unexpected behaviour (loss of contact), following a detailed procedure.
The following table reports the steps and the main conclusion of each action.

Step	Action	Conclusion
1	Preliminary inspection of the E-link connection between MISSUS and BX15, checking functionality with SSC crew	E-link connection at top suspected to be not locked, anyway it works
2	MISSUS isolated with respect to E-link, visual inspection performed	No damages
3	Remove MLI and top panel, visual inspection performed	No damages
4	Remove the side exposed to the external environment, visual inspection performed	All the electronics boards were unhinged from the supports of the rack, due to the impact with ground
5	Verification of suspected loss USB connection (IMU &	Confirmed, weak connection

	cameras), visual inspection performed	between ports, to be verified
6	Recovery and copy of memory card	All data available back-up performed
7	Check impact fuse on the sensor system landing board to verify shock detection	Not switched, the system was not working at landing
8	Verification that last timestamp matches last data packet received	Confirmed, it is a on-board system problem
9	Set-up for PC104 to check functionality, disconnection and checking of power lines performed	Illogical behaviour of PC104 due to: • Voltage drop • Driver

Table 32 MISSUS detailed investigation procedure and main conclusions

The first step has been performed with MISSUS on the gondola, then the experiment has been carefully removed from BX15 and placed in a safe room.

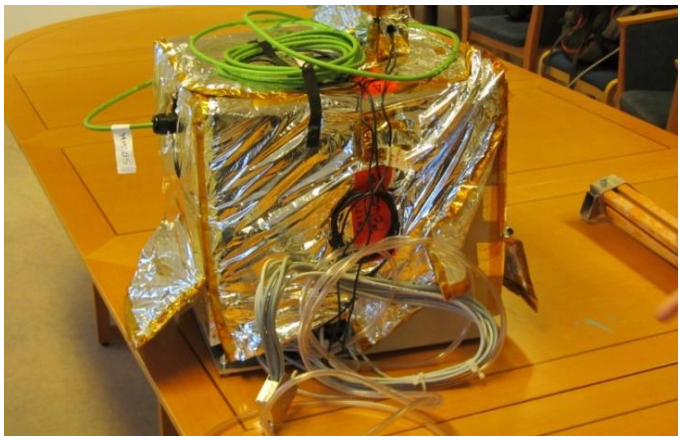

Figure 44 Missus removed from the gondola

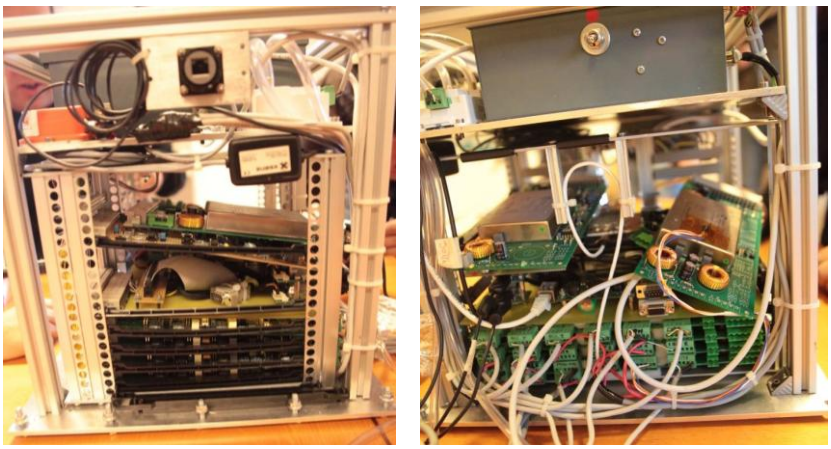

Figure 45 Status of the internal part of the experiment (side and front view)

After the investigation the experiment was completely re-built, founding out that MISSUS worked properly, that all internal parts were not damaged and that the experiment is reusable for future analysis.
The cause of the problem encountered during flight was the PC104, demonstrated to be defective.

Figure 46 MISSUS Experiment Re-built

After the launch campaign the data analysis of the experiment based on a synergic approach started. The data analysis and results are discussed in the following chapter.

Chapter 4

Sensors data analysis

Data analysis represents a fundamental task of the experiment.
MISSUS is able to measure a series of atmospheric parameters and collects other data in order to perform trajectory and gondola attitude reconstruction (altitude, latitude and longitude, roll, pitch and yaw angles and rates, magnetic field).
All these data have been analyzed in post processing according to the data fusion concept which relies on the cross correlations between measurements.
MISSUS Experiment measured the following data during flight:

- Temperature (3 thermometers)
- Pressure
- Magnetic Field (IMU & magnetometer)
- Attitude & Trajectory of the gondola (GPS & IMU)

The data used for the analyses presented in this Chapter are provided both by MISSUS sensors and BX15 sensors, in order to have a complete view of the flight (considering that MISSUS stopped collecting data at +04:06:00) and to compare the available data at the same time.

Data	Sensor/Device	Source
Temperature	Fine RTD sensor, coarse PT100, Pitot tube PT100	MISSUS
Pressure	Absolute pressure sensor	MISSUS,
Altitude	IMU	MISSUS, BX15
Longitude	IMU	MISSUS, BX15
Latitude	IMU	MISSUS, BX15
Yaw angle	IMU, magnetometer	MISSUS
UTC Time	PC104 Timestamp	MISSUS, BX15

Table 33 Sensors data used for the cross correlation

4.1 Data filtering

The data filtering was performed as preliminary operation before the scientific data analysis. The operation was necessary in order to reduce the signal noise and to fulfill the performance requirements of the experiment (see paragraph 1.3.4.2).

4.1.1 Disturbances and white noise

At first sight, all the analog signals are affected by a well noticeable disturbance.
The unexpected behaviour can be seen in Figure 47, which reports the voltage signal of the battery. Usually the voltage should decrease like a monotone exponential function; on the contrary several beats are present and the higher the frequency content, less clear the disturbance.

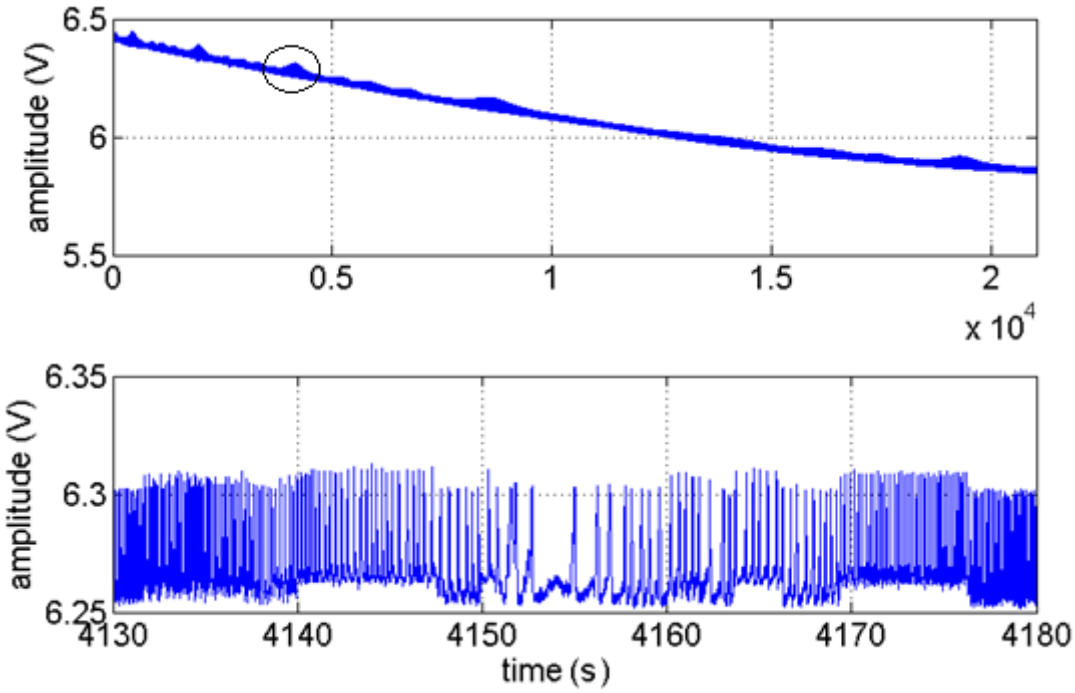

Figure 47 Battery #1 voltage signal, on the top the whole flight; on the bottom the enlargement of the circled area

The noise frequency decreases near to the beats peaks and becomes higher near to the minimum values, with a maximum beat amplitude of 0.05 V (see enlargement of Figure 47 and Figure 48).
In addition the noise is characterized by a higher peak followed by three minor peaks with a variable period (progressively wider) during the flight; this trend can be seen in Figure 47 and better in Figure 51, where the isolated noise component is visible.

Other signal variations were observed: the magnitude order is equal to 0.005 V, which is higher than the ADC LSB precision (0.0003 V) of MISSUS experiment.

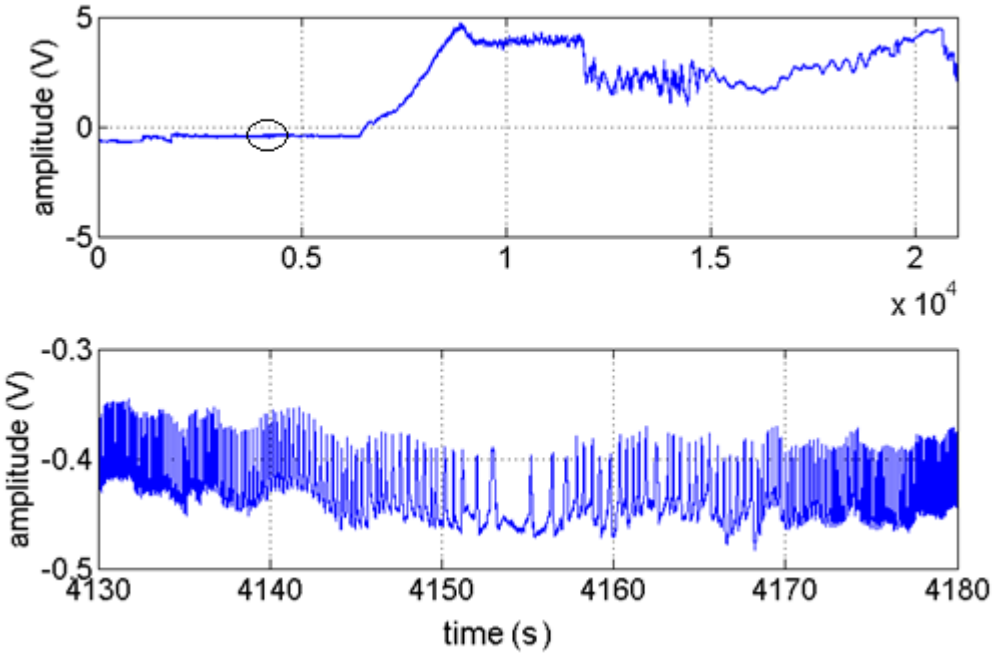

Figure 48 Temperature sensor signal, on the top the whole flight; on the bottom the enlargement of the circled area

The disturbances observed could be related to:

- ADC or electronics before the conditioning boards;
- External magnetic noise.

Considering that all analog signals are affected by the same disturbance (see also Figure 48 as example) and that the noise signal amplitude is the same despite gains are different for each analog channel, the disturbance could have been caused by the presence of a coil generated by the wiring between the analog conditioning boards and the ADC (see the following figure).

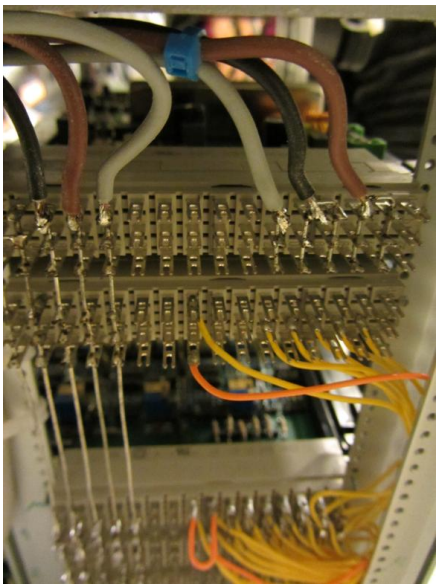

Figure 49 Wiring between the analog conditioning boards and ADC

4.1.2 Wavelet filtering

The data filtering has been performed with the wavelet techniques; the starting point was the interest in the low-frequency content of the signal.
One major advantage afforded by wavelets is the ability to perform local analysis, i.e. to analyze a localized area of a larger signal. Wavelet analysis is capable of revealing aspects of data that other signal analysis techniques miss, aspects like trends, breakdown points, discontinuities in higher derivatives, and self-similarity. Furthermore, because it affords a different view of data than those presented by traditional techniques, wavelet analysis can often compress or de-noise a signal without appreciable degradation.
In Appendix the main advantages of wavelets respect to other techniques, the wavelet transform and its implementation for discrete signals (DWT) are described.

After a preliminary comparison among the different kinds of wavelet and scales, 5 levels of factorization (see Figure 50) have been applied and the biorthogonal wavelet 3.9 (see Ref.[13]) has been used for the filtering and reconstruction process. Please refer to Appendix for the explanation of the filtering and reconstruction algorithm.
The biorthogonal family exhibits the property of linear phase, which is needed for signal reconstruction.

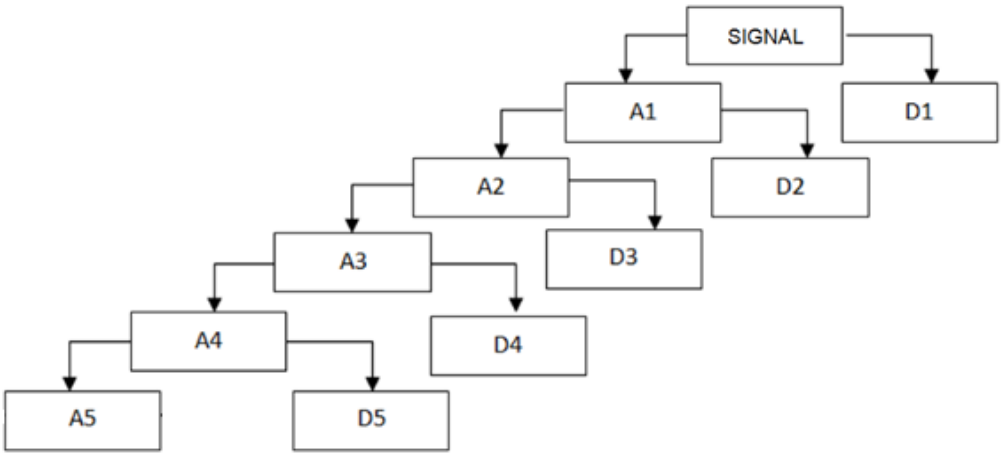

Figure 50 Wavelet decomposition tree used to de-noise the signal: A is approximation, low-frequency components of the signal; D is detail, high-frequency components of the signal

The following figure shows the noise, isolated from the original signal. The higher peaks followed by the three minor peaks, described in the previous paragraph, are clearly visible.

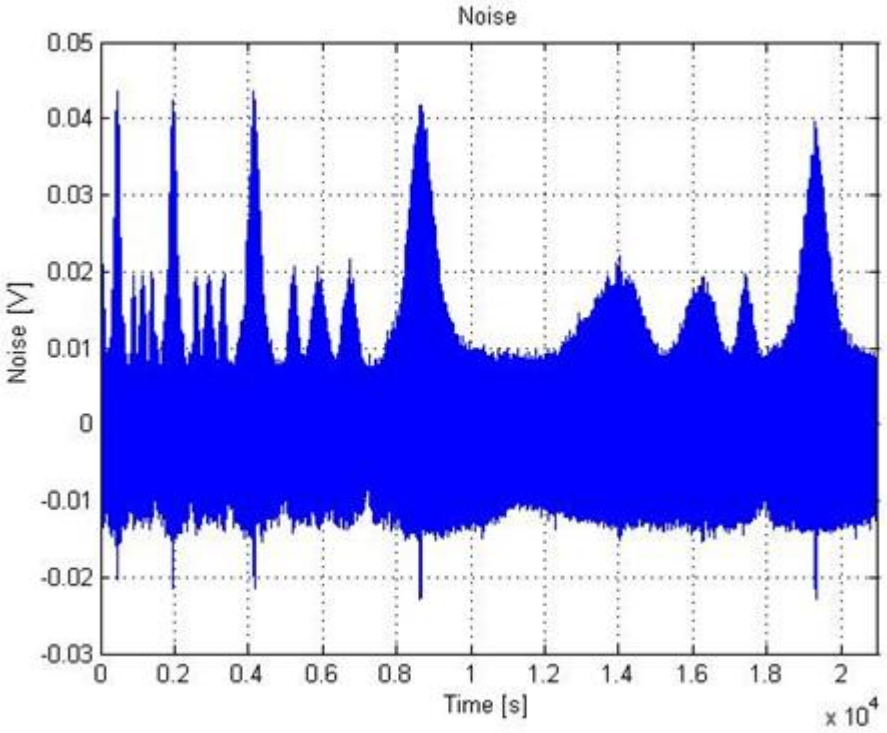

Figure 51 Noise component in the battery #1 voltage signal

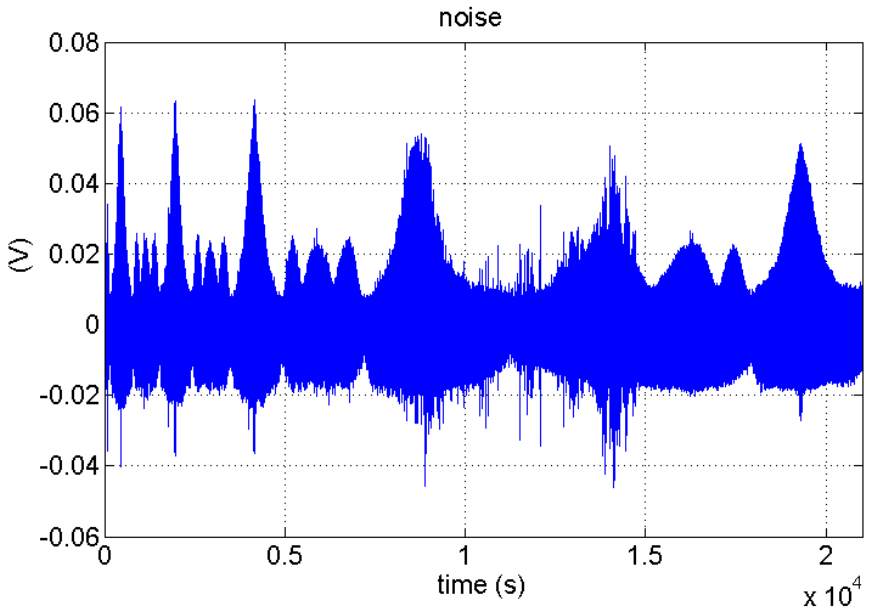

Figure 52 Noise component in the temperature sensor signal

In the next figures the results of the de-noising process is shown: noise is mitigated for the sensors signals and phase displacement is negligible.

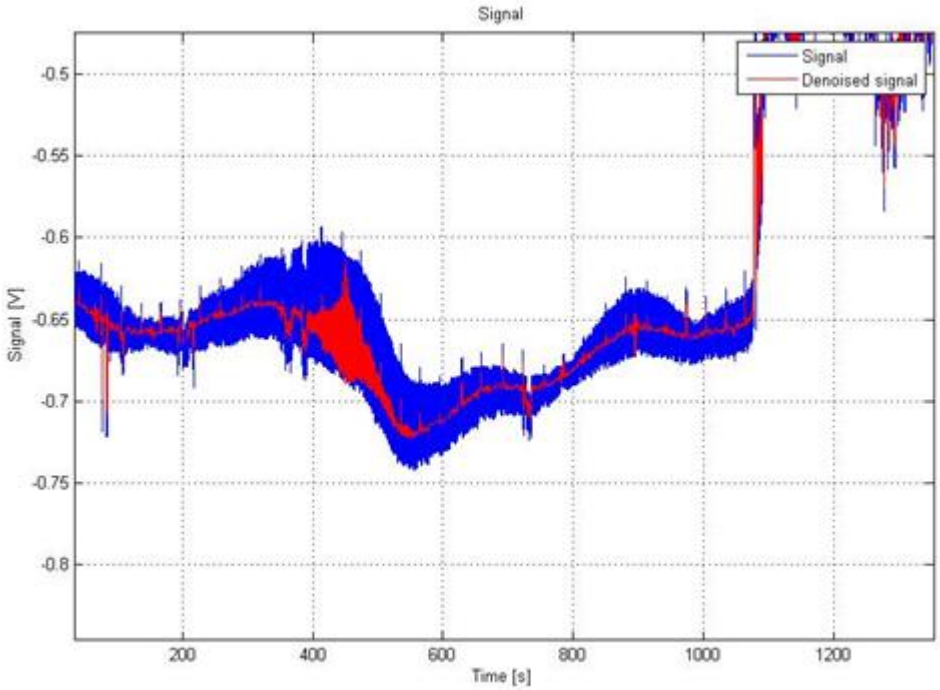

Figure 53 Comparison between the RTD sensor signal and the RTD de-noised signal in the initial phase from power on

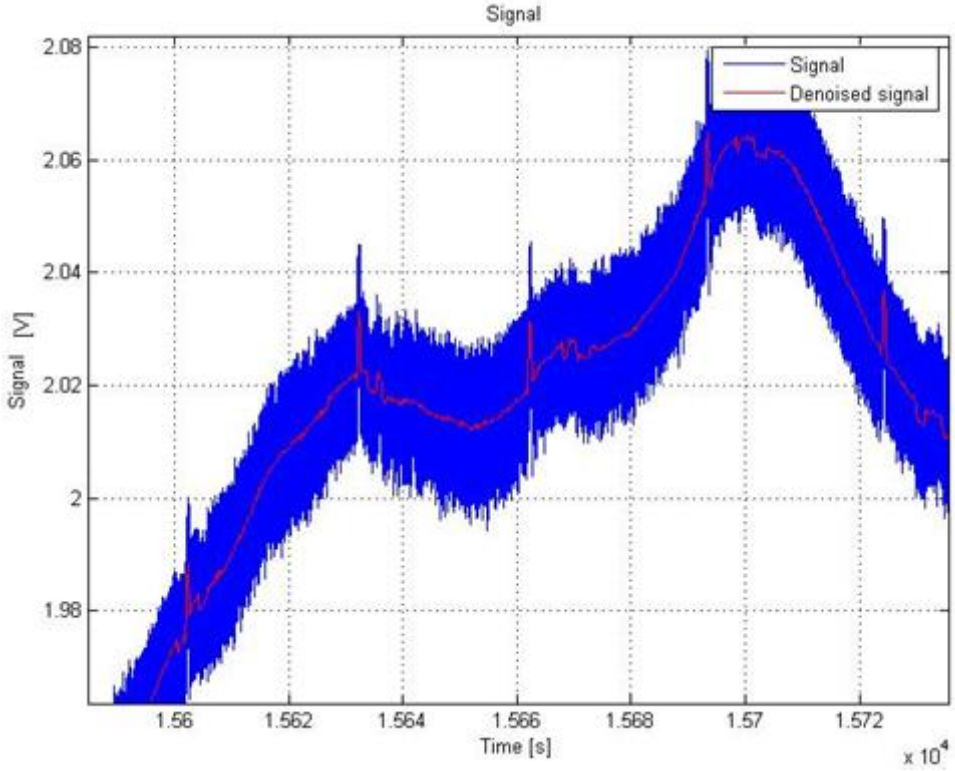

Figure 54 Comparison between the RTD sensor signal and the RTD de-noised signal during the flight

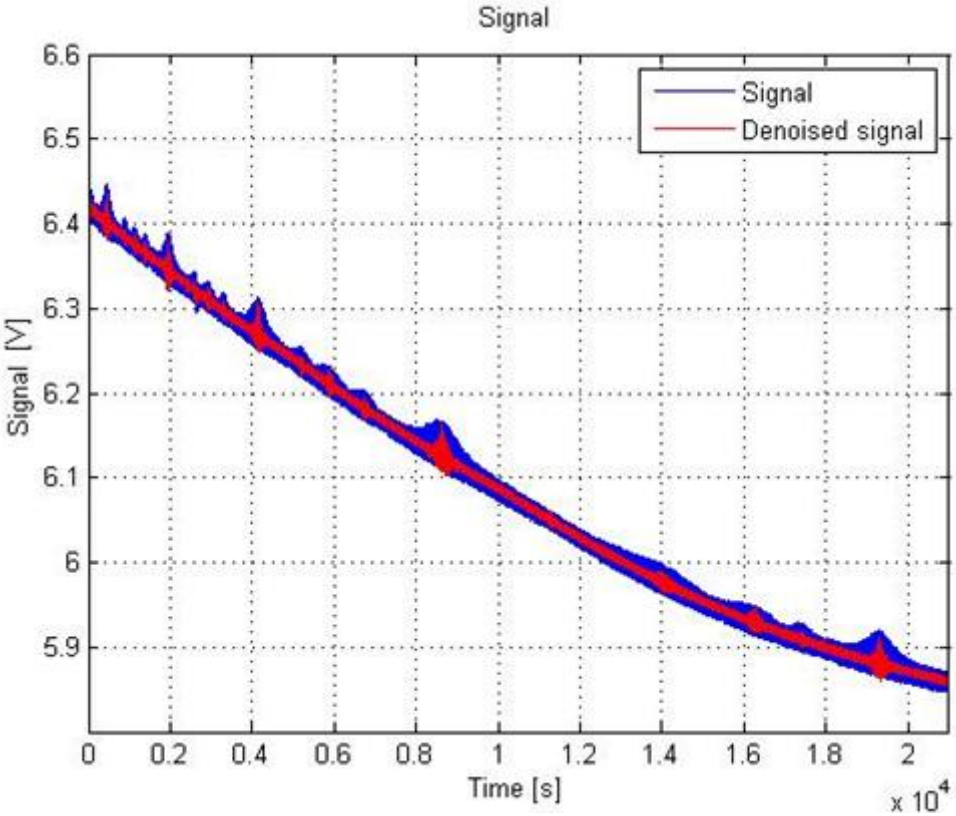

Figure 55 Comparison between Battery #1 signal and filtered signal, the noise is reduced even if the higher peaks are still present.

4.2 Cross correlation of the data

The paragraph focuses on the cross correlation of the meteorological data and on the influences of environmental factors in the measurements (e.g.: clouds, solar radiation, etc). The data used for the following analysis are provided both by MISSUS sensors and BX15 sensors, see Table 33 at the beginning of the Chapter.

Except for the IMU, the sensors on-board MISSUS had analog output for this reason the signal value (voltage) has been converted into scientific measurement value.
The following block diagrams report the conversion process applied.

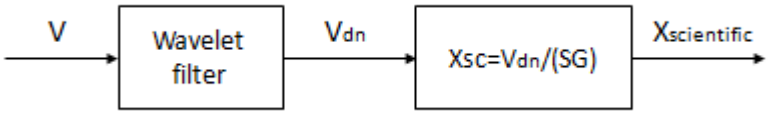

Figure 56 Block diagram for signal conversion: S is sensitivity, G is gain

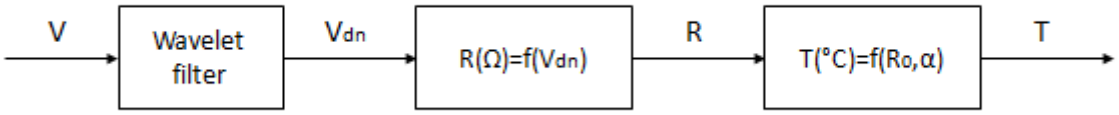

Figure 57 Block diagram for temperature signal conversion

4.2.1 Atmospheric analyses

In this section the meteorological analyses are described: such analyses have been performed in order to characterize the environment up to 25.6 km and compare the atmospheric models with the data collected (in particular the temperature measurements provided by the innovative RTD sensor).

4.2.1.1 Atmosphere characteristics

The atmosphere of the Earth contains a few highly concentrated gases, such as nitrogen (78%), oxygen (21%), and argon (1%), and many trace gases, among them water vapor, carbon dioxide, methane, and ozone. All such gases are constituents of air. Important characteristics of air are its pressure (p), density (ρ), and temperature (ϑ). These parameters vary with altitude, latitude, longitude, and season and are related to each other with a good approximation by the equation of state of ideal gases.

$$p = R\rho\vartheta$$

Where R=287,05 m^2/Ks^2 is the gas constant for dry atmospheric air.
A deviation from the ideal gas law occurs when there is moist air, i.e. the amount of water vapor in atmosphere can't be neglected.

The lower atmosphere of the Earth, from 0 to 100 km, is called homosphere and is divided into four major regions in which temperature changes with altitude. These are, from bottom to top, troposphere, stratosphere, mesosphere, and thermosphere Even if the relevant zone for the BEXUS flight is up to 25.6 km, for sake of completeness we define all the regions up to 100 km:

1. Troposphere: from the surface to a variable height of 8 km near the poles, 15-18 km near the Equator. The temperature, on average, decreases with increasing altitude. It is divided into the boundary layer, which is the region from the surface to about 500 – 3000 m altitude, and the free troposphere, which is the rest of the troposphere.
    - Boundary layer: is the portion of the troposphere influenced by the Earth's surface and that responds to surface forcing with a time scale of about an hour or less [18]. Temperature varies significantly in the boundary layer during the day and between day and night.
    - Free troposphere: is the region extending above the boundary layer. The upper boundary is the tropopause. The tropopause is defined by the World Meteorological Organization (WMO) as the lowest altitude at which the lapse rate decreases to 2 K km^{-1} or less, and at which the lapse rate, averaged between this altitude and any altitude within the next 2 km, does not exceed 2 K km^{-1} [18].

2. Stratosphere: from the tropopause to 50 km of altitude. The temperature is relatively constant with increasing altitude (isothermal) in the first layers then it increases with increasing height. It contains 90% of the Earth's ozone that interacts with radiation and then influences the temperature profile.

3. Mesosphere: from 50 km to 90 km of altitude. Ozone densities are too low for ozone to absorb radiation and affect temperatures. As such, temperature decreases with increasing altitude in a manner similar to the upper troposphere.

4. Thermosphere: above 90 km. The temperature increases with increasing altitude because molecular oxygen and nitrogen there absorb very short wavelengths of solar radiation.

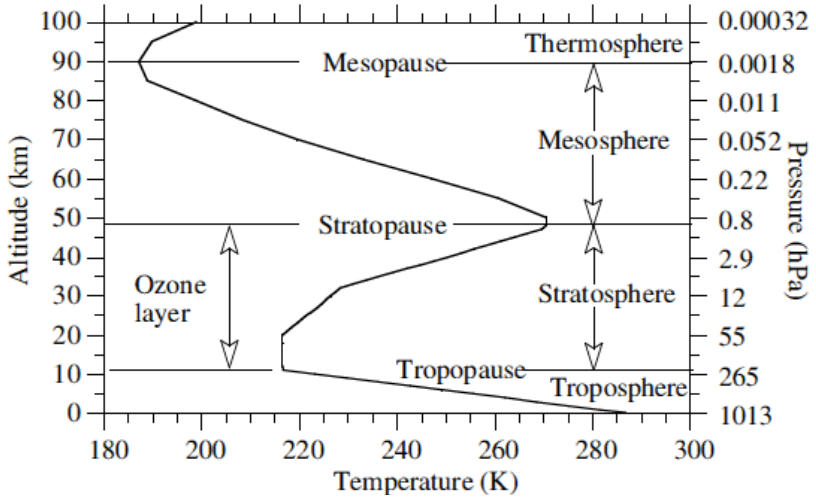

Figure 58 Temperature structure of the Earth's lower atmosphere

4.2.1.2 Atmospheric models

To validate the temperature data collected by the RTD sensor (MarsTem prototype) during the ascending phase, two type of atmospheric models have been used:

- ISA standard atmospheric model from ICAO 1964 [17];
- NRLMSISE-00 model, based on the earlier models MSIS-86 and MSISE-90, but updated with drag data [19].

International Standard Atmosphere (ISA)

The standard atmosphere model is a good starting point considering that it is based on the medium value of the lapse rate for the different layers of the atmosphere (troposphere, stratosphere, etc.) and the different parameters are function of altitude.

The air is considered as a perfect gas, without water vapour and with constant chemical composition. The division in different regions is given by the variation of the mean value of the environmental lapse rate λ defined as:

$$\lambda = \frac{d\vartheta}{dh}$$

Where ϑ is the temperature and h is the altitude.

The portion of interest considered for the analyses are:

- Troposphere: from h_0= 0 m to h_S= 11000 m, the constant lapse rate value is λ_{ISA} = -0.0065 K/m.
- Low stratosphere: from h_S= 11000 m to h_M= 20000 m, the constant lapse rate is null, λ_{ISA} = 0 K/m.

- Mid stratosphere: h_M=20000 m to h_K=32000 m, the constant lapse rate value is λ_{ISA} = -0.0010 K/m.

The temperature then has a linear dependency with altitude and it is then given by the following equations:

$$\vartheta_{ISA}(h) = \vartheta_0 + \lambda_{ISA} h \qquad h \in [h_0, h_S)$$

Where $\vartheta_0 = \vartheta_{ISA}(h_0) = 288.15$ K at the mean sea level. The temperature value reached at h_S is then constant in the low stratosphere

$$\vartheta_{ISA}(h) = \vartheta_S \qquad h \in [h_S, h_M)$$

Then the lapse rate is positive and the temperature increases:

$$\vartheta_{ISA}(h) = \vartheta_S + \lambda_{ISA}(h - h_M) \quad h \in [h_M, h_K)$$

The following table shows the ISA temperatures at different altitudes

Altitude (m)	Temperature (K)	Temperature (°C)
0	288.15	15
5000	255.65	-17.5
11000	216.65	-56.5
20000	216.65	-56.5
25000	221.65	-51.5
32000	228.65	-44.5

Table 34 ISA Temperatures at different altitudes

Since air is assumed at rest and behaves like an ideal gas in static equilibrium under the effect of the forces due solely to the pressure and gravity field (g_0 = 9.80665 m/s^2) we have:

$$\frac{dp}{dh} = -\rho g_0$$

This type of air pressure is called hydrostatic air pressure, which is the pressure due solely to the weight of air in a column above a given altitude [18].

$$\frac{dp}{p} = -\frac{g_0}{R\vartheta}\, dh$$

From the previous differential equation we can evaluate the pressure from the distribution of temperature with altitude (See Ref. [17]). In this way are obtained the pressure and density distributions as function of altitude for the ISA model.
The pressure distribution laws then are:

$$p_{ISA}(h) = p_0 \left(1 + \frac{\lambda_{ISA}}{\vartheta_0} h\right)^{-\frac{g_0}{R\lambda_{ISA}}} \qquad h \in [h_0, h_S)$$

Where $p_0 = p_{ISA}(h_0)$ =101325 Pa at the mean sea level.

$$p_{ISA}(h) = p_S \exp\left(-\frac{g_0}{R\vartheta_S}(h - h_S)\right) \qquad h \in [h_S, h_M)$$

$$p_{ISA}(h) = p_M \left(1 + \frac{\lambda_{ISA}}{\vartheta_M}(h - h_M)\right)^{-\frac{g_0}{R\lambda_{ISA}}} \qquad h \in [h_M, h_K)$$

And for the density we have:

$$\rho_{ISA}(h) = \rho_0 \left(1 + \frac{\lambda_{ISA}}{\vartheta_0} h\right)^{-\left(1+\frac{g_0}{R\lambda_{ISA}}\right)} \qquad h \in [h_0, h_S)$$

Where $\rho_0 = \rho_{ISA}(h_0)$ =1.2250 kg/m^3 at the mean sea level.

$$\rho_{ISA}(h) = \rho_S \exp\left(-\frac{g_0}{R\vartheta_S}(h - h_S)\right) \qquad h \in [h_S, h_M)$$

$$\rho_{ISA}(h) = \rho_M \left(1 + \frac{\lambda_{ISA}}{\vartheta_M}(h - h_M)\right)^{-\left(1+\frac{g_0}{R\lambda_{ISA}}\right)} \qquad h \in [h_M, h_K)$$

The equations shown above were used to calculate pressure and total air density during the flight from the altitude data.

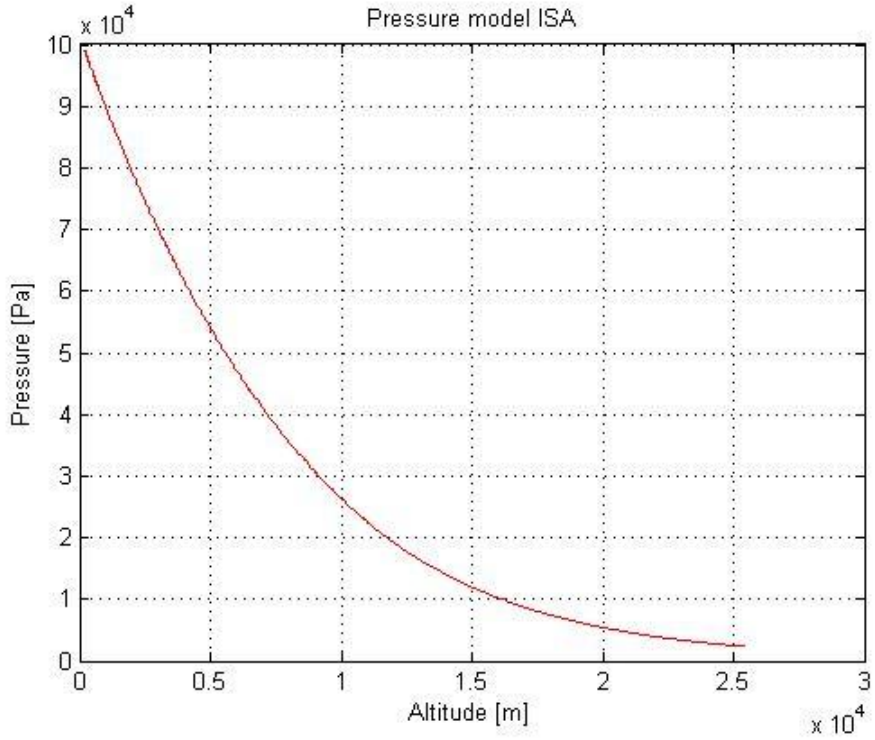

Figure 59 ISA pressure distribution calculated from flight data altitude

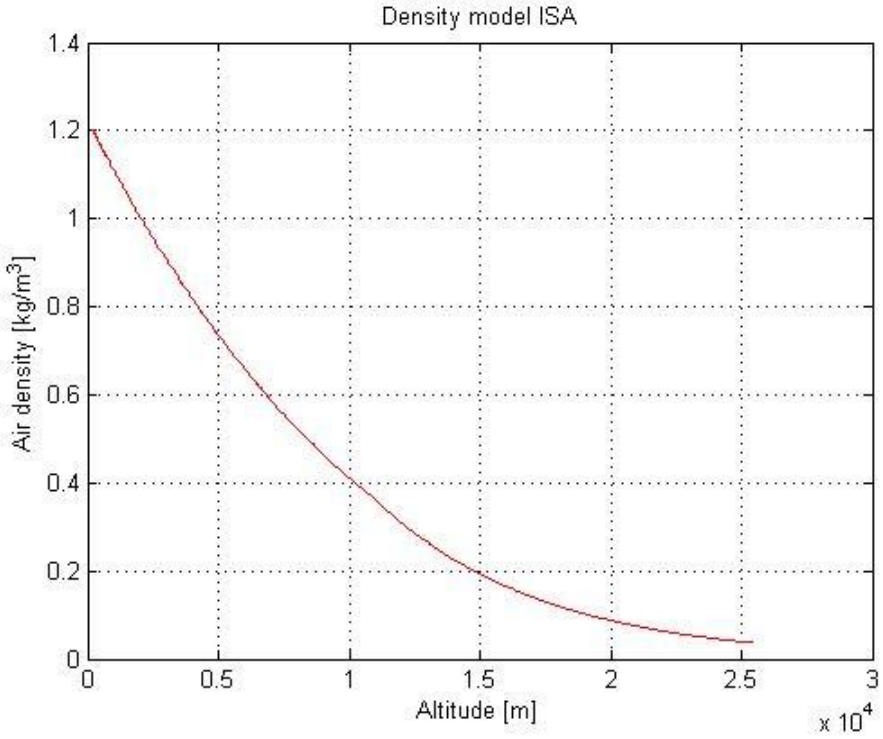

Figure 60 ISA density distribution calculated from flight data altitude

The following table shows pressure and density values at different altitudes for the ISA model.

Altitude (m)	Pressure (Pa)	Density (m/kg^3)
0	101325	1,2250
5000	54019	0,7361
11000	22632	0,3639
20000	5474	0,0880
25000	2511	0,0394
32000	868	0,0132

Table 35 ISA pressure and density at different altitudes

A preliminary comparison has been performed between altitude calculated by pressure measurements using the inverse relation for the ISA model and altitude from the GPS of the IMU. In the following figure this comparison is shows: the disturbances described in the paragraph 4.1.1 are quite evident, but the trend of altitude provided by GPS (black curve) and that obtained by pressure measurements (red curve) is the same.

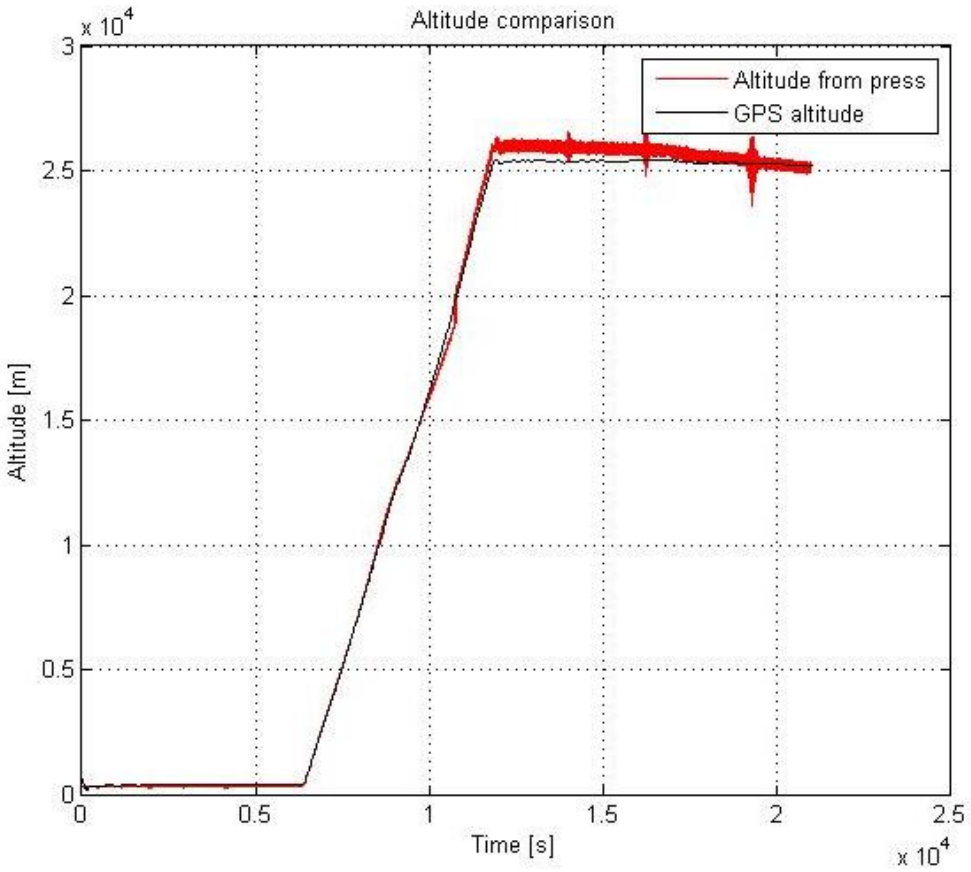

Figure 61 Altitude from GPS and from pressure vs time

Due to the low temperatures of the site and season, the standard ISA has been shifted by a $\Delta\vartheta$ = 5°C, so this is a off-ISA atmosphere; the correction is necessary for the troposphere

layer. In the first layer of troposphere then the linear dependency between altitude and temperature becomes:

$$\vartheta(h) = (\vartheta_0 + \Delta\,\vartheta) + \lambda_{ISA} h$$

Applying the correction above, we obtain the following values of temperature at different altitudes:

Altitude (m)	Temperature (K)	Temperature (°C)
0	283.15	10
5000	250.65	-22.5
11000	211.65	-61.5
20000	211.65	-61.5
25000	216.65	-56.5
32000	223.65	-49.5

Table 36 Temperatures at different altitudes with $\Delta\,\vartheta$ applied

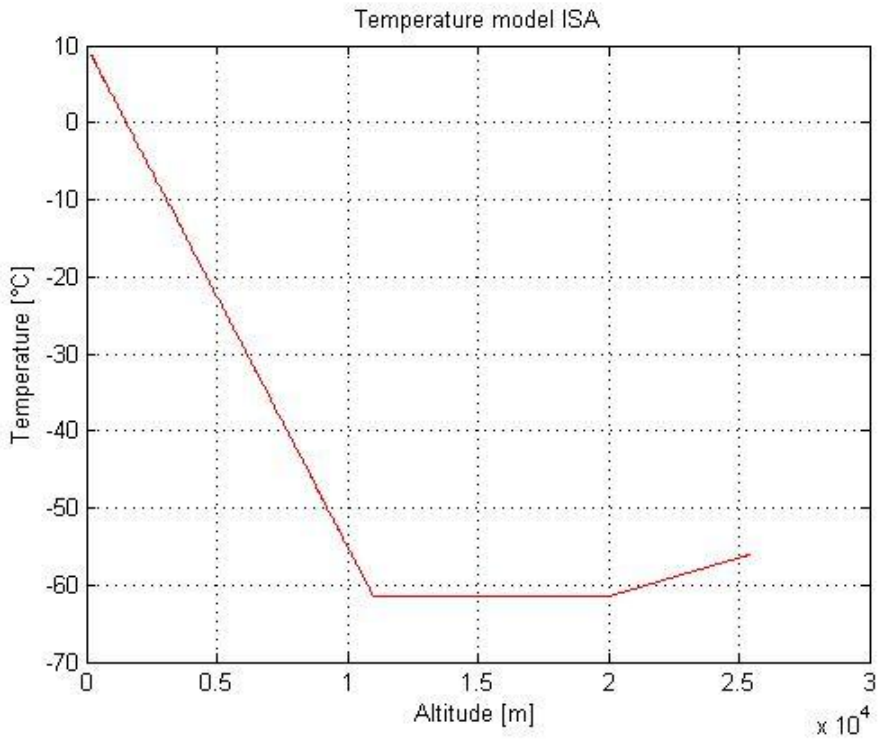

Figure 62 Off- ISA temperature distribution calculated from flight data altitude

NRLMSISE-00

The NRLMSISE-00 model adopted is the empirical, global model of the Earth's atmosphere from ground to space based on the previous MSISE-90.

It models the temperatures and densities of the atmosphere's components. A primary use of this model is to aid predictions of satellite orbital decay due to atmospheric drag.
NRL stands for the US Naval Research Laboratory. MSIS stands for Mass Spectrometer and Incoherent Scatter Radar respectively, the two primary data sources for development of earlier versions of the model. E indicates that the model extends from the ground through exosphere and 00 is the year of release.
The MSISE-90 model describes the neutral temperatures and densities in Earth's atmosphere from ground to thermospheric heights. Below 72.5 km the model is primarily based on the MAP Handbook tabulation of zonal average temperature and pressure by Barnett and Corney, which was also used for the CIRA-86. Below 20 km these data were supplemented with averages from the National Meteorological Center (NMC) [19].

The input parameters of the model are:

- year and day
- time of day (UT seconds)
- altitude
- latitude
- longitude
- 81 days *average F10.7* solar flux
- *daily F10.7* solar flux for previous day
- daily magnetic index

The input parameters were provided by the GPS data during the flight (altitude, latitude, longitude) of 25th September 2012 with UT time from the switch-on of the experiment on the launch pad.
The effects of *daily F10.7* and *average F10.7* are not large or established below 80 km; therefore, for the atmospheric analyses performed is set the default value of 150. These values correspond to the 10.7 cm radio flux at the actual distance of the Earth from the Sun. Also for the daily magnetic index is set the default value of the model function.
The output parameters of the model are:

- Helium Number density
- Oxygen (O) Number density
- Oxygen (O_2) Number density
- Nitrogen (N) Number density
- Nitrogen (N_2) Number density
- Argon Number density
- Hydrogen (H) Number density
- total mass density
- anomalous Oxygen number density

- exospheric temperature
- temperature at altitude

The outputs of interest for comparison with the collected measurements are temperature and total mass density versus altitude during flight. The following figures show the temperature and density profiles obtained from the flight data altitude.

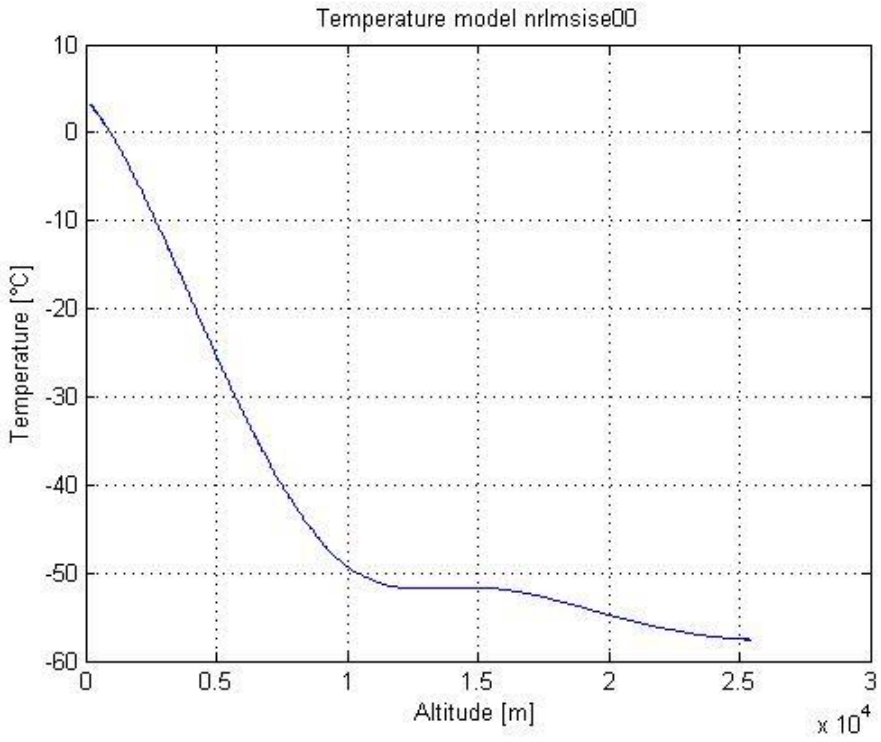

Figure 63 NRLMSISE-00 temperature distribution calculated from flight data

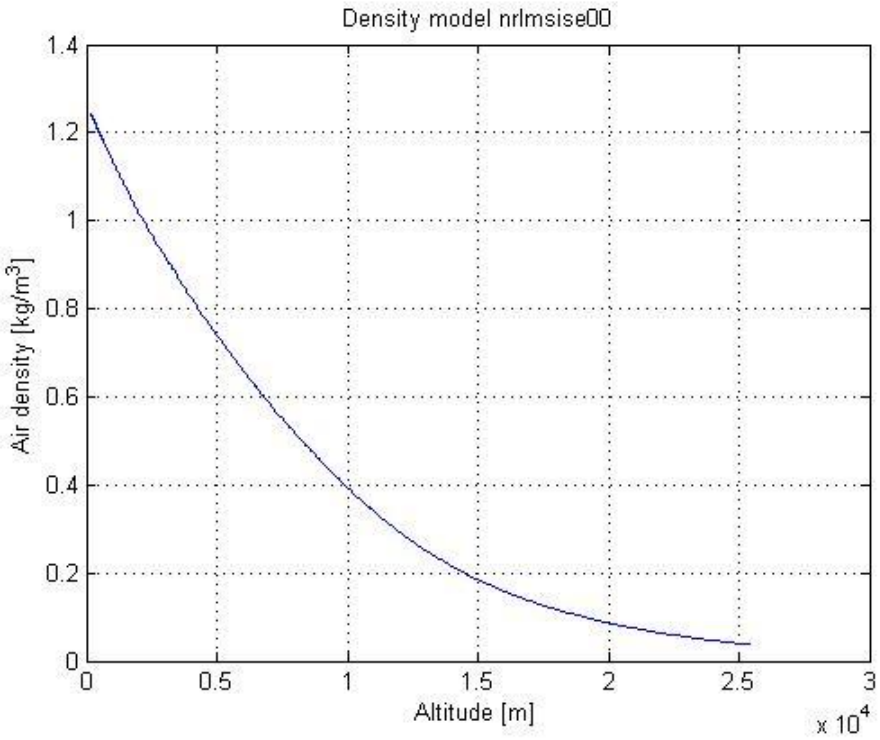

Figure 64 NRLMSISE-00 density distribution calculated from flight data

4.2.1.3 Comparison and discussion

A first comparison has been performed among all temperature measurements provided by the external sensors on-board. It can be seen that data collected by the fine RTD sensor and the coarse reference sensor are characterized by a similar trend since the beginning until the middle and final phases, when temperature starts increasing.

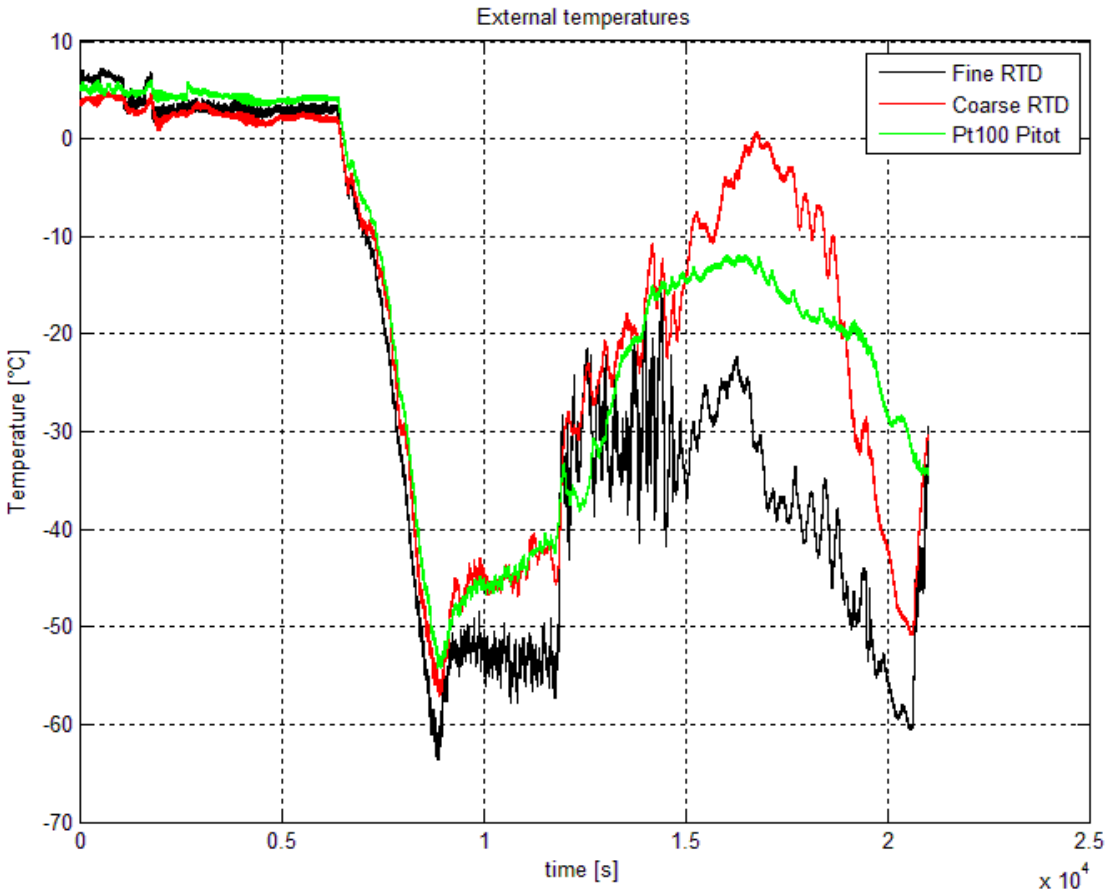

Figure 65 External temperatures vs time from switch on

The different behaviour with respect to the fine RTD can be explained:

- Coarse reference sensor was placed on the titan support of the innovative RTD sensor (therefore measurements are affected by the time-constant of the titanium support) and insulated w.r.t. to the external air by means of kapton;
- Pt100 Pitot was indeed placed on the aluminum surface of the Pitot tube (therefore measurements are affected by the time-constant of the aluminum support), thermally insulated w.r.t. the external environment by means of kapton and aluminum tape and with different sun exposure.

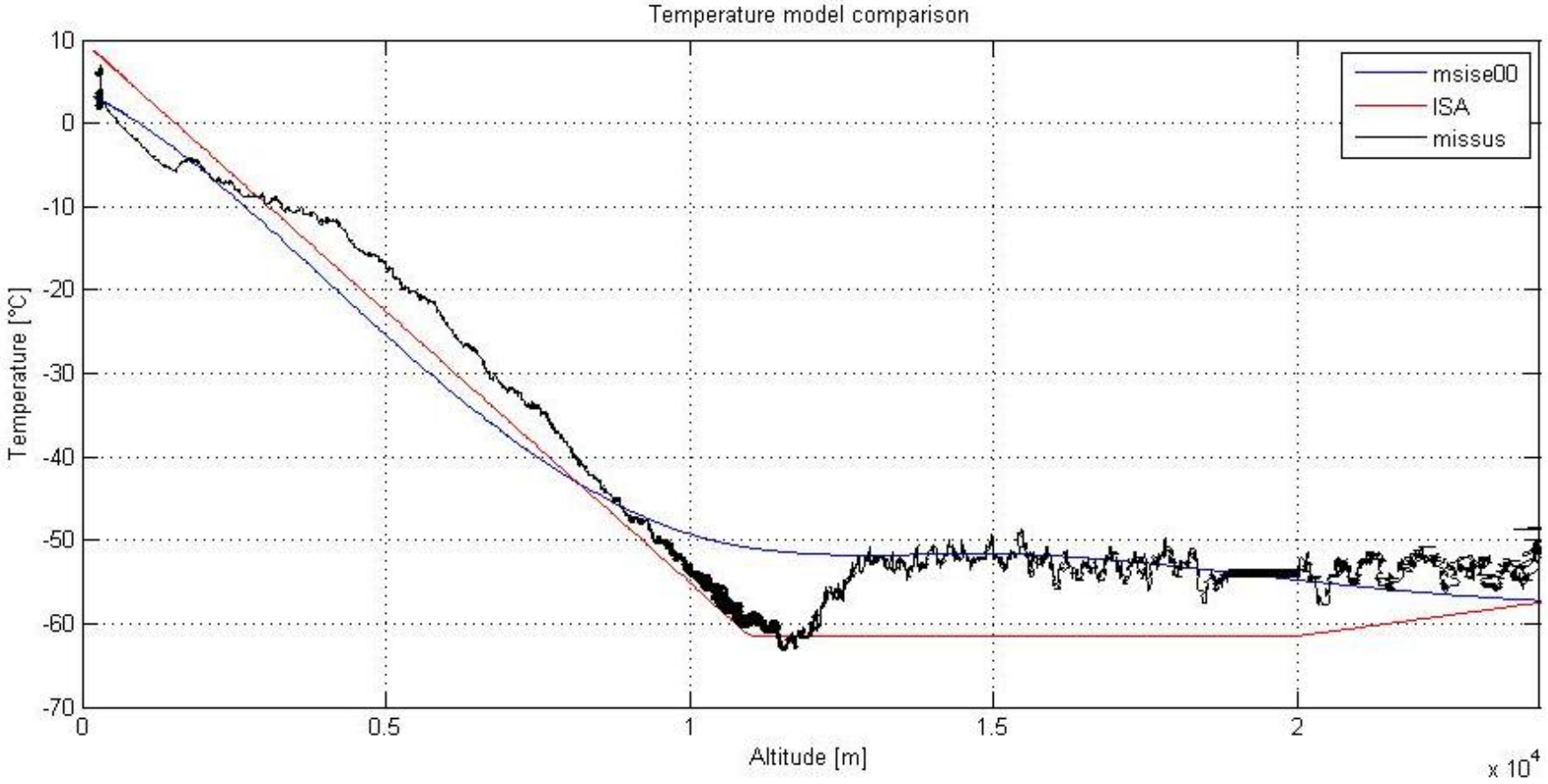

Figure 66 Temperatures from models and from MISSUS vs altitude

The previous figure shows the comparison between temperatures provided by MISSUS innovative RTD (black curve), ISA (red curve) and NRLMSISE-00 model (blue curve). Innovative RTD measurements have been taken into account since it is able to measure fast temperature fluctuations and it is the only sensor directly exposed to the atmosphere.
The following table summarizes the input of the models and the MISSUS data used for the comparison in Figure 66.

TYPE	INPUT
ISA	• Altitude during flight (h)
NRLMSISE	• Year and day of flight • Time of day UTC during flight (t) • Altitude during flight (h) • Latitude during flight • Longitude during flight
MISSUS	• Temperatures (T) measured during flight at the correspondent altitude (h) obtained by pressure measurements (p)

Table 37 Description of the input of the atmospheric models and MISSUS data for Figure 66

In the troposphere zone the temperature trend provided by MISSUS is quite different from the models ones, but it has to take into account the adverse meteorological condition of the day, in particular the presence of clouds and high humidity, (see CALIPSO VFM in Figure 75). Anyway the mean slope of the MISSUS curve is the same of the standard ISA model.

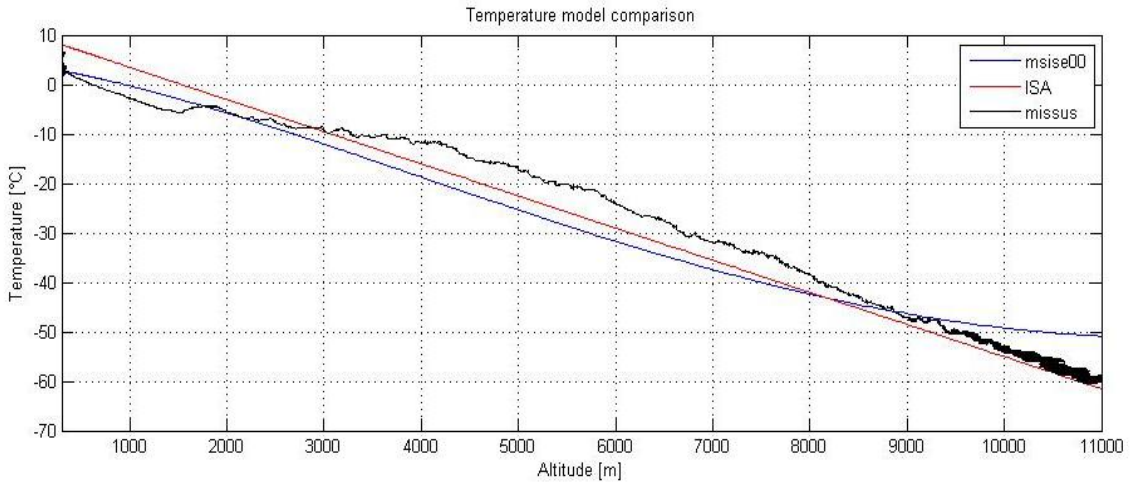

Figure 67 Particular of the temperature trends vs altitude in the troposphere

A drop in the temperature of the atmosphere is evident in the layer between 10 km and 13 km.

The same decreasing trend is observed also for the other temperature sensors. This drop is present on the correspondent foreseen tropopause and a positive not expected lapse rate is observed (see the figure below). This discrepancy is described hereafter. In the stratosphere layer, the trend of the temperature provided by MISSUS is compliant with values provided by the NRLMSISE-00 model.

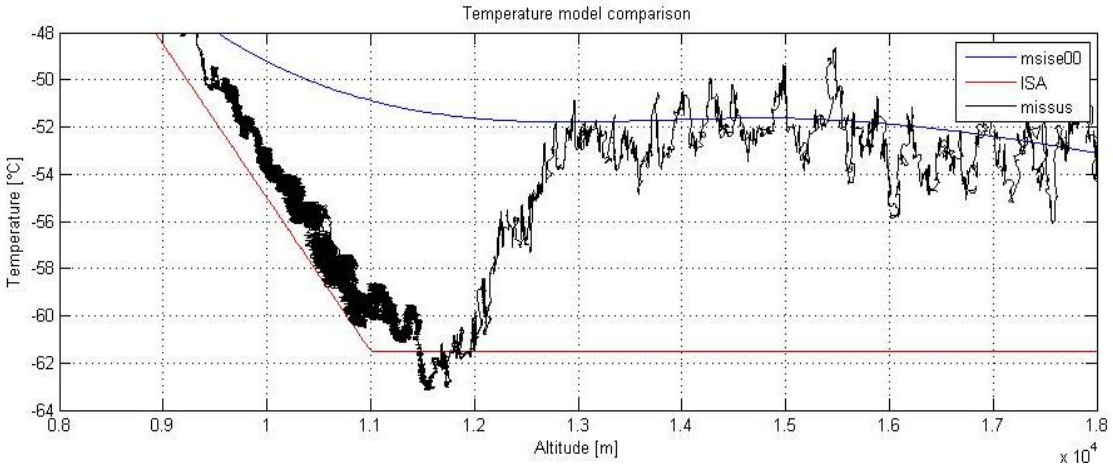

Figure 68 Particular of the temperature drop observed

The following figure shows the temperature profile provided by all MISSUS temperature sensors and the two models. As described before, the drop in temperature and the following increasing trend is well evident.

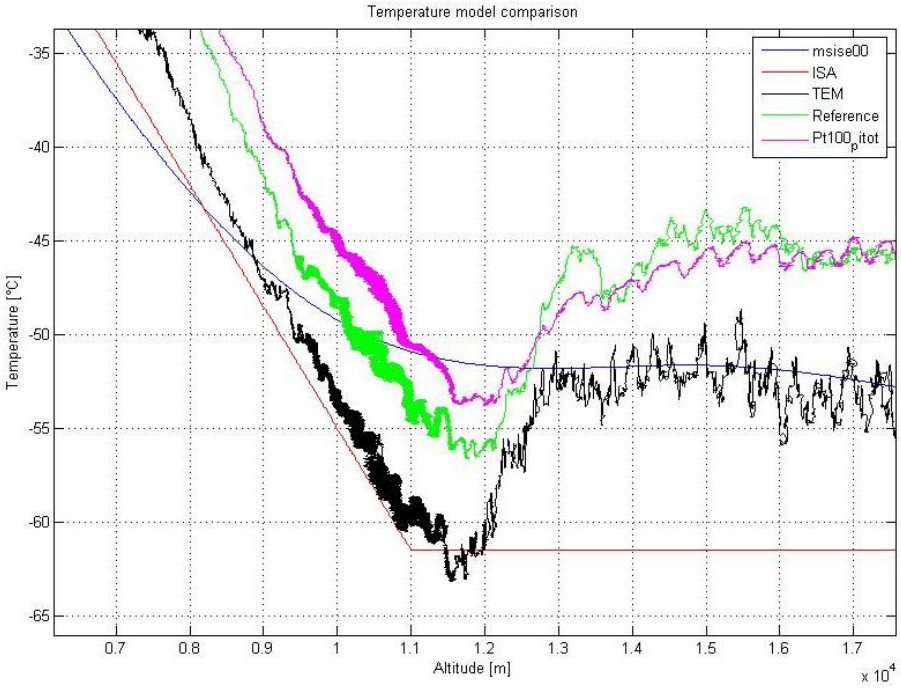

Figure 69 Particular of the temperature drop observed for all MISSUS Temperature sensors

Density has then been obtained by the perfect gas law in which the input parameters are the measured ones.

$$\rho_{air} = \frac{p_{MISSUS}}{RT_{MISSUS}}$$

The result has been compared with the outputs of the atmospheric models described in the previous section.

The following table summarizes the input of the models and the MISSUS data used for the comparison of the atmospheric density (see Figure 70).

TYPE	INPUT
ISA	• Altitude during flight (h)
NRLMSISE	• Year and day of flight • Time of day UTC during flight (t) • Altitude during flight (h) • Latitude during flight • Longitude during flight
MISSUS	• Temperatures (T) and pressures (p) measured during flight

Table 38 Description of the input of the atmospheric models and MISSUS data for Figure 70

The following figure shows the good match between the output obtained from MISSUS sensor measurements and models.

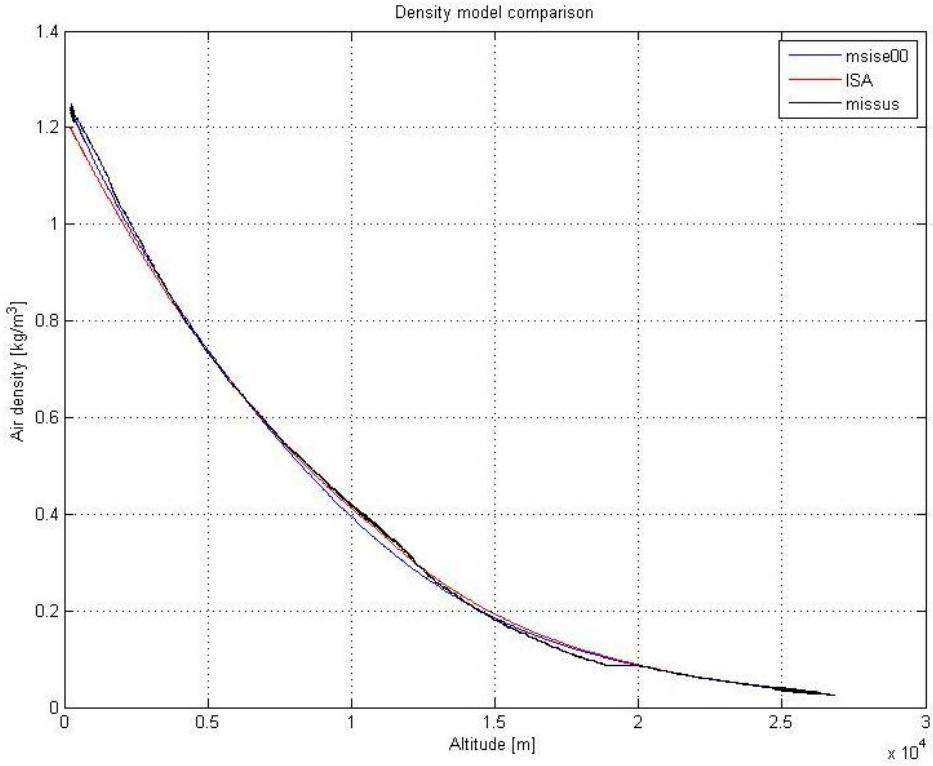

Figure 70 Density from models and from MISSUS vs altitude

The following discrepancies are evidenced:

- in the first layer of troposphere, probably due to the high humidity that causes a deviation from the ideal gas law;
- layer around 10 km, due to the discrepancies between measured temperatures and those predicted by the models (see previous graphs);
- before 20 km (hereafter explanation is attributed to higher measured temperatures w.r.t. predicted ones).

The beginning of the Tropopause zone is clearly visible as expected in the zone between 10 km - 13 km, as described by Zangl and Hoinka (see Ref. [19]) .

Anyway in this layer RTD measurements evidence an inversion of the temperature gradient (positive) after a drop in temperature (as described before). This behavior deviates from the NRLMSISE-00 (the drop is about 10 K, see Figure 68), but then above 13 km of altitude the trend is compliant with the model.

This aspect has been investigated to verify the measurements provided by the sensor, trying to correlate this variation to a physical phenomenon, which could have caused this decreasing trend.

The possible scenarios formulated consider the presence of ice clouds, cold stable layers, winds.

1) The first hypothesis takes into account the data collected by CALIPSO satellite. CALIPSO has been providing nearly continuous measurements of the vertical structure and optical properties of clouds and aerosols from 2006. The CALIPSO payload consists of three co-aligned, near-nadir viewing instruments: a 2-wavelength polarization-sensitive lidar, an imaging infrared radiometer (IIR), and a high-resolution wide field camera (WFC). CALIOP is the name of the CALIPSO lidar and is an acronym for *Cloud-Aerosol Lidar with Orthogonal Polarization.* The lidar profiles provide information on the vertical distribution of aerosols and clouds, cloud particle phase, and classification of aerosol size. The CALIOP laser transmitter subsystem transmits laser light simultaneously at 532 nm and 1064 nm at a pulse repetition rate of 20.16 Hz. The CALIOP receiver subsystem measures backscatter intensity at 1064 nm and at two orthogonally polarized components of the 532 nm backscattered signal (see Figure 72). The IIR provides medium spatial resolution nadir viewing images at 8.65, 10.6, and 12.05 m, providing information on cirrus cloud particle size and infrared emissivity. The WFC digital camera collects daytime high spatial resolution imagery in the 620 - 670 nm wavelength range and is used to ascertain cloud homogeneity, aid in cloud clearing, and provide meteorological context (See Ref. [25]) .

   CALIPSO orbits in formation with other spacecraft in the A-Train satellite constellation, and provides complementary, near-simultaneous, observations with the other active and passive instruments in the constellation to better understand the effects of clouds and aerosols on climate, weather, and air quality.

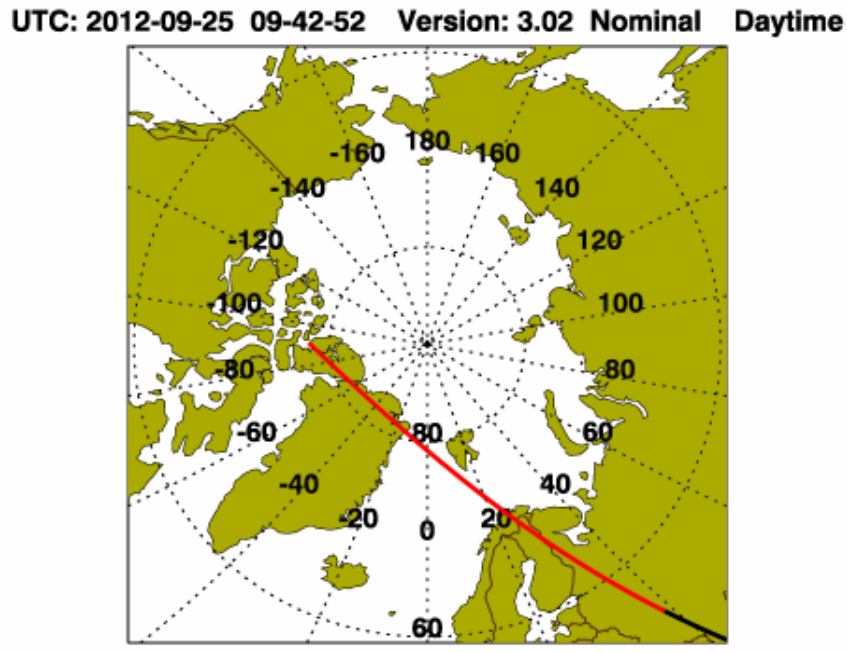

Figure 71 Tracking on ground of CALIPSO satellite

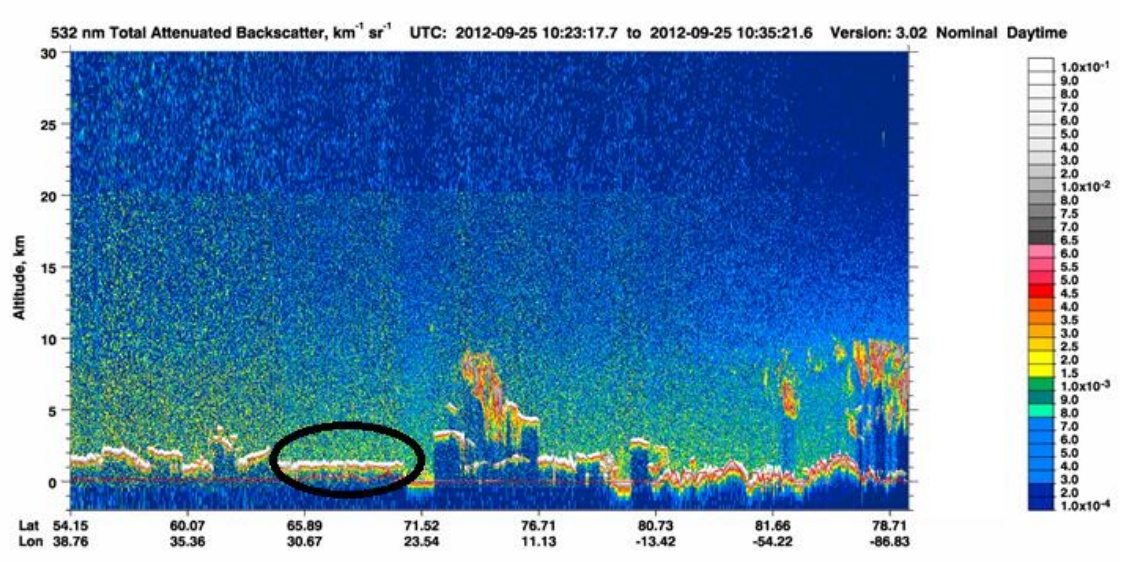

Figure 72 Total Attenuated Backscattered at 532 nm of CALIPSO revealing the presence of clouds in a narrow region crossed during BX flight

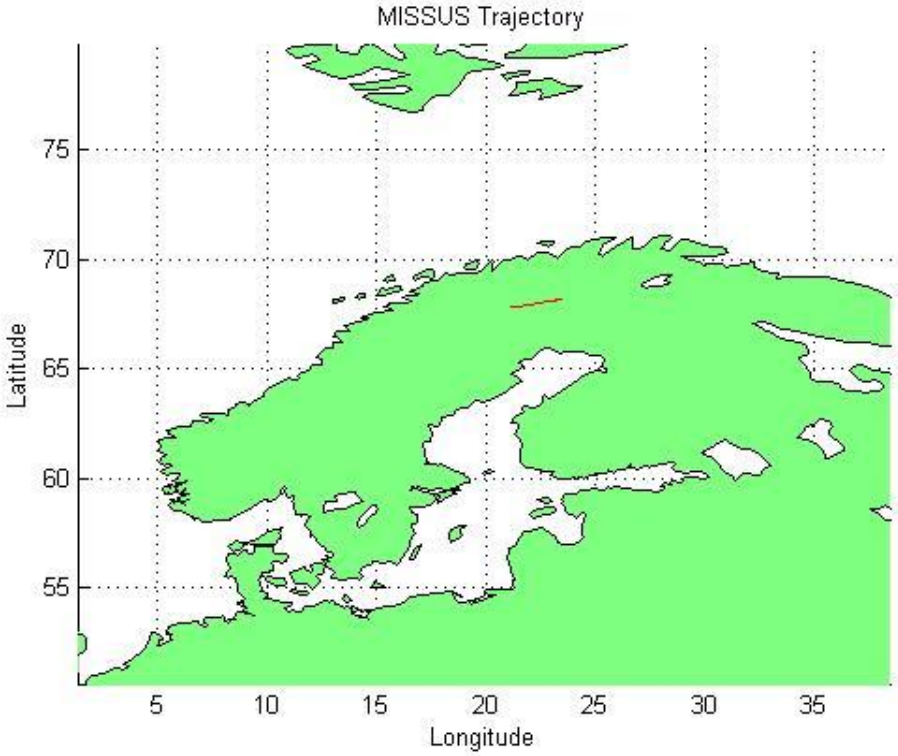

Figure 73 Tracking on ground of MISSUS

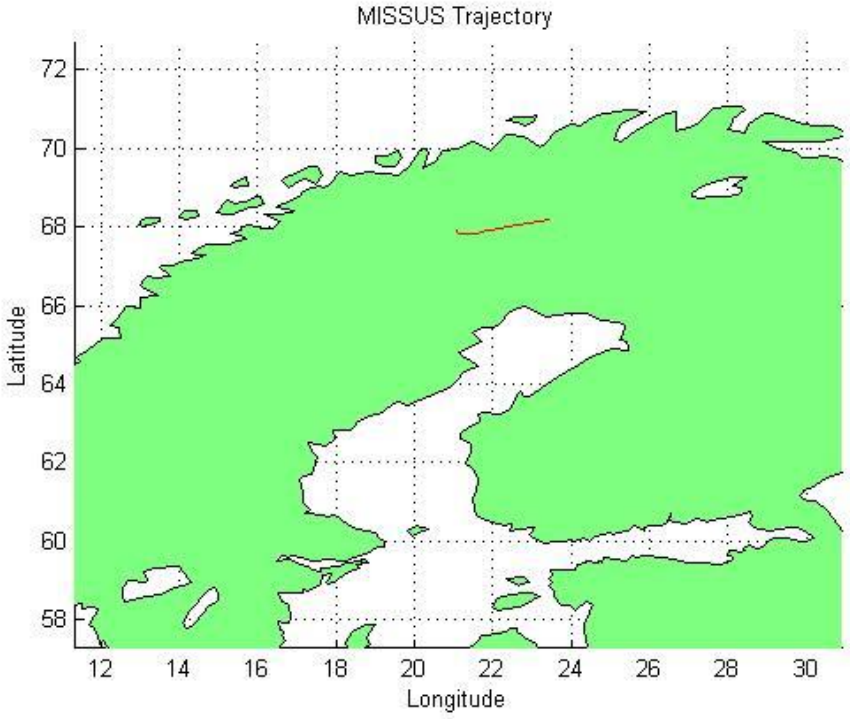

Figure 74 Particular, tracking on ground of MISSUS

CALIPSO data revealed clouds in low troposphere layers in a narrow region crossed during BX15 flight from 10:23 to 10:35 UTC in the Polar area and higher icy clouds around 10 km (see Figure 75 and Figure 76).

The latter are incompatible with BX15 ascent trajectory, which doesn't match with CALIPSO data (icy clouds should have been characterized by a speed of 100 m/s to interfere with BX15 trajectory).

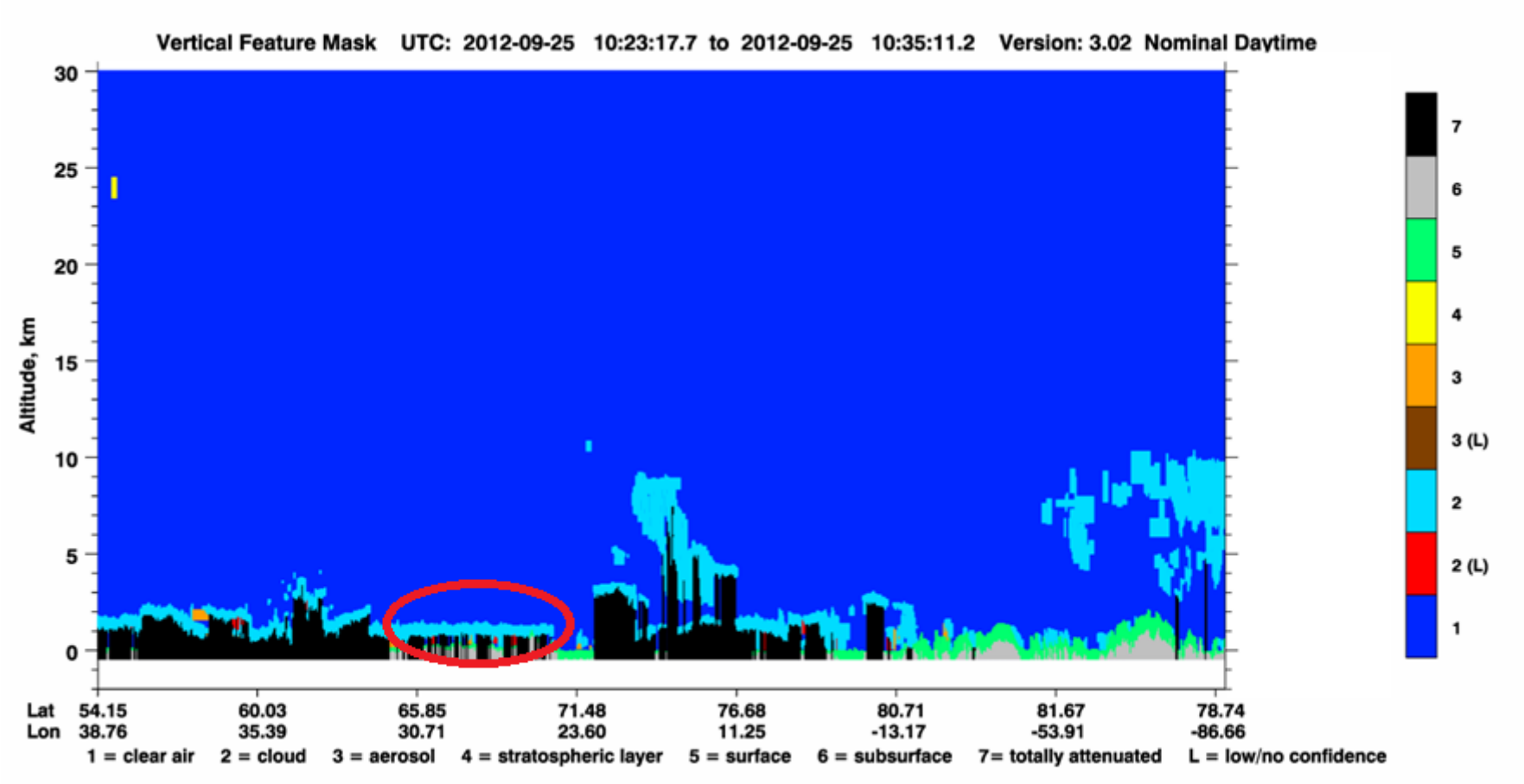

Figure 75 VFM of CALIPSO shows the air profile and clouds, in the circle the low troposphere layer of clouds present during the day of flight

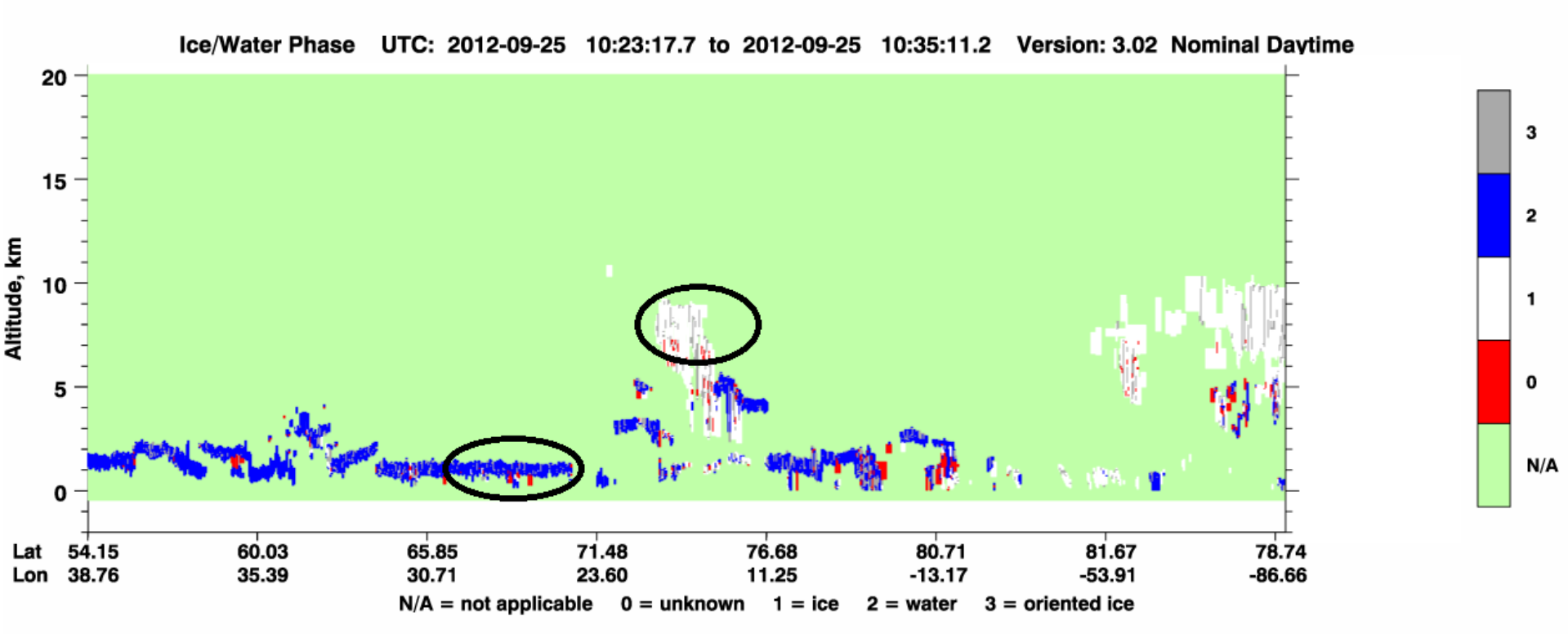

Figure 76 VFM of CALIPSO shows the clouds type (ice/water), in the circle the point of interest for the analysis

2) The second hypothesis considers the presence of a layer of stable cold air.
   Other temperature profiles during the day have been analyzed: the same drop was measured by PTU probes before launch and during flight.
   The amplitude of this drop is about 10°C for the first probe before flight, about 6°C for the second one during the flight.

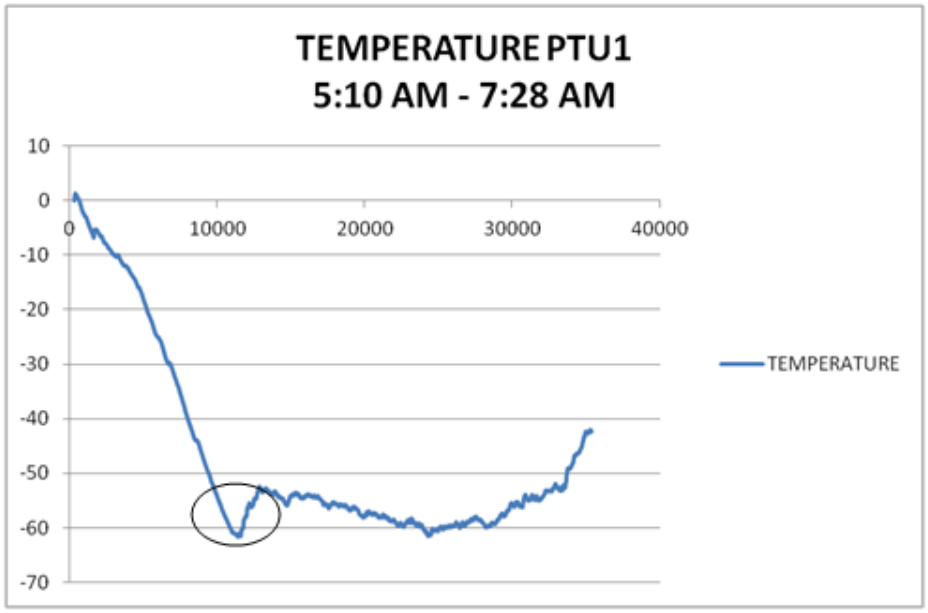

Figure 77 Temperature profiles vs altitude detected by PTU1 ozone sonde

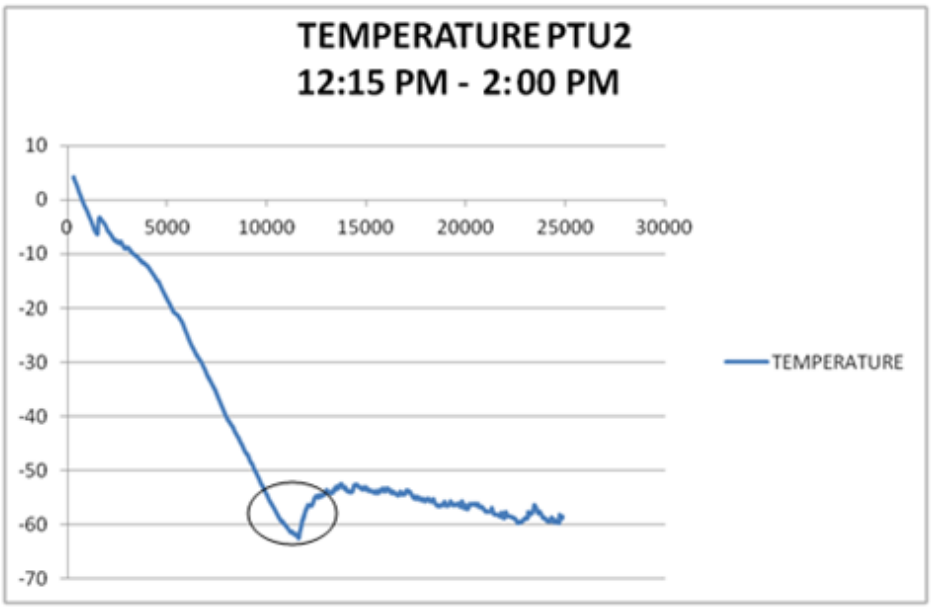

Figure 78 Temperature profiles vs altitude detected by PTU2 ozone sonde

3) The third hypothesis supposes that the gondola crossed a region where stronger horizontal winds are present.
   This is confirmed by PTU wind measurements provided by EuroLaunch during the day of flight, between 8-14 km.
   The drop is observed at the same altitude of winds with higher speed, more than 12 m/s. This leads to the conclusion that also during BX15 flight, the region between 10-13 km was crossed by stronger winds that caused increase in convective thermal exchange.
   The same behavior was also observed in the high resolution vertical profiles of temperature and horizontal wind speed measured by radiosondes launched at Sodankyla, Finland, in January 2001 (See Ref. [27]). This is a further proof of this kind of temperature trend.

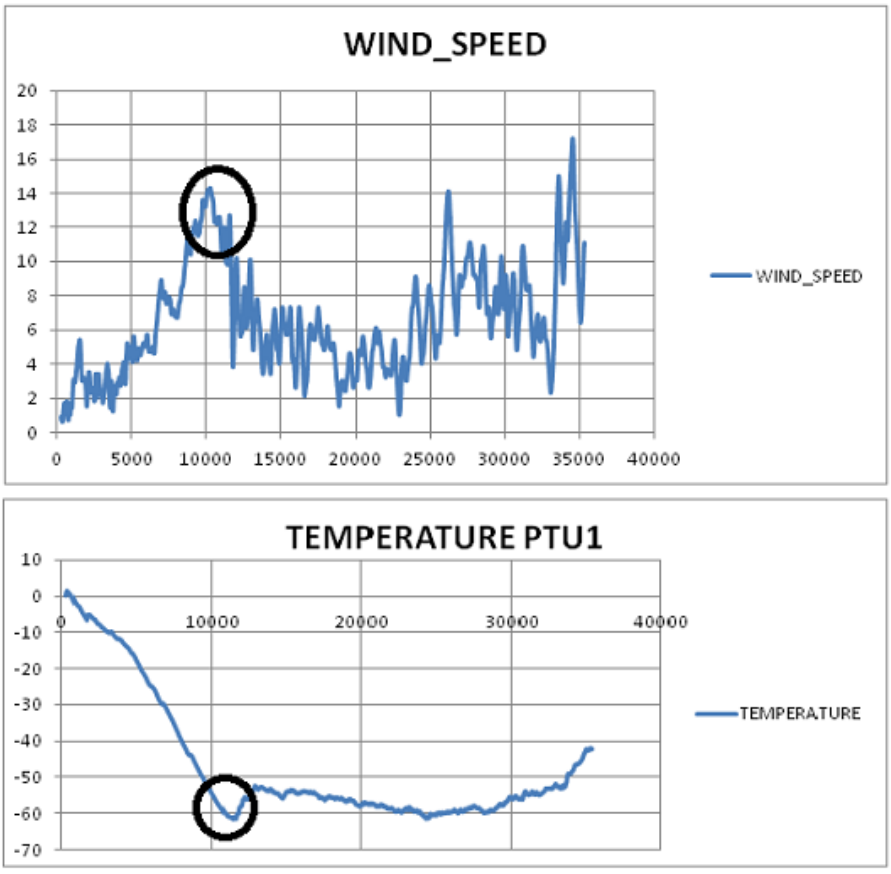

Figure 79 Comparison between wind and temperature profile vs altitude for PTU1, winds are around 14 m/s in the zone of interest, it can be seen the correspondence with drop in temperature

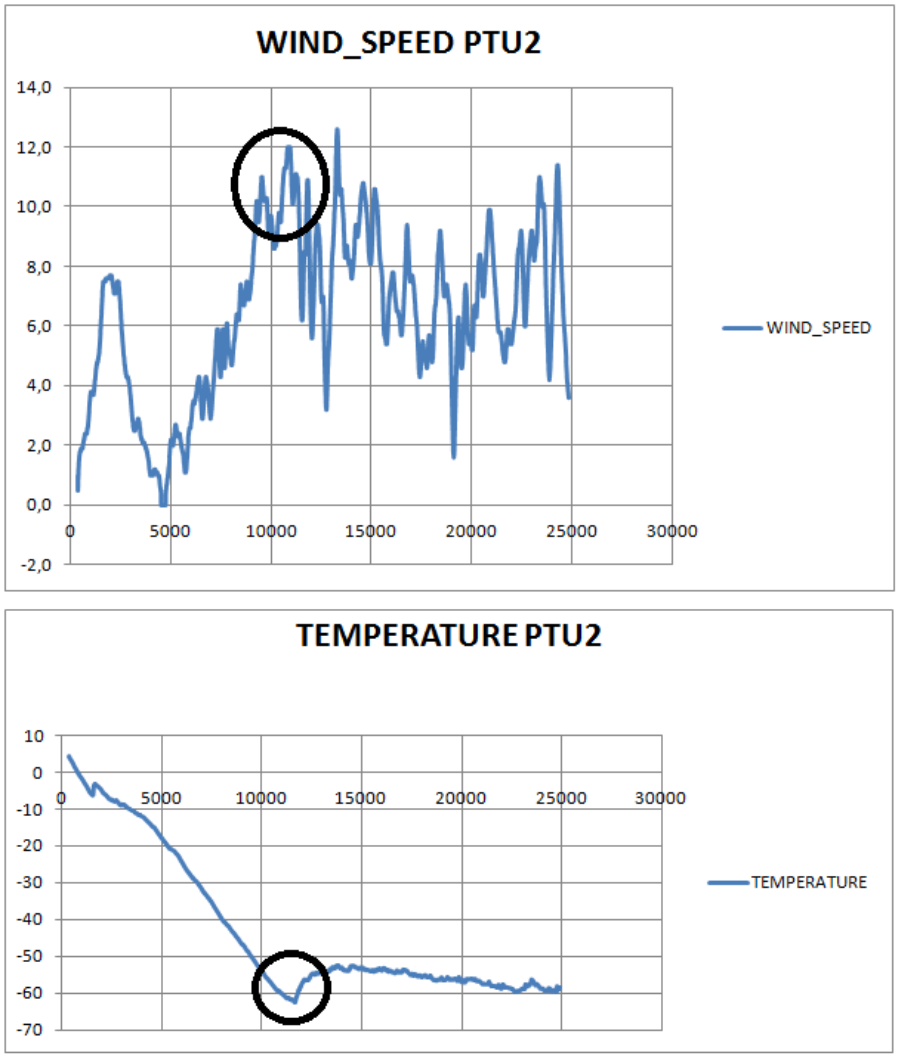

Figure 80 Comparison between wind and temperature profile vs altitude for PTU2 (winds less than 12 m/s); it can be seen the correspondence with drop in temperature

4.2.1.4 Atmospheric stability

The atmosphere is considered stable, stably stratified, when a parcel of air displaced vertically decelerates and returns to its original position. The atmosphere is unstable when a displaced parcel accelerates in the direction in which it is displaced. The atmosphere is neutral when a parcel does not accelerate or decelerate after being displaced.

When the atmosphere is stable near the surface, pollution builds up, since air parcels cannot accelerate out of the stable layer to disperse the pollution. Stability also inhibits clouds of vertical development from forming. When the atmosphere is unstable, emitted pollutants accelerate vertically, decreasing their concentration near the surface. Furthermore clouds of vertical development can form in unstable air.

Stability of the atmosphere during flight has been studied considering two main parameters, already adopted in previous balloon campaigns for RTD innovative temperature sensors (see Ref. [26]):

- Potential temperature,
- Brunt-Vaisala frequency

Potential Temperature

Potential temperature is define as the temperature an unsaturated air parcel attains if it is brought adiabatically from its altitude down to a pressure of 1 bar.
Potential temperature is derived from the first law of thermodynamics and the perfect gas law in an adiabatic process.

$$\frac{dT}{T} = \left(\frac{R}{c_p}\right)\frac{dp}{p}$$

Integrating the previous differential equation from T_0 to T and p_0 to p yields Poisson's equation,

$$T = T_0\left(\frac{p}{p_0}\right)^{\frac{R}{c_p}} = T_0\left(\frac{p}{p_0}\right)^{\kappa}$$

Where

$$\kappa = \frac{c_p - c_v}{c_p} = 0.286$$

When p_0=1 bar, T_0 is called the potential temperature of dry air, since here is not considered the presence of water vapour and becomes

$$\theta_p = T\left(\frac{p_0}{p}\right)^{\kappa}$$

While for the potential temperature of moist air must be applied a correction on the exponential term

$$\theta_{pm} = T\left(\frac{p_0}{p}\right)^{\kappa(1-0.251q_v)}$$

Since q_v, i.e the specific humidity, is usually smaller than 0.03 kg kg^{-1}, neglecting q_v causes an error in κ of less than 0.75 percent [18].
Thus, for simplicity, is usually used the potential temperature of dry air, even when water vapor is present.
For this reason θ_p was used for the stability analysis, where T and p are the temperature and pressure measured during flight by MISSUS sensors.

Potential temperature is conserved (stays constant) if an unsaturated air parcel is displaced adiabatically.

Thus, the stability criteria in terms of potential temperature are:

$$\frac{\partial \theta_p}{\partial h} = \begin{cases} < 0 & \text{unstable} \\ = 0 & \text{neutral} \\ > 0 & \text{stable} \end{cases}$$

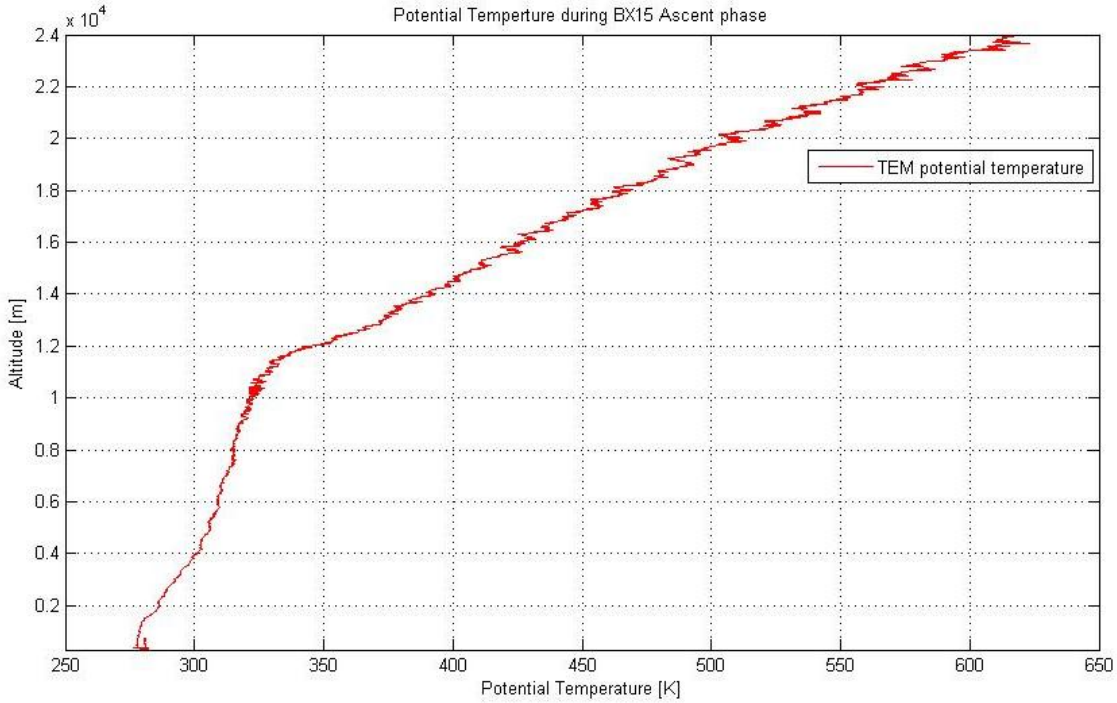

Figure 81 Potential temperature versus altitude for MISSUS during flight

Vertical stability of dry atmosphere is characterized by a constant variation of θ_p (9.8 K/km), whereas, during the ascent phase is often constant, due to convective exchange mechanisms.

The region up to 3000 m shows several convective layers (θ_p is constant), visible in the following graphs.

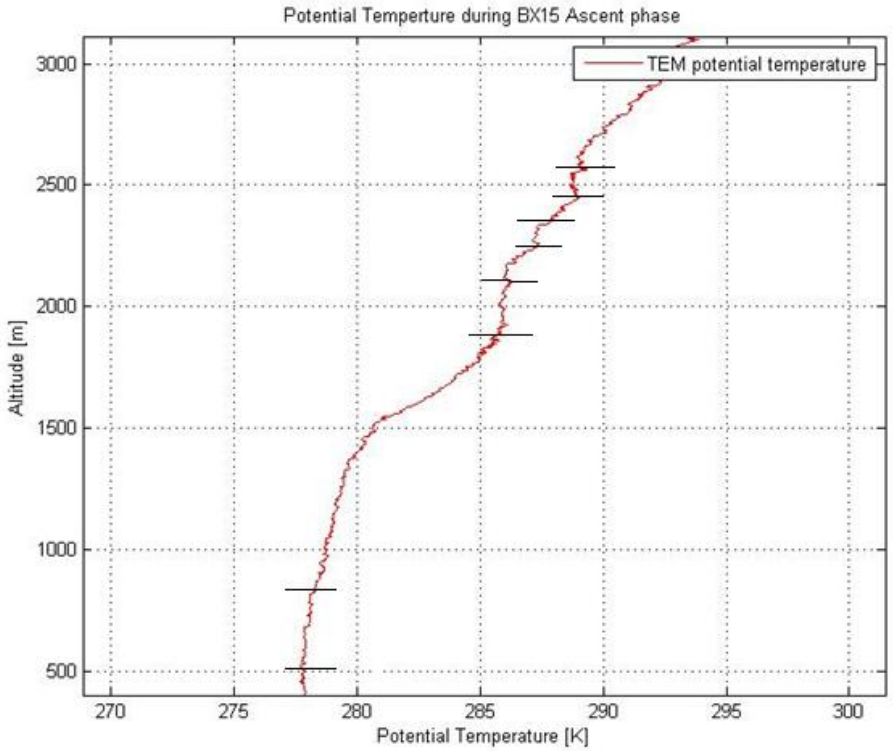

Figure 82 Alternation of convective and stable layers between 500 m and 3000 m

In particular is evident the first layer near the surface (Ekman layer), 500m-800m, in which interactions between ground and atmosphere take place.

The other convective layers that alternate with stable layers are visible between 1900m-2100m; 2260m-2330m; 2440m-2550m.

The figure above shows the alternation of convective and stable (black lines) layers between 500 m and 3000 m.

Unstable regions, above 3000 m, are observed in the layers between 5700m-6200m and 7400m-8500m, see the following plot.

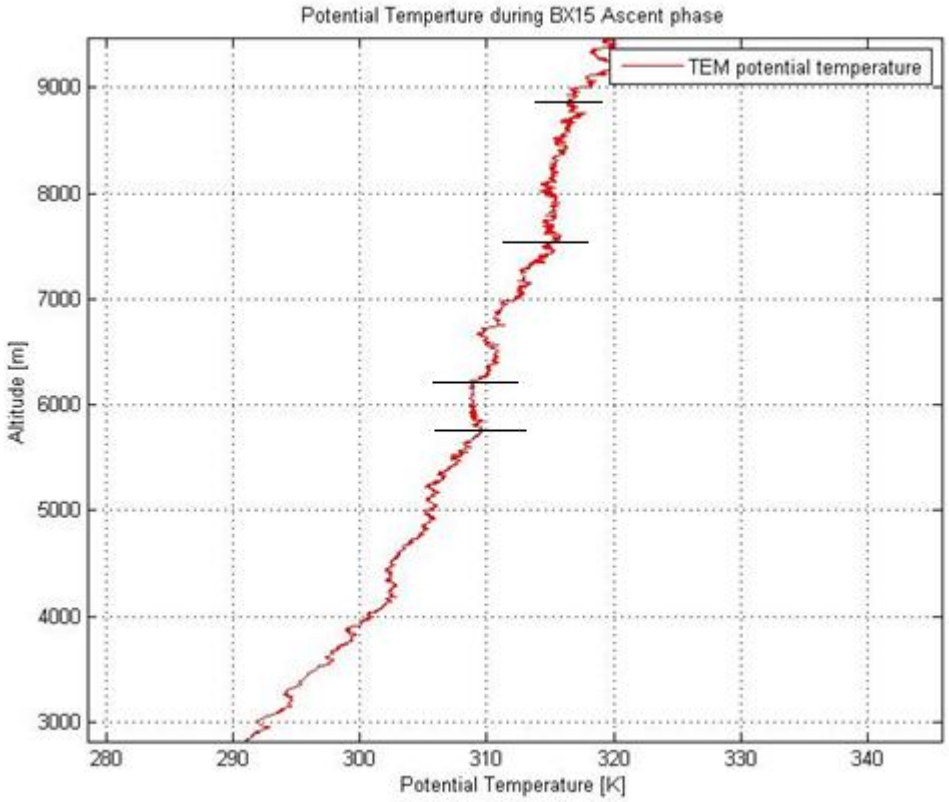

Figure 83 Potential temperature profile between 3000 m and 9000 m, the convective layers are delimited

This kind of behavior, i.e. the alternation of layers with constant and variable potential temperature, supports the presence and persistence of clouds. The day was cloudy and wet, as confirmed by the VFM of CALIPSO in the previous figures.

Even if the trajectory path of the satellite isn't exactly above the flight trajectory, it can be seen that a narrow area was covered by clouds, in particular low troposphere (see Figure 75).

Above the inversion layer (@12 km) a more stable behavior is observed as expected, with constant gradient of the temperature, typical of the stratosphere.

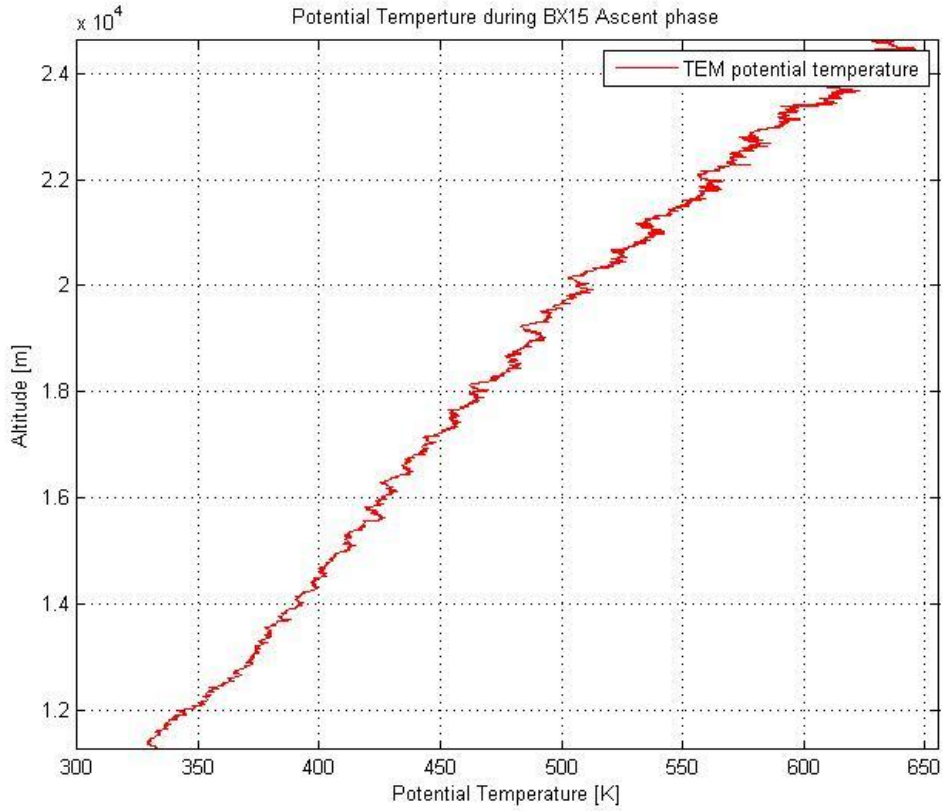

Figure 84 Potential temperature versus altitude in the stratosphere

Brunt-Vaisala frequency

Another way to determine the stability of atmosphere has been studied considering the Brunt-Vaisala frequency (buoyancy frequency). The Brunt-Vaisala square frequency is defined by the following relation:

$$N_{bv}^2 = g\frac{\partial \ln \theta_p}{\partial h} = \frac{g}{T}(\Gamma_d - \Gamma_{Flight})$$

Where

$$\Gamma_d = \frac{g}{c_p} \qquad \Gamma_{Flight} = -\frac{\partial T}{\partial h}$$

And g is the gravitational acceleration, T is the atmospheric measured temperature, c_p is the specific heat at a constant pressure (equal to 1004 J K^{-1} kg^{-1}) and h is the altitude.

If θ_p increases with increasing height ($\Gamma_d > \Gamma_{Flight}$), then $N_{bv}^2 > 0$, and the atmosphere is stable. In such a case, buoyancy acts as a restoring force, causing a perturbed parcel of air to oscillate about its initial altitude with a period $\tau = \pi/N_{bv}^2$.

During the oscillation, kinetic energy is exchanged with potential energy. The oscillations arising from buoyancy restoration are gravity waves.
If θ_p is constant with increasing altitude (N_{bv}^2= 0) the atmosphere is neutral, and displacements occur without resistance from a restoring buoyancy force.
If θ_p decreases with increasing altitude (N_{bv}^2< 0), the atmosphere is unstable, and a parcel's displacement increases exponentially with time. Anyway, for low values of the square of buoyancy frequency, the atmosphere tends to be unstable.

During flight instabilities are seen in the troposphere zone (considering mean trend), before the tropopause, as also confirmed by potential temperature analyses.
It can be seen that a stable behaviour characterizes the stratosphere, in which are present higher values of N_{bv}^2.

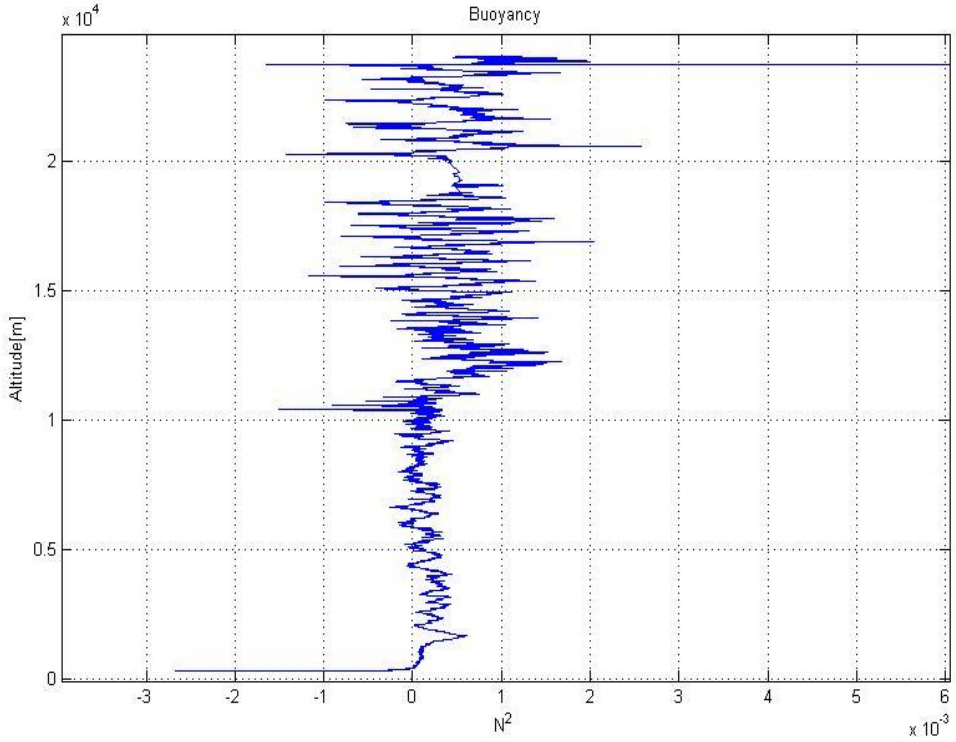

Figure 85 Square buoyancy frequency

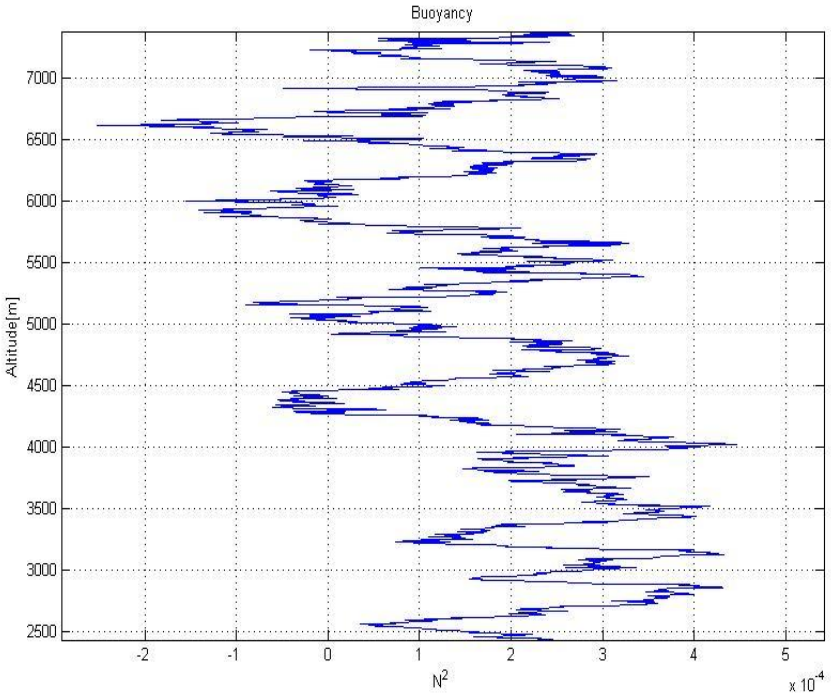

Figure 86 Particular of Square buoyancy frequency between 2500 m and 7000 m, instabilities can be seen from low and negative values

4.2.2 Correlation between yaw rotation and RTD Temperature

In order to see when the thermometer is illuminated by sunlight and to understand how the sun influences temperature measurement, the sun position has been evaluated during the cruise phase of BX15 balloon.

At high altitudes the heat exchange by convection is negligible and the temperature sensor measurements should be deeply affected by the incident solar flux.

The following figure shows the behavior for the temperature measurements of the innovative RTD sensor during flight, the relevant increases of temperature are pointed.

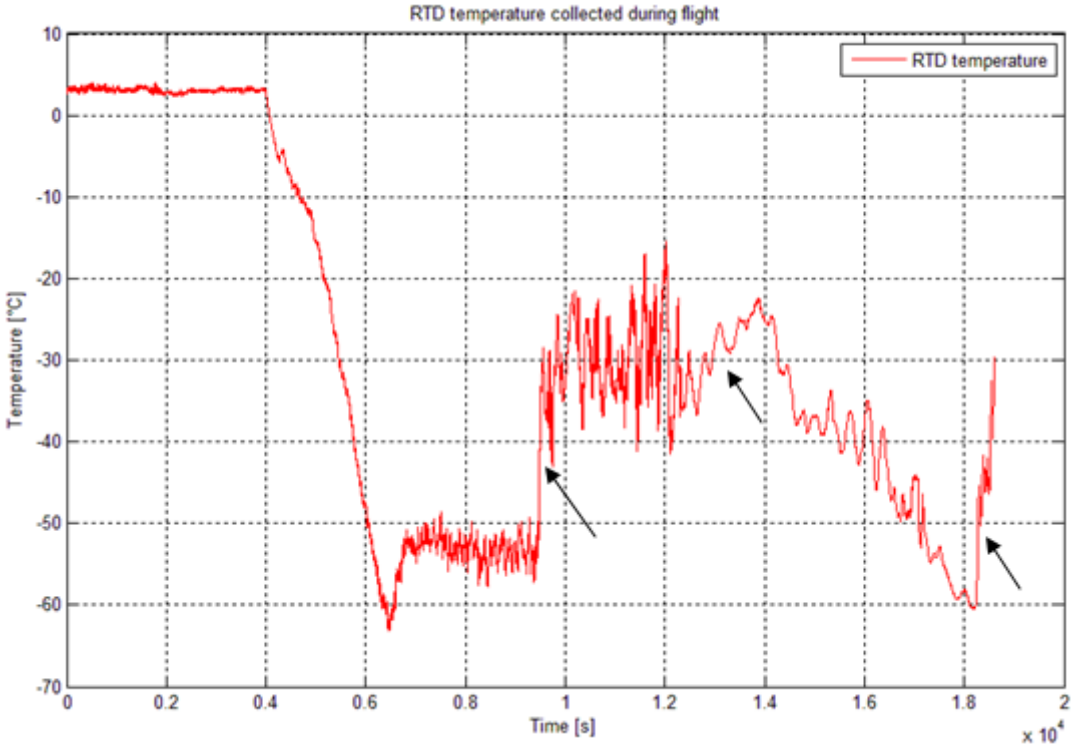

Figure 87 External temperature versus time and indication of the relevant temperature increases

4.2.2.1 Evaluation of the sun position and observations

The sun position during floating was calculated using the Solar position algorithm for solar radiation application by Reda et Andreas [29]. This algorithm (original creation by V. Roy) is based on numerical approximation of the exact equations.
The following table summarized the input of the algorithm.

INPUT	NOTES
TIME	
Year	
Month	
Day	Calendar day
Hour	Local hour
Minutes	
Seconds	
UTC	Offset hour from UTC
LOCATION (of the observer)	
Latitude	North of equator is positive
Longitude	Positive for east of

	Greenwich
Altitude	Above mean sea level

Table 39 Inputs of the sun position algorithm

The output parameters are the zenith angle in degrees from the vertical (0° vertical, 90° in plane) and the sun azimuth in degrees, eastward from the geographic north (N_{geo}=0°, S_{geo}=180°, angles in the range 0° up to 360°).

During the cruise phase the azimuth variation results:

$$207° < \alpha < 242°$$

while the zenith variation is

$$72° < z < 80°$$

The first value of the range corresponds to the UTC start instant of the floating phase (11:49 UTC), the second value to the last UTC instant of MISSUS operative life (14:22 UTC).
The following figure shows the sun position (zenith and azimuth angles) as a function of time.

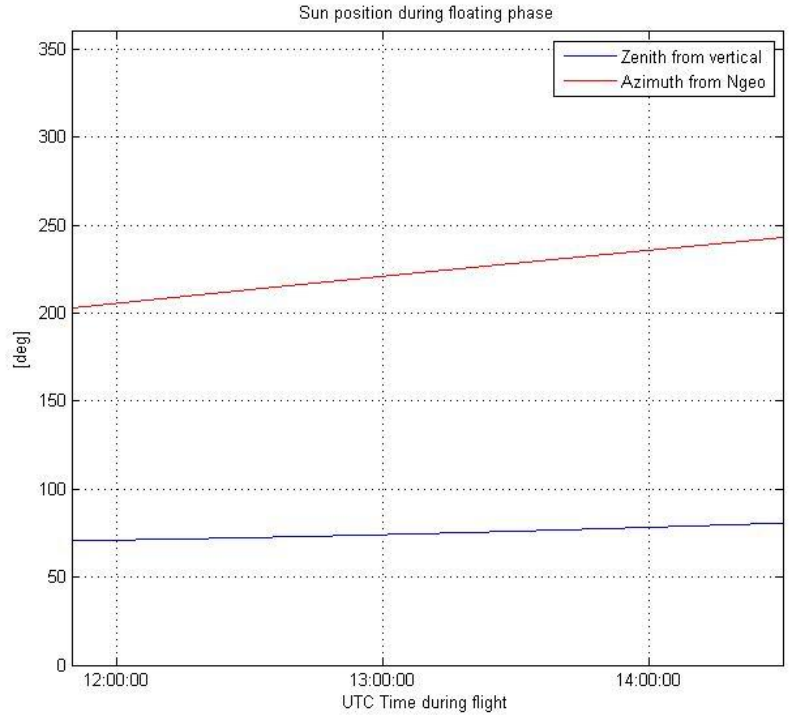

Figure 88 Sun position during cruise: azimuth is measured staring from N geo , zenith from vertical

Since in the body reference the horizon has been considered at the altitude of the plane of the gondola (0° in plane) the zenith angle variation has been transformed in:

$$18° > z > 10°$$

From this starting point the shadow area of the thermometer has been calculated in the NED reference frame placed on the tip of the boom.
In the body frame on the boom the x-axis points the boom direction, the z-axis points the down direction and the y-axis completes the right-handed coordinate system.

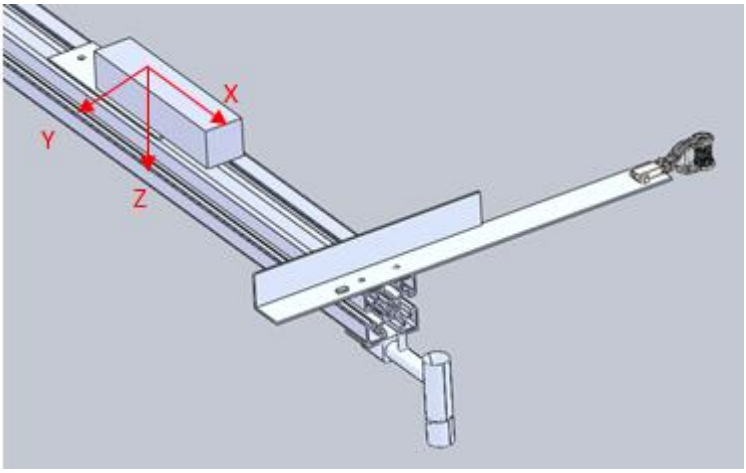

Figure 89 Body frame on the boom

Since the sun is just above the gondola horizon (18° > z >10°), the solar radiation doesn't affect the measurement (considering only the zenith angle): the gondola shields the sensor if pitch angle (mean value of 3°) is not taken into account.

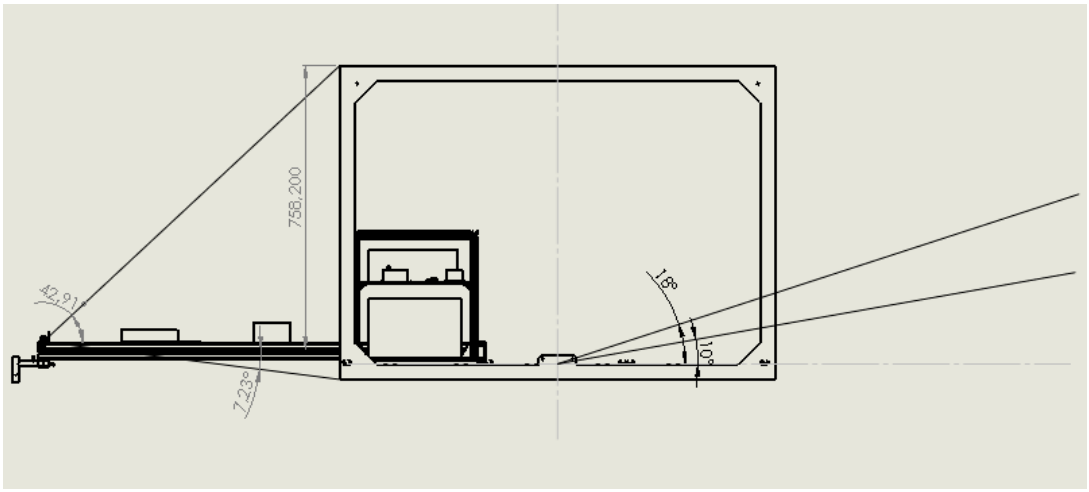

Figure 90 MISSUS in the correct position on the gondola (side view) and inclination of solar beam with respect to the thermometer

The dark zone respect to the boom direction, visible in Figure 91, is:

$$-43.6° < \psi_{boom} < +27.5°$$

taking into account the yaw range (with North geographic as reference), during the cruise phase the thermometer is not illuminated in the following zone:

- Start of floating considered UTC TIME=11:49; 344°<Ψ<54°
- Last measurement collected, UTC TIME=14:22; 18°<Ψ<89.5°

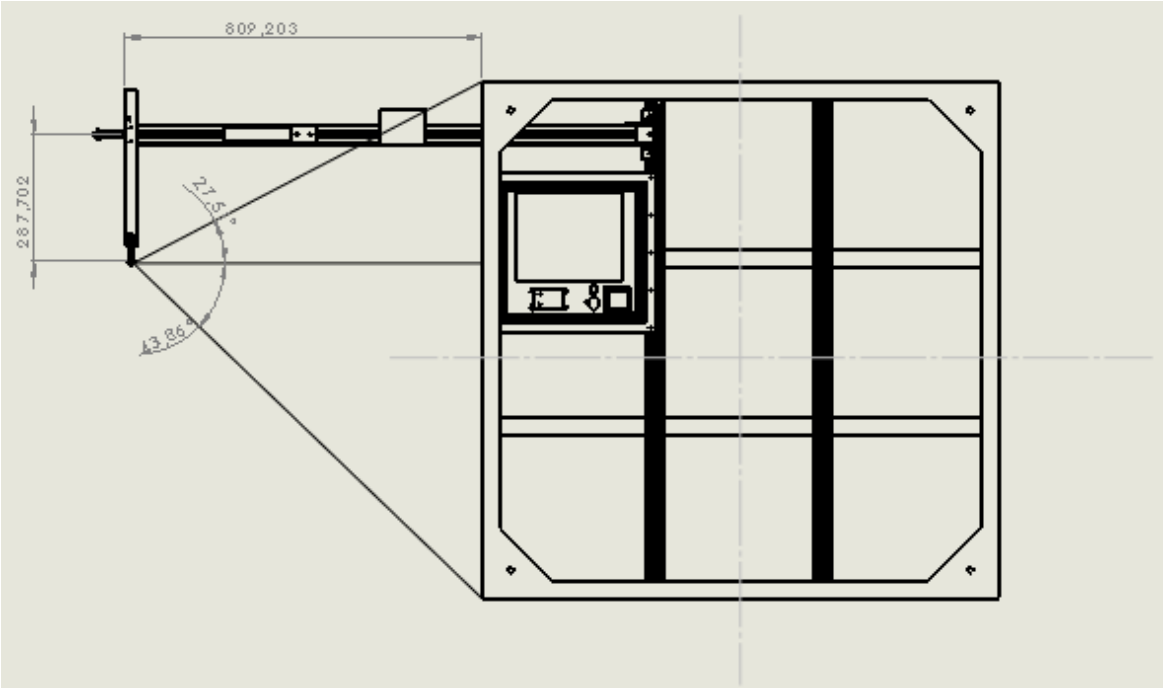

Figure 91 MISSUS in the correct position on the gondola (upper view) and angles which define the thermometer dark zone

In order to estimate the solar radiation effect on the temperature sensor sensitive wire, the temperature profile has been compared with the yaw angle (see following figure).

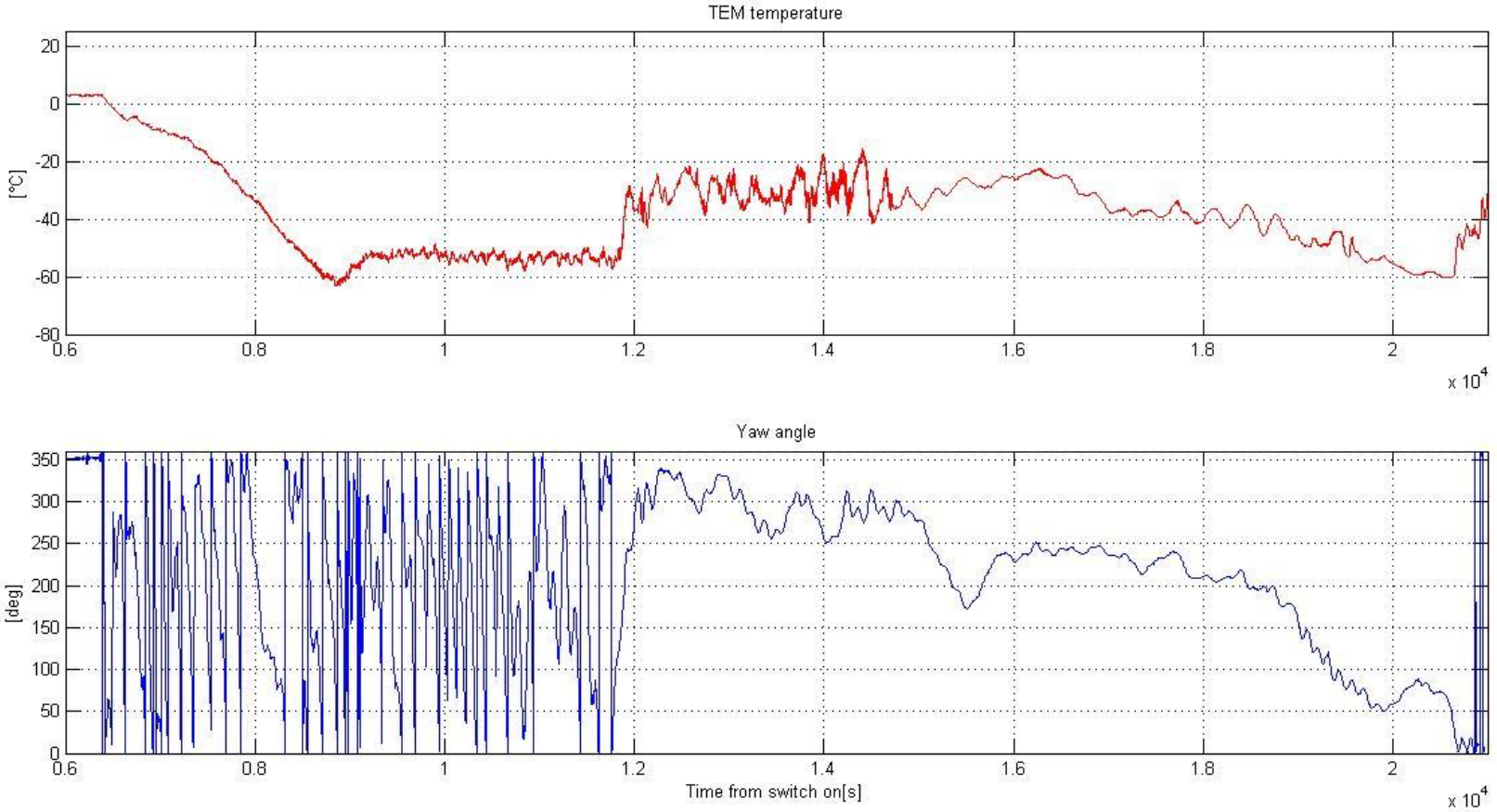

Figure 92 Temperature profile and yaw angle variation during flight

The following table summarizes the relevant events detected during floating phase. The first instant corresponds to UTC TIME =11:49 (floating phase starts 10 minutes later); the last instant considered is at UTC TIME=14:22 (end of MISSUS operative life).

Event	Time instant from switch on [s]	Temperature [°C]	Yaw angle	Notes
Start heating	11850	-53	85°	Compatible with start cruise phase
Temperature peak 1	11950	-28.77	228°	Boom towards the sun direction
Temperature peak 2	12540	-21.90	314.6°	Sensor is still illuminated
Temperature trend maintenance	11950-15040	-20 to -35	228°- 330°	Illuminated area, oscillations in Temp due to not constant illumination
Temperature trend maintenance	15040-18500	-22 to -38	175°- 247°	Illuminated area, oscillations in Temp due to not constant illumination
Start cooling	18500	-44.91	175°	No more fully illumination from sun
Cooling and maintenance	18500-20600	-45 to -60.35	175°- 50°	At 90° starts shadow area for cruise end compatible
Minimum temperature	20580	-60.38	64°	Correspondance with full darkness zone at cruise end
Start heating	20660	-58.06	21°	Perfect correspondance with exit from scadow area at cruise end
Heating	20660-21000	-58.06 to -30.50	21°- 0°	Compatible with illuminated area

Table 40 Correlation between temperature profile and yaw angle

The maximum temperature increase in the calculated illuminated zone respect to the dark zone is about $\Delta T=30°C$.

In the next figure can be seen the illuminated and shadow zones during cruise respect to the yaw rotation of the gondola.

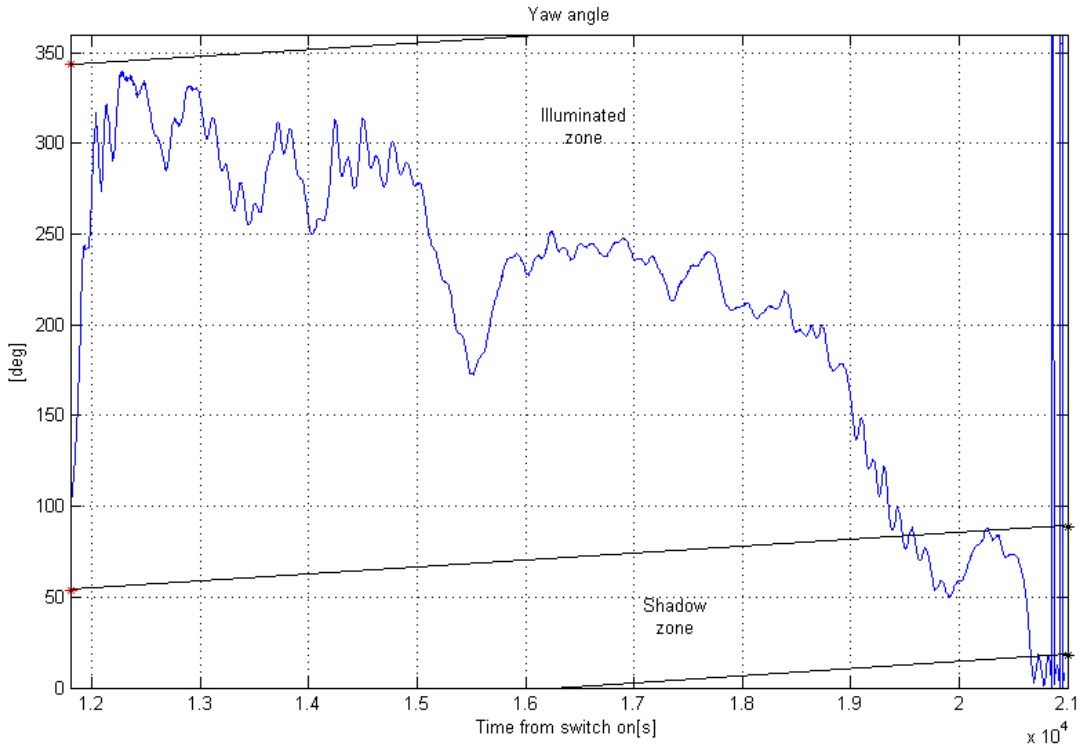

Figure 93 Yaw rotation during cruise and variation of the shadow zone

The following figures show specific intervals of observation, in which the fluctuations of the temperature due to the variable sun exposure are visible (x axis is time).

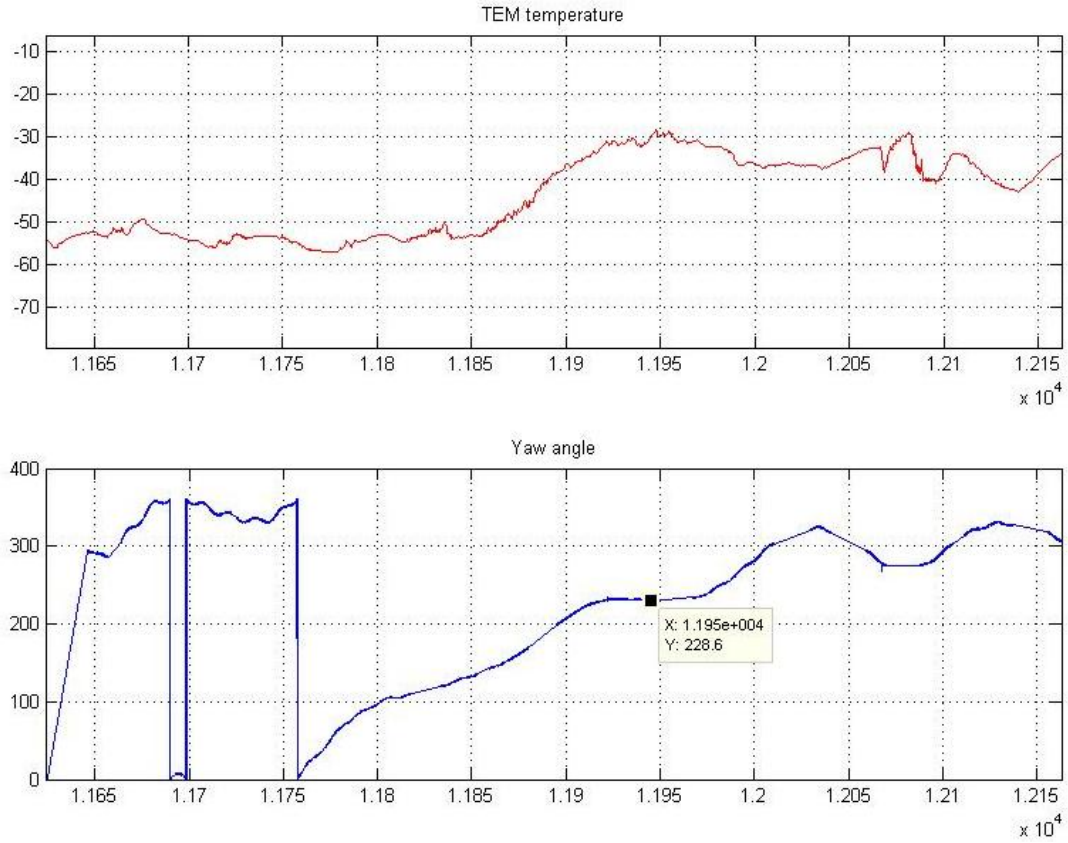

Figure 94 Correlation between temperature signal and yaw angle; temperature peak occurs when yaw angle is 228°

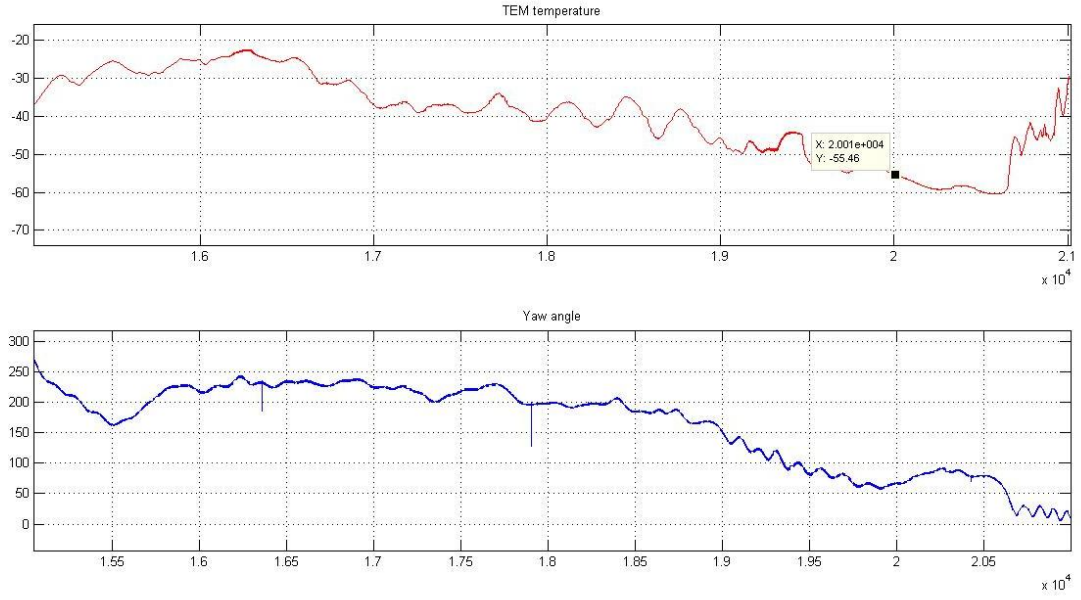

Figure 95 Example of cooling: the sensor comes back in shade at instant 20000s (dark zone: 18°<ψ<90°)

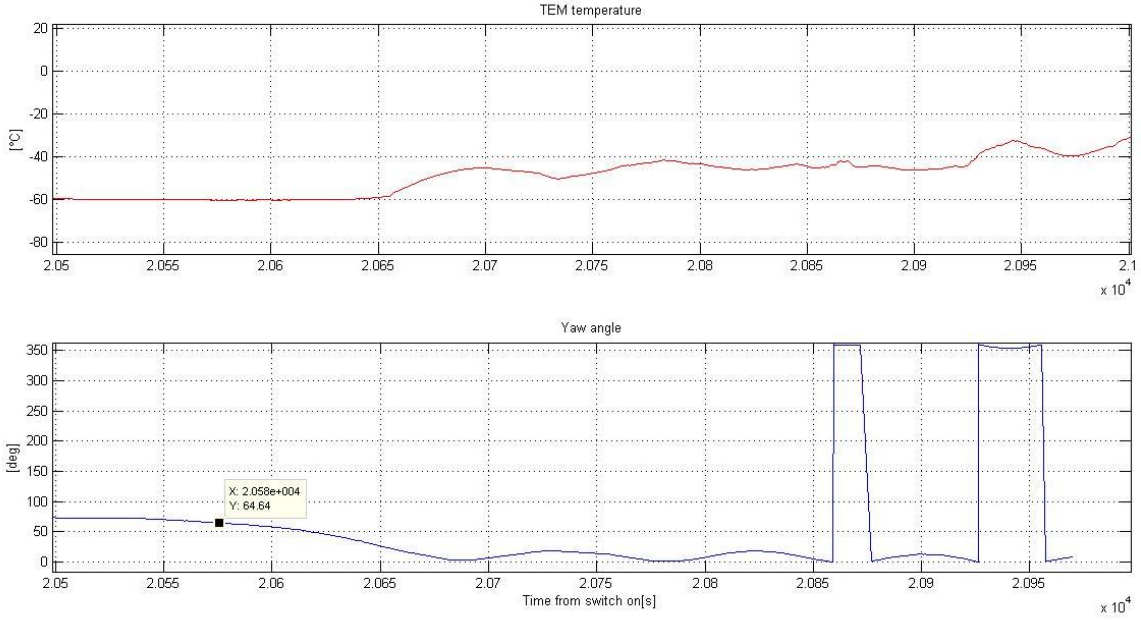

Figure 96 Clear increase of the temperature due to the gondola rotation; exit from shadowed area at ψ=21°

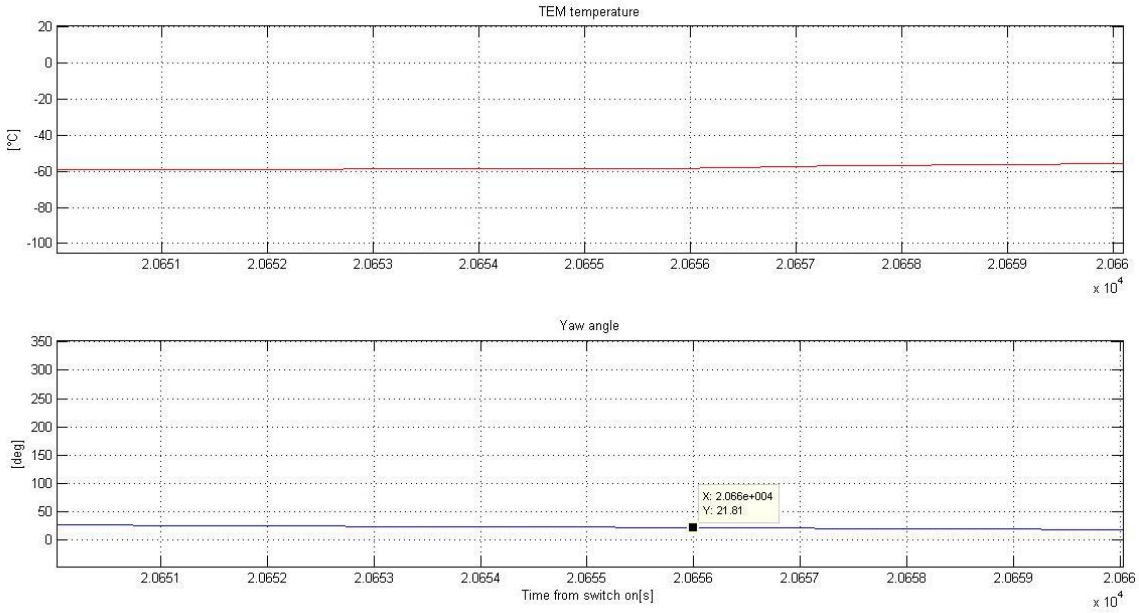

Figure 97 Increase of temperature with the decrease of yaw angle starting from ψ=21°

During the ascent phase the gondola has a high spin which doesn't allow sun influences on measurements. After the last complete rotation (around 12000s) is clearly visible that the increase of temperature occurs in less than 2 minutes, compliant with the moving in the illuminated zone (see Figure 94).

The same happens in the last part of collected data (see Figure 96), where the temperature increase of 20°C occurs in less than 100 s, compatible with the rotation in the sun-exposed zone.
When the sun exposition is maintained also the temperature is higher than that predicted by the atmospheric models (@ 25,6 km), this confirms the hypothesis of influences by illumination. Furthermore between 12000s and 14000s small rotations (clockwise and counter clockwise) of the gondola around the vertical axis are observed; also the temperature trend show different oscillations, however the correlation isn't well defined.
The cooling time is much longer respect to the heating one, around 30 minutes, which corresponds to a slow rotation of the gondola in the dark zone (see Figure 95). The cooling of the sensitive wire of the sensor results less clear. Influences of the thermic inertia of the sensor structure and support device are hypothesized (see Figure 89).
In addition other sources of uncertainty come from the gondola structure and external bodies protruding from the gondola body (other experiments, supports, etc.), which shield the sensor and modify the shadow zone.
We have also to consider the presence of only one innovative RTD sensor on board; two thermometers of the same type would have given a better reference during floating phase to scan the sunlight.

4.2.2.2 RTD wire thermal model

A numerical thermal model has been implemented in *Matlab* in order to deeply understand the phenomenon observed during flight, described in the previous paragraph.
The model allows to calculate the temperature of the sensitive Platinum wire as a function of the flight time by means of transient analysis.

The Platinum wire has been modelled with small spheres in order to evaluate exchange surface, volume and mass.
Each winding of the wire around the PEEK supports has been modelled with eight spherical surface of 1.495E-6 m^2. Then the total surface exposed to the external air has been calculated considering the number of windings (N=16) obtained for the RTD sensor.
The volume has been calculated considering a diameter of the wire of 6.8E-5 m and the length of the sphere of 7E-3 m (same number of spheres each winding and same number of windings as before).
The Platinum wire is characterized by a thermal capacity of 130 J/(kgK) and by the following thermal optical properties: $\alpha_S = 0.3$ (solar absorption coefficient) and $\varepsilon_{IR} = 0.05$ (infrared emissivity coefficient).

The thermal node, that represents the sensitive wire, is characterized by a self-heating $q_i=Ri^2$, i is the supply current (equal to 0.5 mA) and R the thermal resistance function of the temperature (the relation is described later in detail).
The node is directly exposed to the external environment, for this reason is thermally coupled with the sky background by radiation and external air by convection. Sky background and external air have been simulated as boundary nodes. The convection coefficient has been calculated using a simplified model, described hereafter.
In addition the sensitive wire is subjected to solar flux, planetary flux and exchange with the sky background.

Node	Description
BOUNDARY NODES	
B_SKY	Sky Background
B_PLANET	Planet
B_AIR	External air
RTD NODE	
D1	Platinum sensitive wire exposed to the external environment and with internal heat due to self heating

Table 41 Thermal model nodes

Platinum wire properties	Value
Thermal optical properties	
α_S	0.3
ε_{IR}	0.05
Material properties	
ρ[kg/m^3]	21450
c_P [J/(kg K)]	130

Table 42 Platinum properties

Solar radiation

The solar radiation is considered as a thermal input for the model. The direct solar flux, also called solar irradiance, is inversely proportional to the square of the distance to the Sun. The assumed value for the solar constant is:

$$J_S = 1367\ \mathrm{Wm^{-2}}$$

The solar input q_{SUN} has been calculated with the following equation:

$$q_{SUN} = A_i F_{i-SUN} J_S \alpha_S$$

α_S is the absorption coefficient of the platinum wire surface at 0.5 μm wavelength.

The view factor has been assumed equal to 0.25 since the surface directly exposed to the sun illumination is only the front side of the sensitive wire and half of the total windings length around the supports.

Planetary radiation

This thermal input depends on the temperature of the planet's surface and the mutual position of the body and the planet.

$$q_{PLANET} = \sigma A_i (T_{PLANET}^4 - T_i^4) F_{i-PLANET} \varepsilon_i \varepsilon_{PLANET}$$

σ is the Stefan Boltzmann constant 5.6704 E-8 $Wm^{-2}K^{-4}$.
ε_i is the absorption coefficient of the wire surface for a 4μm wavelength (infrared band).
ε_{PLANET} is the emissivity coefficient of the planet's surface at the same wavelength.
T_i is the temperature of the platinum wire.

Sky background

Sky background is set at the temperature of 3-4 K and is assumed to behave like a blackbody.
The heat flux q_{SKY} emitted by the RTD node towards the sky background is given by the following relation:

$$q_{SKY} = \sigma A_i (T_{SKY}^4 - T_i^4) F_{i-SKY} \varepsilon_i$$

Convection

Heat exchange by convection between RTD node and external air is given by the following relation:

$$q_{CONV} = \alpha_{CONV} A_i (T_{Air} - T_i)$$

The convective coefficient α_{CONV} has been estimated using the empirical formula for the forced convection on outer surface of circular duct (See Ref. [31]).
The outer surface is assumed as the total Platinum wire surface exposed to the external air.
The air velocity is supposed parallel to the vertical speed of the gondola, it is calculated from the variation of GPS altitude with time during BX15 flight.

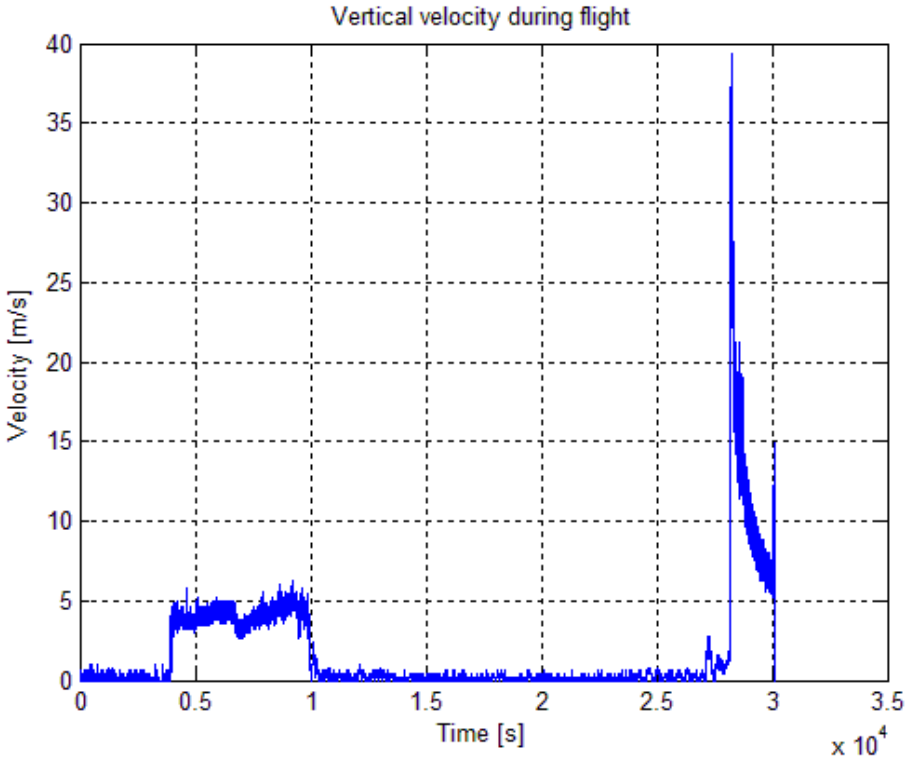

Figure 98 Vertical velocity profile versus time of BX15 flight

The Reynolds number is given by the following relation:

$$Re = \frac{v_{air} d_{eq} \rho_{air}}{\mu_{air}}$$

d_{eq} is the diameter of the cylindrical section (ring) on which the wire is wrapped around and is equal to 0.012 m.

The Nusselt number, assuming the air flow model described before is:

$$Nu = 0{,}43 + CRe^{m}$$

Where *C* and *m* are numerical constants function of the Reynolds number.

Re	C	m
1-4000	0.480	0.5
4000-40000	0.174	0.618
40000-400000	0.0239	0.805

Table 43 Variation of C and m with Re

Then the convective coefficient is:

$$\alpha_{CONV} = \frac{Nu\ \lambda_{air}}{d}$$

The air parameter were evaluated using the NRLMSISE-00 model for density and temperature, while dynamic viscosity μ and thermal conductivity λ were obtained from temperature by Sutherland's law and empirical formula respectively (see Ref.[32]).

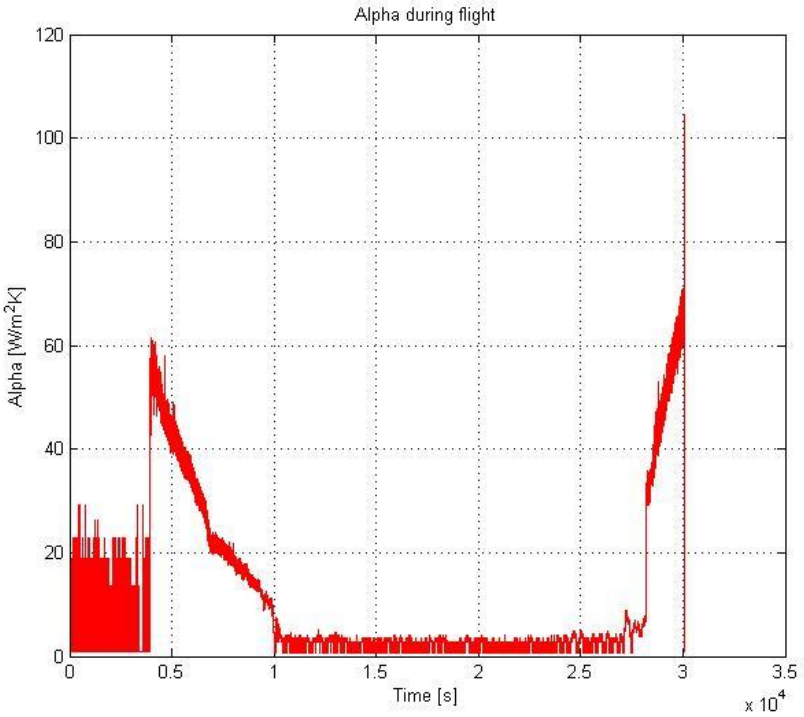

Figure 99 Convective alpha calculated versus time of BX15 flight

Self-heating

The RTD sensor is characterized by a self-heating equal to:

$$q_i = Ri^2$$

Where R is the sensor resistance, function of the temperature with the following relation for T<0:

$$T=AR^3+BR^2+CR+D$$

The interpolation coefficients were determined by the calibration process.

	T<0
A	-0.0000828631131
B	0.0165678475983
C	6.6002754665315
D	-239.3444697318800

Table 44 Interpolation coefficients

And *i* is the supply current equal to 0.5 mA.
Since the internal heating has a negligible effect on the temperature of the wire respect to the other fluxes, a constant value of 0.0000075 W (R=31 Ω) has been considered.

Boundary condition

The boundary nodes have known temperature values:

- The temperature of the Planet has been supposed equal to 283.15 K.
- The temperature of the sky background is equal to 4 K.
- The external air temperature has been calculated with NRLMSISE-00 model using the input data from the BX15 flight (see paragraph 4.2.1.2). The air temperature is then known as a function of time.

The following graph shows the temperature profile obtained and used as boundary condition.

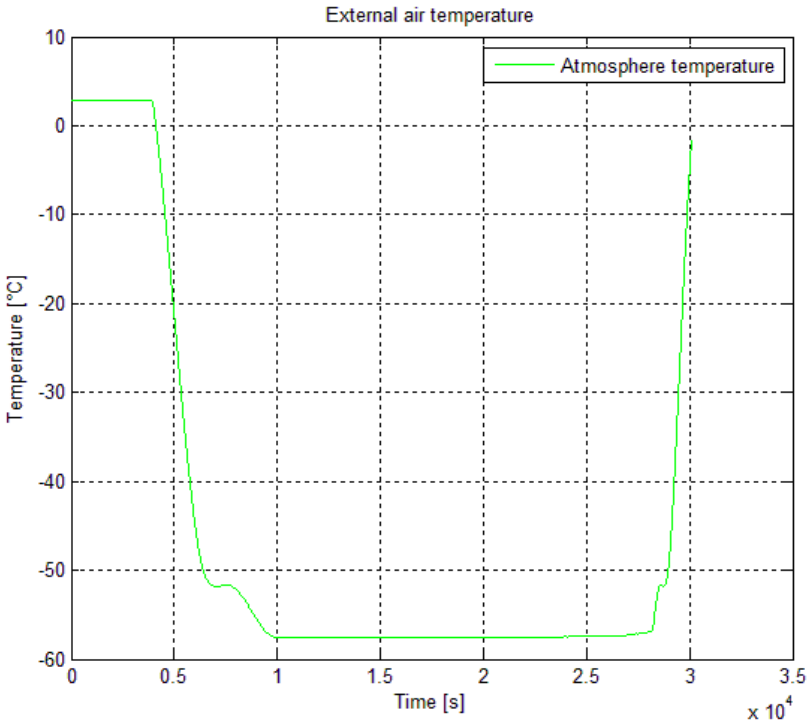

Figure 100 External air temperature of NRLMSISE-00 model versus time

Solution and results

The transient analysis has been performed considering the terms described above (radiation terms, convective term, self-heating term) plus an additional term, which represents the internal energy variation in time.
The thermal balance equation is:

$$q_{SUN} + q_{PLANET} + q_{SKY} + q_{CONV} + q_{S-E} = mc\frac{dT}{d\tau}$$

The term on the right represents the variation of the internal energy of the node due to the thermal evolution: m is the mass of the wire, c is the specific heat, $d\tau$ is the time lapse and dT the temperature variation in the elapsed time.
The following figure shows the temperature trend obtained for the node as function of time.

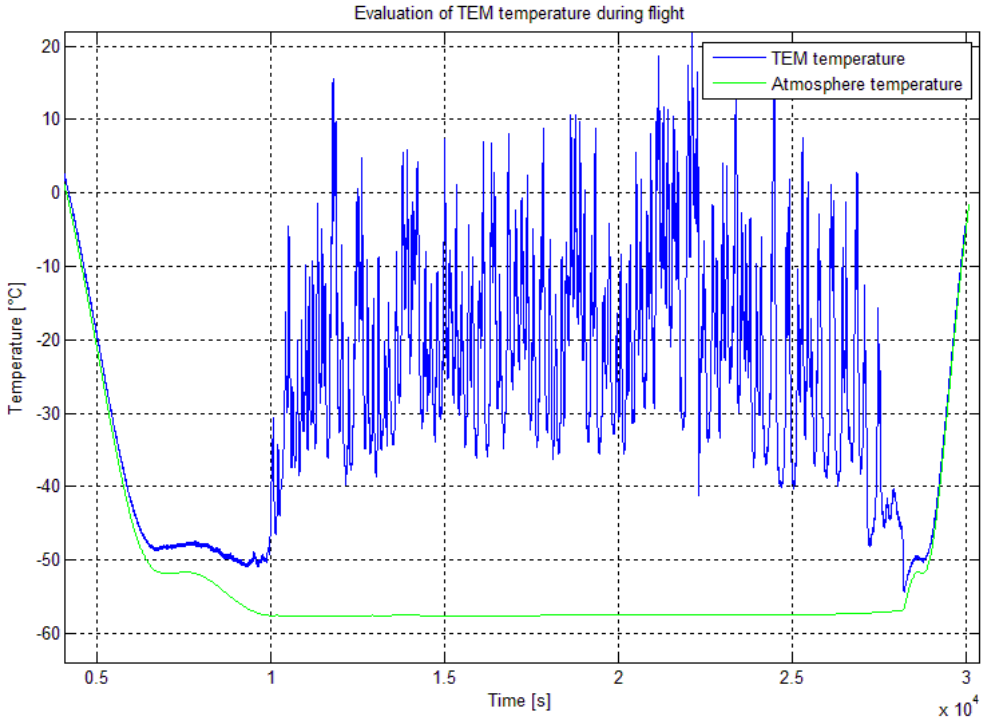

Figure 101 Temperature trends of atmosphere model (green) and platinum wire model (blue)

The model shows and confirms the heating of the platinum wire and the consequent increase in temperature, as observed during floating, when sensor is illuminated. Higher temperature peaks are observed in the model due to the geometrical simplification adopted. In the model the greater oscillations are due to the convective coefficient, which has been only estimated.

The mean temperature obtained during floating from the model is equal to -19.95 °C; the increase of temperature ΔT due to solar radiation results equal to +36.05 °C.

For comparison the temperature of the wire without solar radiation has been evaluated. The cold case is described by the following equation:

$$q_{PLANET} + q_{SKY} + q_{CONV} + q_{S-E} = mc\frac{dT}{d\tau}$$

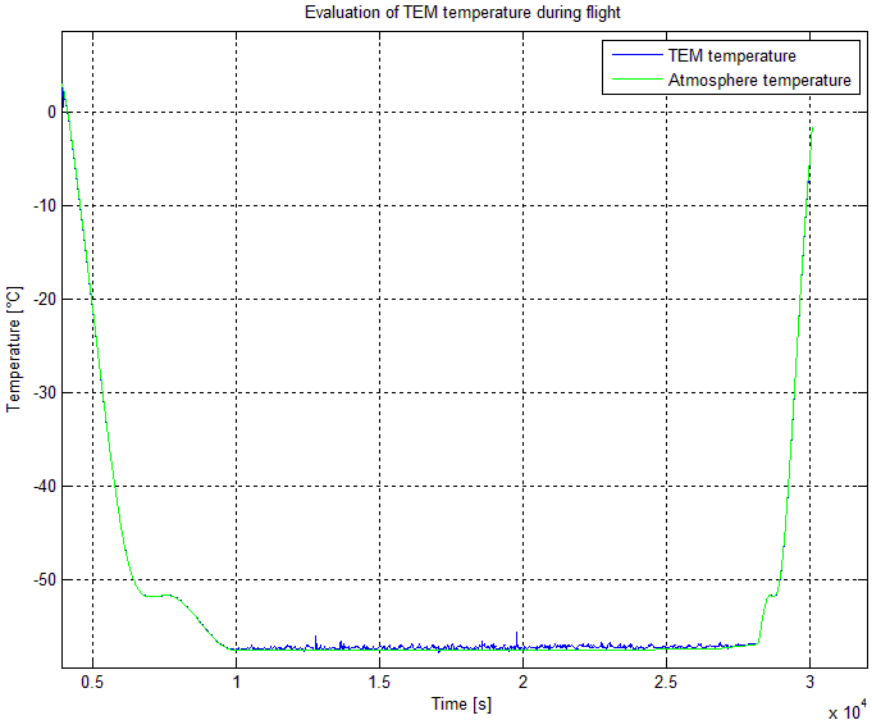

Figure 102 Temperature trends of atmosphere model (green) and platinum wire model (blue) – cold case

The main influence is clearly given by the solar radiation during the cruise phase, absent in the thermal input of the previous graph.

The following figure shows the comparison between the temperature of the wire calculated with the numerical model (blue line), the temperature estimated with the atmospheric model (green line) and the measured temperature (red line).

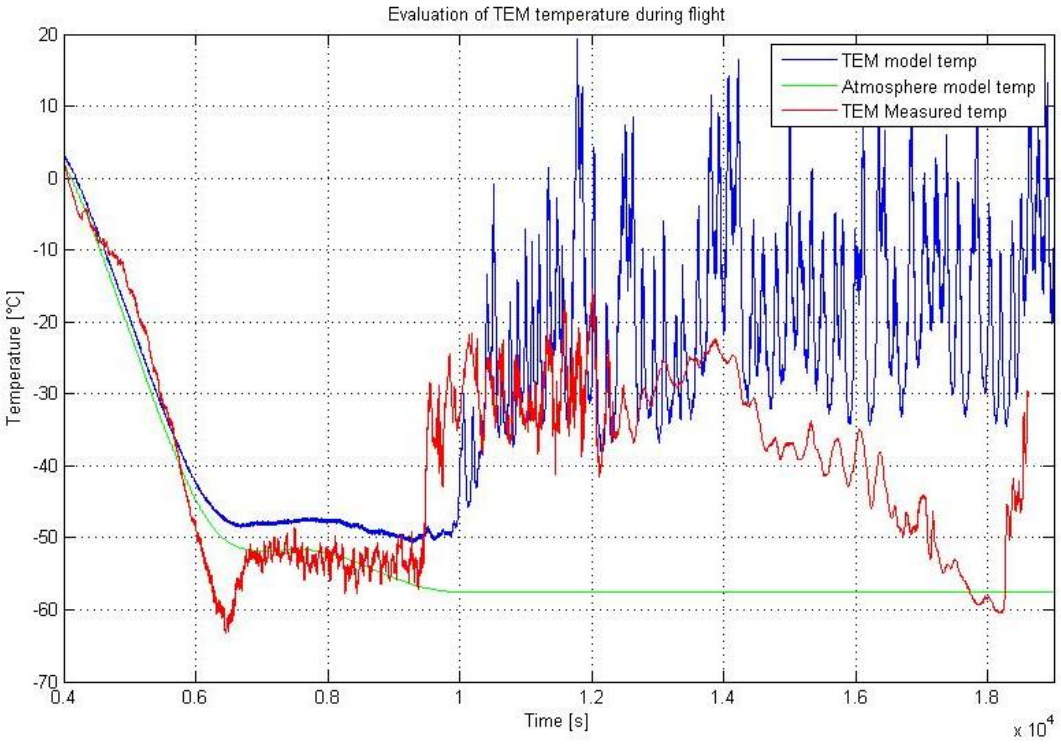

Figure 103 Comparison between estimated temperature (numerical and atmospheric model) and measured temperature

Except for the oscillations described before, the main differences observed are:

- Lower temperatures in the measurements collected respect to the model between 6000 s and 7000 s, the drop in temperature has been explained in paragraph 4.2.1.3.
- Higher increase in temperature in the model than in the measurements after 7000 s, in this phase the gondola is still ascending and it's rotating (as visible from the yaw data), the illumination isn't constant.
- The temperature increases before in the sensor measurements (about 9000 s), the convection coefficient must be lower than that estimated.

The increase of temperature ($\Delta T=36.05°C$) due to solar radiation obtained from the model is higher than that of flight data ($\Delta T=30°C$), anyway we can't relate this effect to the only presence or not of the sun in the real measurements.

In addition we have to take in account other environmental factors, such as unexpected flux perturbation, radiative effect of the structure, altitude oscillations, variable rotation due to the gondola attitude.

However this is a good starting point to plan future TVC tests in order to understand the real influence of solar radiation on the sensor.

4.3 Future work

In this section we discuss the possible tests to be performed to obtain further confirmations about the behavior of the temperature sensor during flight.
Thermal vacuum tests with solar simulator could be useful in order to verify the metrological behavior of the MarsTem prototype (in this paragraph we call it MISSUS Tem) due to the different illumination conditions. In addition, the solar simulator will allow to isolate the effect of solar flux from other environmental factors, encountered during flight.
Moreover further tests will be performed in order to compare the thermal behavior of MISSUS Tem with that one of the MarsTem Flight Model.
In the new version of MarsTem some original improvements have been introduced and implemented in the design from the previous model - MISSUS Tem - with the aim to minimize the effect of the solar radiation on the sensitive wire.

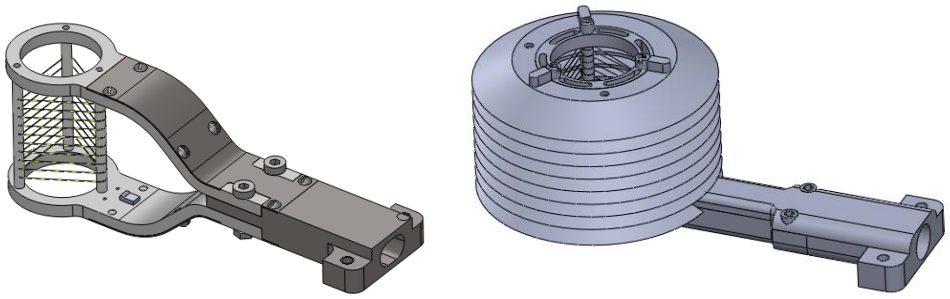

Figure 104 Comparison between the two RTD sensors: on the left MISSUS Tem, on the right the new version of MarsTem

The thermal vacuum tests with MISSUS Tem and MarsTem shall reproduce the environmental conditions during the flight on stratospheric balloon at 25 km and also pressure and temperature conditions on Mars ground, on which the MarsTem will operate.
In this way the tests will allow to achieve the following objectives:

- Verify the collected data of MISSUS Tem on stratospheric balloon flight with the results obtained with the same simulated conditions.
- Compare the collected data of MISSUS Tem with the results obtained with Mars on ground simulated conditions.
- Compare the thermal behaviour of MISSUS Tem with MarsTem in the different simulated conditions.

During the measurements on Mars ground MarsTem, on board DREAMS package, is exposed to sun illumination which has relevant influence on sensitive platinum wire due to

the reduced convective exchange mechanism in low pressure environment, pressure is equal to 6 mbar.
The same condition of thermal exchange can be applied to the stratospheric balloon flight on which flew the prototype, MISSUS Tem.
The main difference between the two cases is the quantity of solar radiation, on Earth the mean solar constant is 1367 W/m^2, on Mars is 653 W/m^2, and the composition of the atmosphere of the Planet.

In order to simulate the radiative and thermal environment in TVC an external beam generated by a Xenon lamp (up to 10 kW) will simulate the Sun, while a cryostat plate will allow to control the air temperature inside a control volume, delimited by a copper shell. The cryostat plate can be thermally controlled in the range from -190 °C up to +200 °C, thanks to a PID control, a set of thermo-resistances and liquid nitrogen.

In the following figures a possible configuration to perform the test is shown, hereafter the configuration proposed is described.

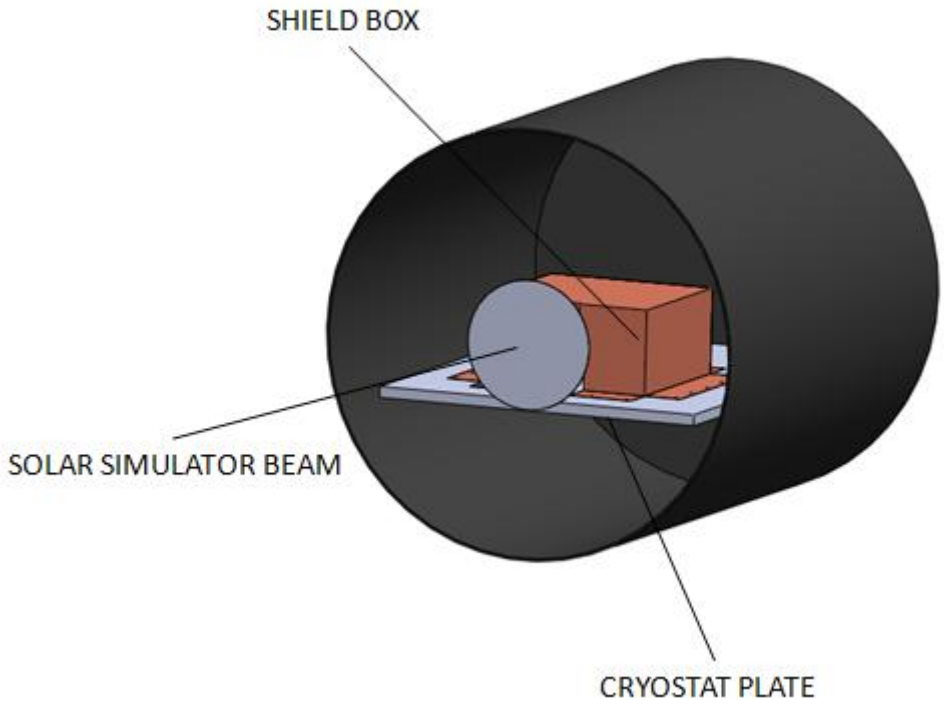

Figure 105 Proposed testbed inside TVC: the gray circle represents the solar simulator beam, the control volume is limited by the shield box

The two sensors will be located inside the (360x350x180) mm^3 shield box. The shell will be fastened with bolts to the cryostat plate, in order to thermally control the air inside the control volume.

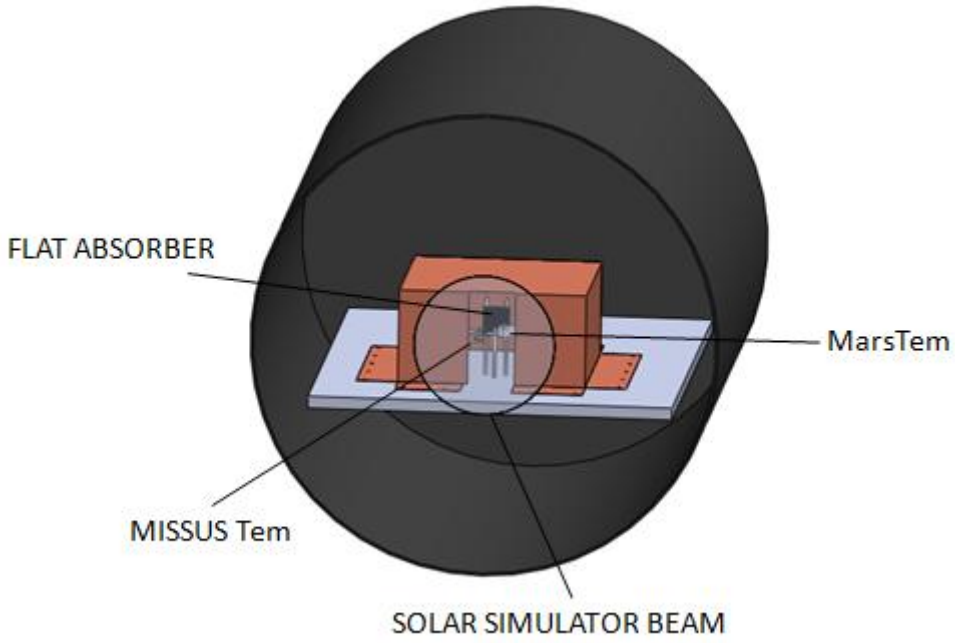

Figure 106 Configuration of the objects of the test - MISSUS Tem, MarsTem - inside the TVC

Next to the sensors inside the shield box can be seen a black square surface (side 50 mm), attached on support rods. The surface acts as flat absorber allowing to monitor the heating due to the solar simulator, applying the Stefan Boltzmann law.

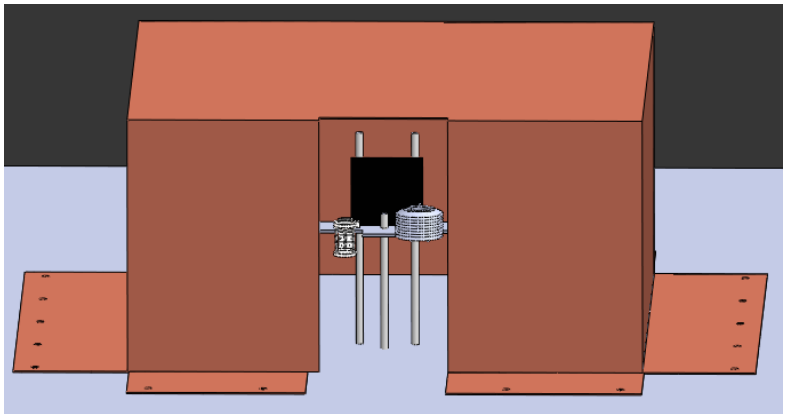

Figure 107 Particular of the previous figure: on the left MISSUS Tem, on the right MarsTem

The shield box is provided with a small rectangular window in order to expose the sensors and the flat absorber surface to the illumination of the Xenon lamp.
The control volume, except for the window area, will be thermally insulated with High Temperature MLI: the MLI lies on the sides directly exposed to the solar simulator flux in order to avoid overheating of the copper box.

The two sensors can be fastened to a plate support fixed to a PEEK threaded rod in order to avoid high conductivity between the Titanium support structure of the sensitive Platinum wire and the cryostat plate.
During the tests the internal chamber pressure, the cryostat plate temperature, the output temperatures of the innovative sensors, temperatures in different points of interest (black surface, shield box, supports, etc.), time length of the different steps of the test shall be monitored.
The proposed positions of the temperature sensors can be seen in the sketches below.

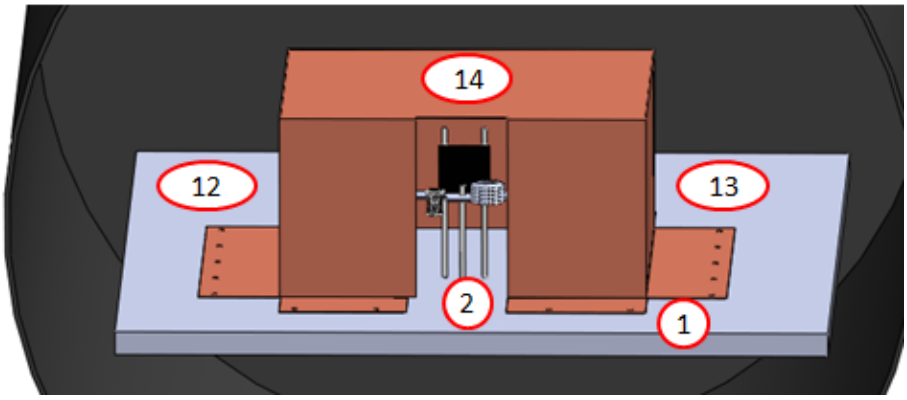

Figure 108 Position of the temperature sensors, front view

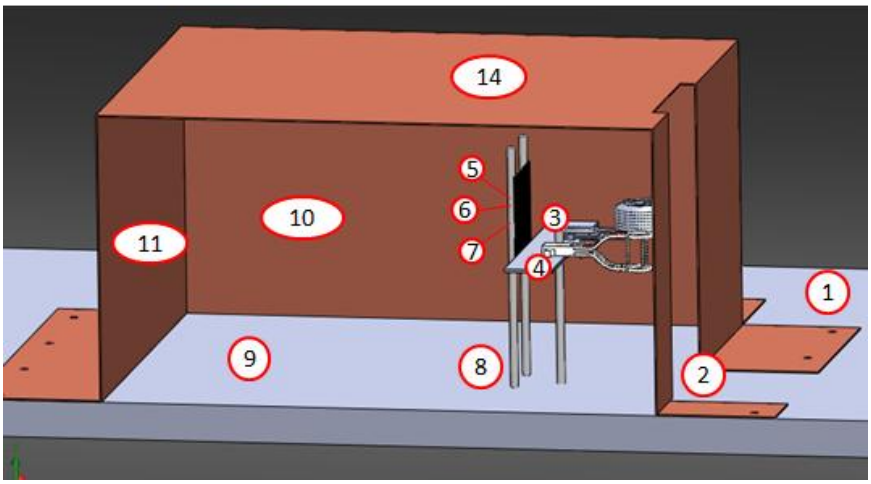

Figure 109 Position of the temperature sensors, side view

In order to achieve the objectives described before five different conditions should be simulated:

1. MarsTem sensors working on Mars ground without sun, night phase: solar simulator is switched off, and cryostat plate temperature is fixed at T_{CRIO_MN}. T_{CRIO_MN} represents the minimum temperature (-97°C) of the CO_2 Mars atmosphere during the night.

2. MarsTem sensors working on Mars ground during the day, daylight phase: solar simulator is switched on (direct flux equal to 653.21 W/m^2), and cryostat plate temperature is fixed at T $_{CRIO\_MD}$. T $_{CRIO\_MD}$ represents the maximum temperature (8°C) of the CO_2 Mars atmosphere during the day.
3. MarsTem sensors working on Mars ground during dust storm, reduced solar flux due to opacity (OD): solar simulator is switched on (incident flux equal to 640 W/m^2), and cryostat plate temperature is fixed at T $_{CRIO\_MD}$.

The environment temperatures and the solar fluxes that the sensor will encounter on Mars can be seen in the following figures.

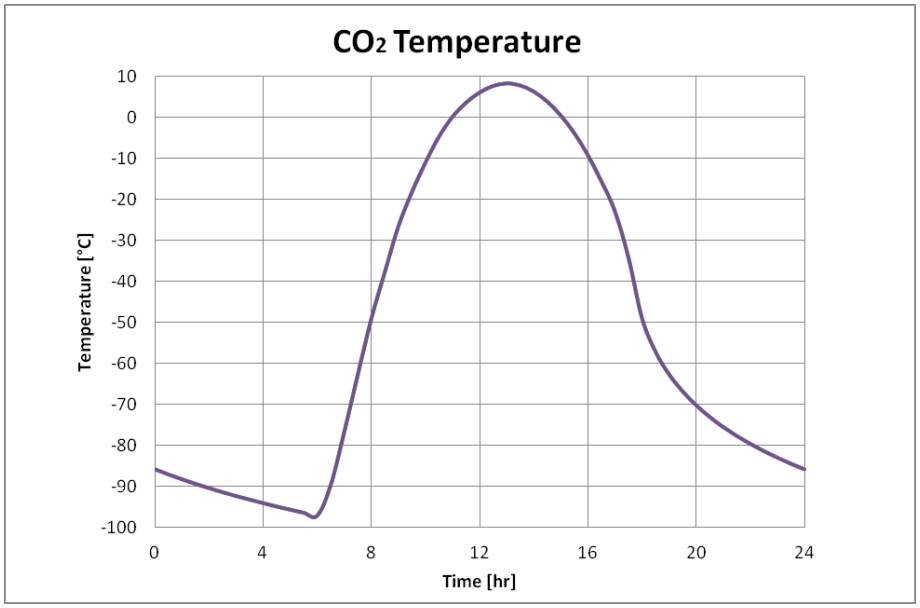

Figure 110 Temperature profile of CO_2 during Martian day

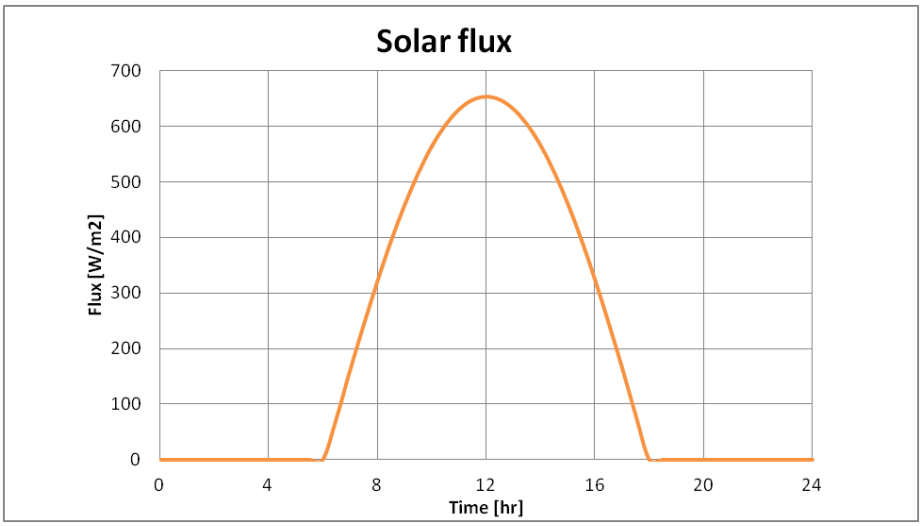

Figure 111 Radiative solar flux on Mars ground

The other conditions will simulate the Stratospheric balloon flight environment:

4. MarsTem sensors working on Stratospheric Earth flight not illuminated by the sun: solar simulator is switched off and cryostat plate temperature is fixed at $T_{CRIO\_E.}$ T_{CRIO_E} represents the temperature of the air (-62°C) in the stratosphere during the flight.
5. MarsTem sensors working on Stratospheric Earth flight illuminated by the sun: solar simulator is switched on (direct flux equal to 1367 W/m^2), and cryostat temperature is fixed at $T_{CRIO\_E.}$

In addition pressure should be set to 6 mbar for all the tests, in this way the condition of low pressure environment can be simulated.

Conclusions

At the beginning of the work two main objectives were defined:

- Manage the project MISSUS in order to design and realize a multi sensor scientific payload from the preliminary definition to the post flight analysis.
- Validate and check the performance of the MarsTem prototype onboard MISSUS with real data sets, achieving in this way the scientific goals of the experiment.

First let's consider the management of the project: the four main activities (work areas identification, resources analysis, schedule and risks definition) of this task have been accomplished, however some aspects must be underlined.
The original planned experiment has been modified during the project to its final version due to reasons of time scheduling (e.g. change HW/SW system) human and economic resources (e.g. sensors cost) and risks.
The work packages have been correctly distributed, nevertheless clear hierarchies have to be identified from the beginning. Moreover the responsibility on the specific task must be fully carried out from cooperating with other members to independent decisions without wait for input.
It is fundamental the availability of the funds and identify the contingencies as soon as possible. Due to the delayed availability all the schedule has been shifted and a great amount of work has been concentrated in the last period before flight. For this reason it is necessary to plan buffer time and wide margins for critical tasks and monitor well their progress from the beginning.
The project risks were correctly identified. It turned out that most of them were prevented, the personnel risks were mitigated and, despite the defective onboard computer, the objectives of the mission weren't compromised.

In the second part of the dissertation the cross correlation of the temperature data and other meteorological data have been undertaken.
The preliminary operation of data filtering was performed in order to reduce the signal noise. The wavelet de-noise technique has shown good results without appreciable degradation of the sensor signal. The technique adopted can be refined for future mission analysis, moreover further tests could be implemented in order to understand what could have caused the particular disturbs detected. In addition, for future experiments, more attention should be paid on filter devices and shielding in order to prevent electromagnetic interferences during the sampling.

The analysis of the environment up to 25.6 km (maximum altitude reached) have allowed to validate the temperature data collected by the innovative RTD sensor, prototype of the MarsTem. Furthermore the thermo-structure of the atmosphere has been evaluated by comparison with the implemented ISA model and the NRLMSISE-00 model. Local variations on the temperature measurements have been observed; the aspect has been investigated and can be related to the presence of stronger winds respect to other troposphere layers.

Stability of the atmosphere has been studied revealing several layers of stable air followed by unstable layers, especially in the troposphere. This kind of behavior supports the formation and presence of clouds, as confirmed by the VFM of CALIPSO satellite that crossed the region during balloon flight. The increase in stability is found to be at higher altitudes than troposphere, as expected; the stratosphere stability is also confirmed by the buoyancy frequency profile.

Another analysis has been undertaken for the cruise phase in order to see if and how the solar flux influences the temperature measurements. Therefore the sun position has been calculated respect to the sensor reference frame. In this way it has been possible to correlate the yaw rotation of the gondola with temperature variation due to the dark/illuminated zone. To assess the phenomenon observed a thermal model of the sensitive platinum wire has been implemented. The model shows and confirms the heating of the wire due to the solar flux in the cruise phase.

Since temperature and attitude data are strictly correlated, it can be interesting to develop a data fusion algorithm in order to improve the measurements.

However the real influence of illumination can be quantified only isolating solar flux from other flight factors. From this starting point thermal vacuum tests with solar simulator could be useful in order to verify the collected data of the sensor.

Furthermore the tests can be performed with the new version of the MarsTem in Mars like conditions. This scenario will allow to compare the thermal behavior of the two sensors, the prototype and the new version, together with the Earth thin atmosphere data of the flight.

References

[1] A. Spiga, *Elements of comparison between Martian and terrestrial mesoscale meteorological phenomena: Katabatic winds and boundary layer convection, Planetary and Space Science*, vol.59, pp.915-922, 2011

[2] ESA; *The Exomars Programme 2016-2018*; http://exploration.esa.int/science-e/www/object/index.cfm?fobjectid=46124 (Consulted in December 2012)

[3] ESA; *ExoMars orbiter and EDM Mission (2016)*; http://exploration.esa.int/science-e/www/object/index.cfm?fobjectid=46124 (Consulted in January 2013)

[4] EuroLaunch; *RXBX_REF_SED guidelines v3-0_14Dec10*; 2010

[5] C. Palla, D. Bettio, V. Botti, S. Chiodini, D. Cornale, F. Cucciarrè, E. De Villa Bais, M. Didonè, G. Tovo, I. Vidali; *Student Experiment Document BX15_MISSUS_SED_v5-0_31Dec12*; 2012

[6] ECSS-E-ST-10C; *Space Engineering, System engineering general requirement*s; 6 March 2009

[7] ECSS-M-ST-80C; *Space project Management, Risk Management*; 31 July 2008

[8] Wilfried Ley, Klaus Wittmann, Willi Hallmann; *Handbook of Space Technology*; Wiley; 2009

[9] ECSS-M-ST-10C Rev. 1; *Space project Management, Project Planning and implementation*; 6 March 2009

[10] H. Page; *RXBX_SEL_Introduction and Project Management*; 6 December 2011

[11] M. Inga, M. Fittock, EuroLaunch; *BEXUS-14/15 Campaign Requirements Plan, BX1415_CAM_CRPv1_2_22Sep12*; 2012

[12] F. Angrilli; *Corso di Misure Meccaniche e Termiche e Collaudi*; Vol. 1/2; CEDAM, Padova; 2005

[13] Matlab 2009; *Wavelet toolbox*; 1984-2008 The MathWorks, Inc.

[14] Brani Vidakovic, Peter Mueller; *Wavelets for kids - A tutorial introduction*; Duke University, Durham, NC USA; 1994

[15] Rami Cohen; *Signal denoising using wavelets*, Project Report; Department of Electrical Engineering, Technion, Israel Institute of Technology; February 2012

[16] S. G. Mallat; *A wavelet tour of signal processing: the sparse way*, 3rd edition; Academic Press; 2009

[17] L. Trainelli; *Lezioni di Meccanica del Volo 2 – Modello dell'Atmosfera*; 9 March 2008

[18] Mark Z. Jacobson, Stanford University; *Fundamentals of Atmospheric Modeling*, Second Edition; Cambridge University Press; 2005

[19] ModelWeb catalogue and Archive, *Atmosphere models*; http://ccmc.gsfc.nasa.gov/modelweb/atmos/nrlmsise00.html; (Consulted in October 2012)

[20] Günther Zangl, Klaus P. Hoinka; *The Tropopause in the Polar Regions***;** American Meteorological Society; 15 July 2001

[21] D. A. Hooper and J. Arvelius; *Monitoring of the Arctic winter tropopause: a comparison of radiosonde, ozonesonde and MST radar observations*; MRI Atmospheric Research Programme, Swedish Institute of Space Physics, Kiruna; 2000

[22] Michael Tjernström, Rune Grand Graversen; *The vertical structure of the lower Arctic troposphere analysed from observations and the ERA-40 reanalysis*; Royal Meteorological Society; 24 February 2009

[23] Maarten H. P. Ambaum and Brian J. Hoskins; *The NAO Troposphere–Stratosphere Connection*; Department of Meteorology, University of Reading, Reading, Berkshire, United Kingdom; 15 July 2002

[24] Cooperative Institute for Research in the Atmosphere (CIRA); *CloudSat Project, CloudSat Standard Data Products Handbook*; Colorado State University, Fort Collins; 25 April 2008

[25] K. Powell, M. Vaughan, D. Winker, KP. Lee, M. Pitts, C. Trepte, P. Detweiler, W. Hunt, J. Lambeth, P. Lucker, T. Murray, O. Hagolle, A. Lifermann, M. Faivre, A.

Garnier, J. Pelon; *CALIPSO Data Management System, Data Product Catalog Rev. 3.4*; Doc. Numb.: PC-SCI-50; NASA; 22 December 2011

[26] G. Colombatti , F. Ferri, F. Angrilli , M. Fulchignoni and the HASI balloon team, *Atmospheric stability & turbulence from temperature profiles over Sicily during summer 2002 & 2003 HASI balloon campaigns*; CISAS "G.Colombo" - Università di Padova, Université Paris VII – LESIA; 2003

[27] Rigel Kivi, Esko Kyro, Andreas Dornbrack and Thomas Birner; *Observations of vertically thick polar stratospheric clouds and record low temperature in the Arctic vortex*, Geophysical research letters, vol. 28, no. 19, pages 3661-3664; October 1, 2001

[28] *CALIPSO Level 2 lidar Vertical Feature Mask* _ 25 September 2012, http://www-calipso.larc.nasa.gov (Consulted in November 2012)

[29] I. Reda, A. Andreas; *Solar position algorithm for solar radiation application*; National Renewable Energy Laboratory (NREL) Technical report NREL/TP-560-34302; 2003

[30] I. Vidali; *MarsTem, un termometro per la misura della temperatura atmosferica marziana: progettazione, prototipazione e studio degli effetti dovuti all'autoriscaldamento*; 2012

[31] C. Bonacina, A. Cavallini, L. Mattarolo; *Trasmissione del Calore*; CLEUP; 1985

[32] Ashish Tewari; *Atmospheric and Space Flight Dynamics, Modeling and simulation with MATLAB and Simulink*; Birkhauser; 2006

Acronyms

This section contains a list of all abbreviations used in the document.

ADC	Analog-to-digital Converter
ASI	Agenzia Spaziale Italiana
BEXUS	Balloon Experiment for University Students
CALIPSO	Cloud – Aerosol LIDAR Infrared Pathfinder Satellite Observations
CDR	Critical Design Review
CEST	Central European Summer Time
CIRA	COSPAR International Reference Atmosphere
CISAS	Center for Studies and Activities for Space
CRP	Campaign Requirement Plan
CWT	Continuous Wavelet Transform
DLR	Deutsches Zentrum für Luft- und Raumfahrt
DP	Delivery Proposal
DREAMS	Dust characterization, Risk assessment and Environment Analyzer on the Martian Surface
DWT	Discrete Wavelet Transform
EAR	Experiment Acceptance Review
EBASS	Esrange Balloon Service System (piloting system)
ECSS	European Space Corporation for Space Standardization
EDM	Entry, Descent and Landing Demonstrator Module
E-Link	Ethernet up & downlink system
ESA	European Space Agency
ESRANGE	Esrange space center
ESTEC	European Space Research and Technology Centre, ESA (NL)
FCT	Flight Compatibility Test
FRR	Flight Readiness Review
GPS	Global Positioning System
GSE	Ground Support Equipment
H&S	Health and Safety
H/W	Hardware
HASI	Huygens Atmospheric Structure Instrument
IMU	Inertial Measurement Unit
IPR	Integration Progress Review

ITS	International Temperature Scale
MAIT	Manufacturing, Assembly, Integration & Testing
MISSUS	Meteorological Integrated Sensor Suite for Stratospheric analysis
MLI	Multi-layer Insulator
MoRaBa	Mobile Raketen Basis (DLR, EuroLaunch)
NASA	National Aeronautics and Space Administration
NED	North East Down
PDR	Preliminary Design Review
PEEK	Polyether Ether Ketone
PM	Project management
PTU	Pressure Temperature Humidity
RF	Radio Frequency
RH	Relative Humidity
RTC	Real Time Clock
RTD	Resistance Thermal Detector
SED	Student Experiment Documentation
SNSB	Swedish National Space Board
SoRa	Sounding Radar
SSC	Swedish Space Corporation (EuroLaunch)
STFT	Short-Time Fourier Transform
TBC	To Be Confirmed
TVC	Thermal Vacuum Chamber
TVT	Thermal Vacuum Test
UTC	Universal Time Coordinate
w.r.t.	with respect to
WBS	Work Breakdown Structures
WP	Work Package
WS	Work Shop

Appendix

Commercial sensors data

1. Commercial RTD sensor
   http://www.minco.com/products/sensors.aspx?id=37

2. Humidity sensor - Honeywell HIH-4000 series
   http://www.phanderson.com/hih-4000.pdf

3. Triaxial magnetometer - Bartington Mag-03MS1000
   http://www.bartington.com/Literaturepdf/Datasheets/Mag03%20DS0013.pdf

4. Absolute pressure sensor - Freescale MPX-2200 series
   http://www.freescale.com/files/sensors/doc/data_sheet/MPX2200.pdf

5. Differential pressure sensor Vaisala PDT101
   http://www.vaisala.com/en/products/pressure/Pages/PDT101.aspx

6. IMU - XSENS MTi-G
   http://www.xsens.com/images/stories/products/PDF_Brochures/mtig%20leaflet.pdf

7. Triaxial accelerometer - Dytran7523A5
   http://www.dytran.com/img/products/7523A1.pdf

8. RTD sensors to monitor temperature of components
   http://it.rs-online.com/web/p/termoresistenza-al-platino/6117801/

Price breakdown form

1. Preliminary version

Description	NUMBER	EXPENSE [€]	INCOME [€]
1 DIRECT COST			
SENSORS			
Absolute pressure sensor	2	32.00	
Relative pressure sensor	1	800.00	
Humidity sensor	1	50.00	
Sonic Anemometer	1	5'000.00	
Thermocouple/commercial RTD sensor	1	30.00	
Triaxial accelerometer	1	600.00	
Camera	1	180.00	
MATERIALS			
Raw materials & major ext. products		650.00	
Components for thermometer		250.00	
Structure materials		100.00	
Electronics		1'700.00	
Battery		200.00	
TOTAL DIRECT COST		9'592.00	
2 MACHINING		2'000.00	
TOTAL MACHINING		2'000.00	
3 FUNDING			
University, CISAS and School in sciences technologies and measurement for space (estimated)			8'912.00
Sponsors (estimated)			2'680.00
TOTAL NECESSARY FUNDING			11'592.00
TOTAL		**11'592.00**	**11'592.00**

2. Updated version mid-project

	EXPENCE			INCOME
	NUMBER	**PRICE**	**TOTAL**	
Purchase of sensors and material				
Absolute pressure sensor	2	€16.00	€32.00	
Differential pressure sensor	1	€835.00	€835.00	
Humidity sensor	1	€50.00	€50.00	
Accelerometer	1	€600.00	€600.00	
Fine commercial RTD	1		€186.75	
Kapton heater for Pitot tube	1		€69.75	
RTD sensors for diagnostic	3	€7.92	€23.76	
Other heaters	3	€36.50	€109.50	
Pitot tube	1		€1’560.00	
Innovative temperature sensor	2		€1’900.00	
Main structure components			€273.10	
Battery	3		€1’371.00	
TOTAL purchase materials			€7’010.86	
Technical assistance				
Electronics (estimation)			€1’000.00	
Web site			€12.09	
TOTAL technical assistance			€1’012.09	
Travels				
Travel to ESTEC, Team member1			€370.53	
Travel to ESTEC, Team member2			€352.78	
Travel to ESTEC, Team member3			€400.00	
Travel to ESTEC, Team member4			€413.34	
Travel to ESRANGE, Team member1			€1’300.13	
Travel to ESRANGE, Team member2			€1’300.00	
TOTAL travels			€4’136.78	
Funds				
Università degli studi di Padova				€ 1’000.00
Sponsors (Borgoverde SrL, etc.)				€ 8940.00
Other Sponsors (TBC)				€ 5’000.00
TOTAL Funds				€14’940
TOTAL			**€12’159.73**	**€14’940**

Overview of Wavelet theory

A wavelet is a wave-like oscillation with an amplitude that starts out at zero, increases, and then decreases back to zero.

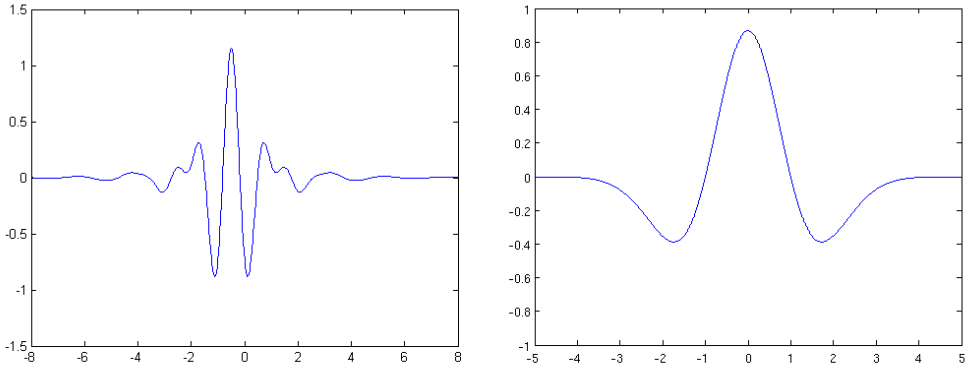

Figure A - 1 Examples of wavelet functions: Meyer wavelet (left), Mexican hat wavelet (right)

The wavelet transform is often compared with the Fourier transform (signals represented as a sum of sinusoids), but there are some important differences.
Fourier basis functions are localized in frequency but not in time. Small frequency changes in the Fourier transform will produce changes everywhere in the time domain. Wavelets are local in both frequency/scale (via dilations) and in time (via translations). Furthermore, many classes of functions can be represented by wavelets in a more compact way [14].
Wavelet analysis represents the next logical step to Short-time Fourier transform, the STFT is also time and frequency localized, but there are issues with the frequency/time resolution trade-off.

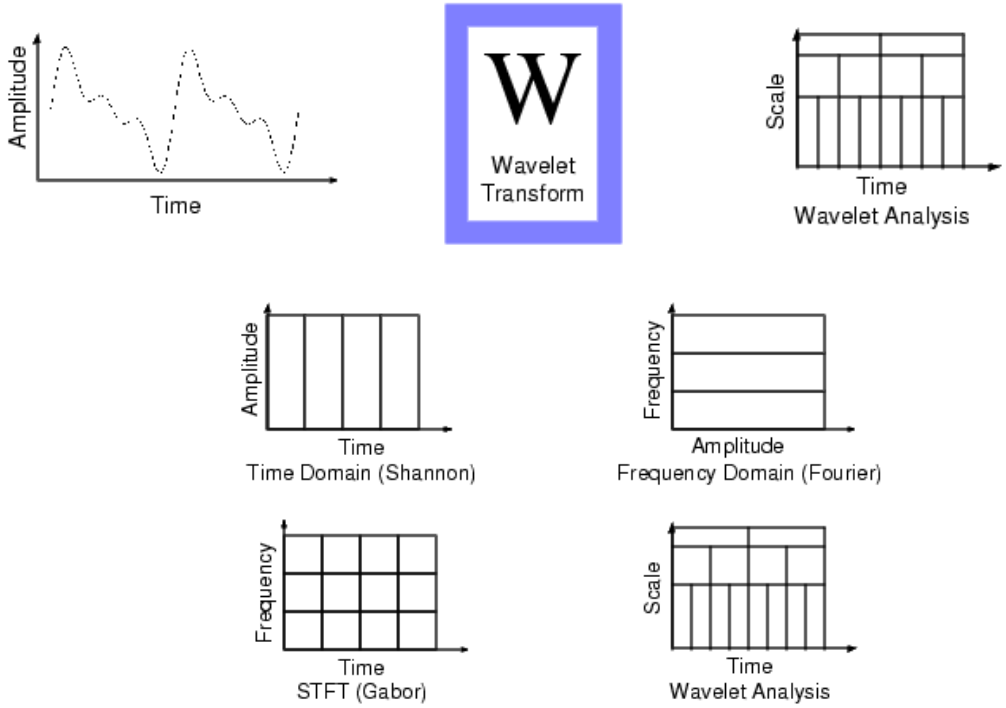

Figure A - 2 Contrast of wavelet analysis with the time-based, frequency based, and STFT views of a signal, Ref. [13]

Given a mother wavelet $\psi(t)$ (which can be considered simply as a basis function of L^2), the continuous wavelet transform (CWT) of a function $x(t)$ (assuming that $x \in L^2$) is defined as:

$$X(a,b) = \frac{1}{\sqrt{a}} \int_{-\infty}^{\infty} \psi\left(\frac{t-b}{a}\right) x(t)dt$$

The scale or dilation parameter a corresponds to frequency information ($a \sim \text{frequency}^{-1}$) and the translation parameter b relates to the location of the wavelet function as it is shifted through the signal, so it corresponds to the time information in the transform. The integral above can be seen as a convolution operation of the signal and a basis function ψ (t) (up to dilations and translations).

Unlike Fourier transform, in which the basis is $e^{i\omega t}$, there are many possible choices of $\psi(t)$. In practice, the transform which is used is the discrete wavelet transform (DWT) which transforms discrete (digital) signals to discrete coefficients in the wavelet domain. This transform is essentially a sampled version of CWT. Instead of working with $a, b \in R$, the values of $X(a, b)$ are calculated over a discrete grid:

$$a = 2^{-j}\ ,\ b = k \cdot 2^{-j} \qquad j,k \in Z$$

where this type of discretization is called *dyadic dilation* and *dyadic position*, respectively. [15]

Considering the DWT, the transform can be computed efficiently using Mallat's algorithm (see Ref. [16]). Essentially the algorithm is a fast hierarchical scheme for deriving the required inner products (which appears in CWT equation above, as a function of *a* and *b*) using a set of consecutive low and high pass filters, followed by a decimation.

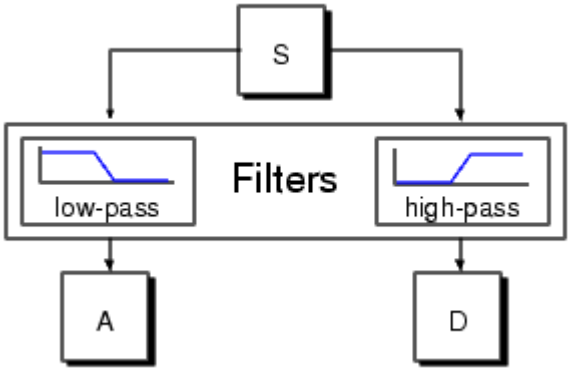

Figure A - 3 The filtering process at its most basic level

The approximations are the high-scale, low-frequency components of the signal. The details are the low-scale, high-frequency components.
The low-pass (LP) and high-pass (HP) filters used in this algorithm are determined according to the mother wavelet in use.

Supposing that the original signal S consists of 1000 samples, two sequences (A and D) of 1000 samples are produced, then they are decimated (500 samples) to obtain the DWT coefficients (cA and cD).

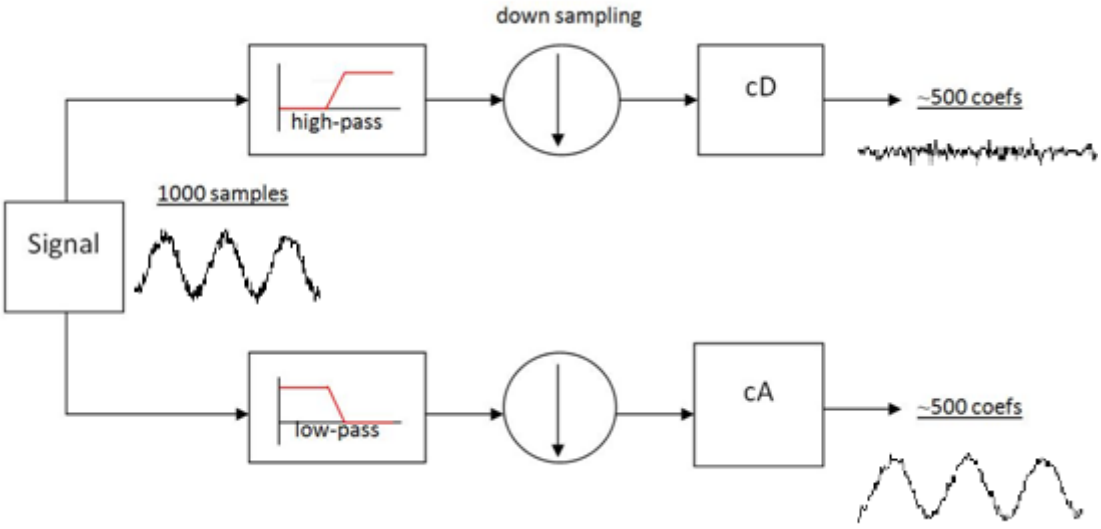

Figure A - 4 One stage filtering, schematic diagram with real signal inserted

The process can be iterated, with successive approximations, so that one signal is broken down into many lower resolution components.

The reconstruction of the signal is performed with the inverse process (see figure below): approximation level is obtained considering null values for the detailed coefficients, H' and L' are the reconstruction filters.

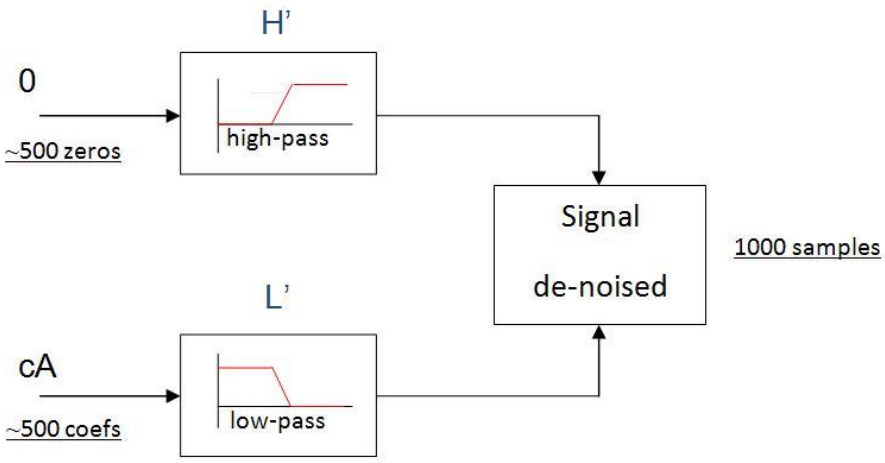

Figure A - 5 Reconstruction of approximated signal

Acknowledgments

I wish to thank you all the people that supported me in this work and during the last year of my Master degree. I hope they know how much their help and advices were worth to me, if not, here we are to tell them!
I prefer to continue in Italian, because in this way I would say it to them!

Sarò un po' informale ma credo sia la maniera migliore per dimostrare la mia gratitudine!
Non ho dubbi da dove incominciare: dai miei genitori! Certo è un classico, ma perché darlo per scontato! Non è solo un supporto formale, ma di vita! Grazie perché mi hanno fatto crescere cullandomi, incoraggiandomi, sgridandomi, spronandomi,…e soprattutto nell'ultimo periodo, quando le insicurezze e la stanchezza di un anno intenso si facevano sentire, perché mi hanno mostrato il cammino percorso, creduto in me e fatto capire che nonostante le difficoltà ce la potevo fare!
Il mio fratellino, si fa per dire (vero Baaalls?), merita un grande abbraccio, perché con la sua scioltezza ha saputo sdrammatizzare i momenti di tensione divertendomi! Lo ringrazio anche per tutte le chiacchierate assieme con la sveglia all'alba, su e giù per tracciati e tornanti con neve, sole e vento! Questa tesi è in percentuale anche sua per le piccole correzioni datemi, obbligandolo a leggere alcuni spezzoni del malloppo!

Ringrazio il Prof. per la disponibilità dimostratami e in particolare per l'opportunità che mi ha dato di partecipare a questo progetto, all'inizio solo un'idea, una proposta appesa su una bacheca del Dim!
Grazie alla Fra per il supporto tecnico, per ciò che mi ha insegnato e per l'incrollabile aiuto da ingegnere e da amica, nonostante gli herpes da stress, metaforici e reali, che le ho procurato!
Grazie a Giacomo per i preziosi consigli, le correzioni, gli spunti e il tempo dedicato alle interminabili riunioni di data analysis per interpretare e analizzare al meglio quanto a disposizione!

Grazie alla Dany, o Dan, o Danuzza, perché ha saputo ascoltare e sopportare i miei scleri estivi, perché mi conosce da un sacco e so che su di lei posso sempre contare!
Grazie a Dadà, a Rich, alla Fra coinqui, alla Fra new entry, a Paguz, a Luca, alla Ele che sono sempre pronti a tollerare, rispondere, aiutare, discutere nelle serate in compagnia, durante i viaggi, fra partite, musica, film e balli!
Grazie ad Eli ed Anna, a volte basta davvero qualche parola per sentirsi meglio!
Grazie alle amiche con la I: Ile, per le confidenze davanti ad una cioccolata calda; la cara Ila, per il suo supporto a non mollare!

Un ringraziamento va anche al MISSUS team, perché ne abbiamo passate di cotte e di crude! Quest'anno e più di lavoro assieme è stata una vera esperienza di vita, a volte proprio "tough", ma ne è valsa la pena!

Ringrazio il gruppo IAS '88, ultimamente di ritrovi goderecci per il Veneto, per questi anni di studi e non solo passati assieme!

Grazie agli amici vicini e lontani e a tutti quelli che hanno condiviso e condividono le mie passioni, i miei valori, le mie ragioni, i miei sentimenti.

Chiara